Institut für Nutzpflanzenwissenschaften und Ressourcenschutz
INRES – Pflanzenkrankheiten und Pflanzenschutz

Phenotyping of wheat resistance to *Fusarium* head blight using hyperspectral imaging

Dissertation

zur Erlangung des Grades
Doktor der Agrarwissenschaften (Dr. agr.)

der Landwirtschaftlichen Fakultät
der Rheinischen Friedrich-Wilhelms-Universität Bonn

von

Elias Alisaac

aus

Sadad – Syrien

Bonn 2021

Referentin: Prof. Dr. Anne-Katrin Mahlein

Korreferent: Prof. Dr. Jens Léon

Korreferent: Prof. Dr. Petr Karlovsky

Tag der mündlichen Prüfung: 18.12. 2020

Angefertigt mit Genehmigung der Landwirtschaftlichen Fakultät der Universität Bonn

To the cradle of the civilization
and the land of the first alphabet
to my homeland
Syria

Acknowledgments

At the end of this journey, I would like to express my sincere appreciation to the people who supported me to accomplish this work especially Prof. Dr. Heinz-Wilhelm Dehne who passed away too early on 23rd of May 2019. Prof. Dehne supported my application in the German embassy and helped me to enroll at the University of Bonn. May God have mercy on him.

Many thanks and appreciations go to Prof. Dr. Anne-Katrin Mahlein who believed in me and stood in my side from the beginning and during the difficult times that I went through. Many thanks, Anne, there are no words to express my thanks and appreciations.

In addition, I would like to thank Prof. Dr. Petr Karlovsky and his team at the University of Goettingen who hosted me in his laboratory and gave me the chance to do the molecular investigations related to this work.

Many thanks go to Prof. Dr. Jens Léon for his time, and remarks regarding this work, thanks are extended as well to my committee for their time during the examination process.

I would like to thank also the administration of the Faculty of Agriculture at the University of Bonn represented by the Dean and the promotion office, in addition to the administration and the teamwork of the department of Plant Diseases and Plant Protection at the Institute of Crop Science and Resource Conservation (INRES).

I also appreciate the financial support of the German Federal Ministry of Education and Research (BMBF) within the funding program “Networks of excellence in agricultural and nutrition research - CROP.SENSe.net” (Funding code: 0315529), Junior Research Group “Hyperspectral phenotyping of resistance reactions of barley”.

I am grateful and thankful to the Catholic Academic Exchange Service (KAAD) for their financial and social support during my Ph.D. and sincere thanks to Dr. Nora Kalbarczyk and Mrs. Santra Sontowski at the department of the Middle East.

Finally, to my parents, who planted my ambition and were always my supporters. To the twin of my soul, my brother Amer, we always shared the tears of happiness and sadness, and to my little angel, my sister Mariam and her beloved family, thank you for being in my life.

Elias

Declaration

I, the undersigned, hereby declare that this thesis is my own original work carried out in the Institute of Crop Science and Resource Conservation (INRES)-Plant Diseases and Plant Protection and that all sources have been accurately reported and acknowledged in the text and a list of references provided. And this thesis has not been previously submitted for another degree at this or any other university.

21.01.2021 

Elias Alisaac

Contents

Abbreviation

ΔT	Average Temperature Difference
3-ADON	3-Acetyl-Deoxynivalenol
4-ANIV	4-Acetyl-Nivalenol
4-ANIV-G	4-ANIV-Glucoside
15-ADON	15-Acetyl-Deoxynivalenol
AUDPC	Area Under Disease Progress Curve
AFB1	Aflatoxin B1
BBCH	Biologische Bundesanstalt, Bundessortenamt and CHemical industry
BEA	Beauvericin
CABI	Centre for Agriculture and Bioscience International
CAI	Cellulose Absorption Index
CCD	Charge-Coupled Device
CFI	Chlorophyll Fluorescence Imaging
CWA	Continuous Wavelet Analysis
CZID	Czapek Dox Iprodione Dichloran Agar
daa	Days After Anthesis
dai	Days After Inoculation
DAS	Diacetoxy-Scirpenol
DCPA	Dichloran-Chloramphenicol Peptone Agar
DMI	Demethylation Inhibitor
DNA	Deoxyribonucleic Acid
DON	Deoxynivalenol
DON-3-G	DON-3-Glucoside
DS	Disease Severity
ELISA	Enzyme-Linked Immunosorbent Assay
ENs	Enniatins
ENA	Enniatin A
ENB	Enniatin B
F_0	Basic Fluorescence
FA	Fusaric Acid
FAO	Food and Agriculture Organization of the United Nations
FDA	Factorial Discriminant Analysis
FDK	*Fusarium*-Damaged Kernels
FHB	*Fusarium* Head Blight
FLDA	Fisher Linear Discriminant Analysis
Fm	Maximum Fluorescence
FP	Fusaproliferin
FUMs	Fumonisins
Fv	Variable Fluorescence
GS	Growth Stage
HPLC	High-Performance Liquid Chromatography
HSI	Hyperspectral Imaging
HT-2-3-G	HT-2-3-Glucoside
IGS	Intergenic Spacer
IRT	Infrared Thermography
ITS	Internal Transcribed Spacers
LDA	Linear Discriminant Analysis
LED	Light-Emitting Diode

LSPDA	Low Strength Potato Dextrose Agar
MAS	Monoacetoxy-Scirpenol
MCz	Modified Czapek Dox Agar
MGA	Malachite Green Agar
MON	Moniliformin
MSI	Moisture Stress Index
mSR	modified Simple Ratio
MTD	Maximum Temperature Difference
VDNI	Normalized Difference Nitrogen Index
NDVI	Normalized Differences Vegetation Index
NEO	Neosolaniol
NIR	Near-Infrared Range
NIV	Nivalenol
NIV-3-G	NIV-3-Glucoside
NMDS	Non-metric Multi-Dimensional Scaling
NN	Neural Network
NS	Nash and Snyder Medium
PCA	Principal Component Analysis
PCR	Polymerase Chain Reaction
PDA	Potato Dextrose Agar
PDB	Potato Dextrose Broth
PDID	Potato Dextrose Iprodione Dichloran Agar
PLS	Partial Least Squares
PRI	Photochemical Reflection Index
PSII	Photosystem II
PSND	Pigment Specific Normalized Difference
PSRI	Plant Senescence Reflectance Index
PSSR	Pigment-Specific Simple Ratio
QDA	Quadratic Discriminant Analysis
qPCR	Quantitative Real-Time Polymerase Chain Reaction
QTLs	Quantitative Trait Loci
RBF	Radial Basis Function
RGB	Red Green Blue
RH	Relative Humidity
SAM	Spectral Angle Mapper
SIPI	Structure Insensitive Pigment Index
SVIs	Spectral Vegetation Indices
SVM	Support Vector Machine
SWIR	Short-Wave Infrared Range
T-2-3-G	T-2-3-Glucoside
VIS	Visible Range
WI	Water Index
Y [II]	Efficient Quantum Yield
ZEA	Zearalenone
ZEA-14-G	ZEA-14-glucoside

Summary

The integrated management of *Fusarium* head blight (FHB) on wheat depends on the implementation of agricultural practices, cultivation of resistant varieties, and fungicides application. Reducing yield losses and mycotoxin contamination caused by FHB on wheat requires fungicides application at a suitable time during the pathogenicity. This, in turn, needs accurate monitoring for disease incidence under field conditions to support the decision-making strategy to apply fungicides. In addition, the development of resistant variety demands screening of a large number of wheat entries for several years of the selection process. Furthermore, it needs mycotoxin quantification in wheat kernels of the advanced lines at the later stages of the breeding program. This research investigated the feasibility of optical sensors i.e. hyperspectral imaging (HSI), infrared thermography (IRT), and chlorophyll fluorescence imaging (CFI) to monitor FHB infection on wheat. In addition, it aimed at designing an automated model to rank wheat varieties according to their resistance to FHB based on HSI data. Moreover, it investigated the applicability of HSI to assess *Fusarium* infection and mycotoxin contamination in wheat kernels and flour. As well as the effect of infection timing on fungal development and mycotoxin contamination in wheat kernels.

The results of this research showed that optical sensors proved to be an effective tool to detect FHB infection on wheat spikelets and to follow the damage of *Fusarium* on wheat spikes. IRT was most sensitive to identify the early response of wheat to FHB infection followed by HSI and CFI. The combination of IRT-HSI led to superior accuracy during the pathogenicity.

The results proved also the possibility for automatic ranking of wheat varieties according to their resistance to FHB based on the spectral vegetation indices (SVIs) derived from HSI. In addition, HSI showed feasibility to screen wheat kernels and flour for *Fusarium* infection and mycotoxin contamination. Combining these tools will accelerate the phenotyping and support the decision-making process in breeding programs by providing objective information about wheat resistance to FHB and mycotoxin contamination in wheat kernels and flour.

This study demonstrated that *Fusarium graminearum* grows from the inoculation site downward. Moreover, it showed that *F. graminearum* can infect wheat spikes and cause deoxynivalenol (DON) contamination in wheat kernels not only at anthesis but also later stages of kernel development. In addition, it showed that infection timing plays a significant role in fungal growth and DON contamination. DON contamination was confined to the colonized kernels. Variety resistance and DON content have a close effect on DON detoxification in infected wheat kernels.

The results of the current work showed that optical sensors, mainly IRT and HSI are promising tools to monitor FHB infection on wheat. These tools can be used to prevent quality and quantity losses caused by FHB in wheat yield. Besides, the results showed the feasibility of HSI to phenotype wheat resistance to FHB on the spike scale as well as to phenotype FHB infection and mycotoxin contamination on the kernel scale. This would be an effective advantage to accelerate the phenotyping process in the breeding programs. The results emphasized that the masked mycotoxin deoxynivalenol-3-glucoside should be legislated and monitored during the food and feed processing due to the high levels of this mycotoxin even with the late infection with FHB.

Zusammenfassung

Das integrierte Management der Ährenfusariosen (FHB) an Weizen beinhaltet landwirtschaftlichen Praktiken, Kultivierung von resistenten Sorten und Fungizid- Behandlungen. Die Reduzierung von Ertragsverlusten und der Mycotoxin-Belastung durch FHB an Weizen erfordert eine Fungizid-Behandlung in einem engen Zeitfenster während der Pathogenese. Hierfür ist eine akkurate Überwachung des Krankheitsbefalls im Freiland entscheidend, um den Zeitpunkt der Fungizid Behandlung zu unterstützen. Für die Entwicklung von resistenten Sorten wurden im Selektionsprozess über mehrere Jahre eine hohe Anzahl an Tochterpflanzen untersucht. In der Endphase des Züchtungsprogrammes wird eine Mycotoxin-Quantifizierung der Weizenkörner vorgenommen. In dieser Arbeit wurde die Eignung von optischen Sensoren für Hyperspektrale Bildgebung (HSI), Infrarot Thermografie (IRT) und Chlorophyllfluoreszenz Bildgebung (CFI) zur Überwachung des FHB Befalls an Weizen untersucht. Zusätzlich zielten die Untersuchungen auf den Entwurf eines automatischen Models, basierend auf den HSI Daten, für die Einordnung von Weizen Sorten nach ihren FHB Resistenzen ab. Außerdem wurde an der Anwendbarkeit des HSI zur Beurteilung der *Fusarium*-Infektion und Mycotoxin-Belastung an Weizenkörnern und Weizenmehl geforscht. Anschließend wurde der Effekt des Infektionszeitpunktes an der Pilzentwicklung und der Mycotoxin-Belastung an Weizenkörnern untersucht.

Die Ergebnisse der Forschung zeigten, dass die optischen Sensoren effektive Werkzeuge für die Detektion des FHB Befalls an Weizen Ährchen sowie die Nachverfolgung an Weizen Ähren sind. IRT war sensitiver als HSI und CFI für die Identifizierung von frühen Reaktionen des Weizens durch die FHB-Infektionen. Die Kombination von IRT und HSI führte zu einem hohen Maß an Genauigkeit während der Pathogenität.

Die Ergebnisse zeigten, dass eine automatische Einordnung von Weizen Sorten nach ihrer Resistenz gegen FHB, basierend auf den spektralen Vegetationsindizes (SVIs), abgeleitet von den Bildern der HSI, möglich ist. Durch die HSI lässt sich das selektieren von mit *Fusarium*-infizierten und Mycotoxin belasteten Weizenkörnern und Weizenmehl realisieren. Die Kombination dieser Werkzeuge beschleunigt die Phänotypisierung und unterstützt die Entscheidungsfindung im Züchtungsprogramms.

Die vorliegende Arbeit konnte zeigen, dass *Fusarium graminearum* ausgehend von der Stelle der Inokulation nach unten wächst. Weiterhin wurde gezeigt, dass *F. graminearum* Weizenähren nicht nur während der Anthese infizietn und Deoxynivalenol (DON) Kontamination in Weizenkörnern verursachen kann, sondern auch, wenn die Inokulation zu einem späteren Zeitpunkt der Korn-Entwicklung stattfindet. Der Zeitpunkt der Infektion spielt eine signifikante Rolle für das Pilzwachstum und die DON Kontamination. Die DON Kontamination war auf kolonisierte Weizenkörner begrenzt. Sortenresistenz und DON Gehalt haben einen direkten Einfluss auf die DON Detoxifikation in infizierten Weizenkörnern.

Die Ergebnisse der vorliegenden Arbeiten zeigten, dass optische Sensoren, hauptsächlich IRT und HSI, vielversprechende Instrumente zur Überwachung der FHB-Infektion bei Weizen sind. Diese Instrumente können eingesetzt werden, um durch FHB verursachte Qualitäts- und Mengenverluste im Weizenertrag zu verhindern. Außerdem zeigten die Ergebnisse die Eignung von HSI zur Phänotypisierung der Weizenresistenz gegen FHB auf der Ährenskala sowie zur Phänotypisierung der FHB-Infektion und Mycotoxin-Belastung auf der Kornskala. Dies kann ein effektiver Vorteil sein, um den Phänotypisierung in den Züchtungsprogrammen zu beschleunigen. Die Ergebnisse verdeutlichten, dass das maskierte Mycotoxin deoxynivalenol-3-glucoside aufgrund der hohen Konzentrationen dieses Mycotoxins auch bei der späten Infektion mit FHB gesetzlich geregelt und während der Lebens- und Futtermittelverarbeitung überwacht werden sollte.

1. **Introduction**

Wheat is an essential food around the world, in addition to its use as feed and fiber for livestock and energy production. It is the first crop in the world with a harvested area of 220 million hectares/year and a production of 714 million tons/year (average of 10 years). During the last decade, the wheat yield reached 3252 kg/ha with an average increase of 436 kg/ha than the previous decade (FAO 2020). The genus wheat (*Triticum* L. 1753) is a member of the grass family *Poaceae* with two cultivated species: the tetraploid durum wheat *Triticum durum* 2n = 28 with the genome set AABB and the hexaploid bread wheat *Triticum aestivum* 2n = 42 with the genome set AABBDD (CABI 2020). Wheat yield is affected by biotic and abiotic stresses; this is mediated by the environmental conditions and the genetic prevalence. Among biotic stresses, pathogens (i.e. fungi, viruses, and bacteria) may contribute to average global losses of 21.5% of wheat yield (Savary et al. 2019).

Fusarium head blight (FHB) is one of the most relevant fungal diseases of wheat associated with different fungal species from the genus *Fusarium* (Parry et al. 1995; Summerell 2019). FHB causes significant losses in wheat yield because affected grains are small, shrunken, of low mass and quality, and contaminated with mycotoxins which are harmful to humans and in animal nutrition (McMullen et al. 2012). The main mycotoxins produced by *Fusarium* species are trichothecenes, zearalenones, fumonisins, and the emerging toxins i.e. beauvericin, enniatins, fusaproliferin, and moniliformin (Ferrigo et al. 2016).

Because of the high toxicity of *Fusarium* mycotoxins and its effect on wheat yield, it is important to integrate plant protection practices such as crop rotation, resistant varieties, and cultural practices up to the application of fungicide within the management strategy. To safeguard wheat yield and to produce products with high quality especially, the application of fungicides is necessary under certain environmental conditions. To apply suitable fungicides successfully, it is important to look for new methods to predict and early detect FHB epidemics on cereals (Mahlein et al. 2018). This will be essential in making the decision to apply fungicides at a suitable time of infection.

Besides direct control, a highly effective strategy to control FHB is breeding varieties with appropriate resistance against this disease complex. Effective cultivar development needs interdisciplinary research, integrating plant breeding, phytopathology, and informatics. It also needs precise and innovative methods for identifying and characterizing disease symptoms in an early stage of pathogenicity (Furbank and Tester 2011). Because conventional

characterization of host plant genotypes is laborious, time-consuming and cost-intensive this is a limiting factor in plant breeding programs. Here, proximal sensing with optical sensors is a promising characterizing method. Various sensors are suitable for detection, identification, and quantification of plant diseases like thermography, fluorescence, and spectral sensors (Mahlein 2016). Recently hyperspectral imaging showed efficiency as a precise and non-destructive tool in characterizing cereal resistance to fungal diseases, e.g. powdery mildew in barley (Kuska et al. 2017; Thomas et al. 2017); quantifying wheat resistance to FHB (Alisaac et al. 2018), and combined with thermography and chlorophyll fluorescence for early detection and monitoring of FHB development on wheat (Mahlein et al. 2019).

The host-pathogen interaction of *Fusarium* spp. and wheat plants is highly influenced by the pathogen virulence as well by the host plant resistance. This leads to detectable differences in the optical properties of the host plant according to its resistance. It is expected that specific regions of the electromagnetic spectrum are influenced depending on the host resistance or at least correlated with host plant resistance, in addition to changes in the host plant temperature and chlorophyll apparatus activity. The detection of these subtle differences demands specific sensors combined with precise data analysis methods. To prove this hypothesis; hyperspectral cameras in the visible-near infrared range (VIS-NIR) 400-1000 nm and the short-wave infrared range (SWIR) 1000-2500 nm and thermal camera in the spectral range 7500-14000 nm were used in this study. Mainly, in monitoring and quantifying *Fusarium* infection on different wheat varieties with different degrees of disease resistance and to assess *Fusarium* infection and mycotoxin contamination in wheat kernels and flour.

2. Objectives

1. To reveal the best performance in disease monitoring using individual or combination of different sensors datasets (i.e. thermal, fluorescence, and hyperspectral imaging) supported by machine learning approach.
2. To design a method based on spectral reflectance data for ranking wheat varieties according to their resistance to FHB by reproducing the area under disease progress curve (AUDPC) depending on the data derived from VIS, NIR, and SWIR ranges.
3. To assess *Fusarium* infection and mycotoxin contamination in wheat kernels and flour using hyperspectral imaging.
4. To investigate the effect of the infection timing on disease development and mycotoxin accumulation in wheat spike.

3. Literature Review

3.1. *Fusarium* Head Blight

Fusarium head blight is also known as *Fusarium* ear blight or scab was first described in England by Smith (1884) as a new disease of wheat, barley, and ryegrass, attributing the infection to the casual agents *Fusisporium culmorum, hordei* and *Lolii* W.Sm. It was recorded as an important disease in the USA at the end of the 19th century. By the beginning of the 20th century, FHB was known in wheat production regions worldwide (Parry et al. 1995). In the 1990s, McMullen et al. (1997) characterized it as a re-emerging disease due to the frequent epidemics on wheat in the USA and Canada from 1991-1996. They assigned this to the fundamental changes in agricultural practices mainly reduced tillage. FHB is also known as a disease complex since more than one species from the genus *Fusarium* are involved in this disease in addition to two species from the genus *Microdochium* (Xu et al. 2008). The main difference between the both is that *Fusarium* species produce a wide spectrum of mycotoxins while *Microdochium* species do not produce mycotoxins (Xu et al. 2008).

3.1.1. Pathogen Taxonomy

Since 2013, and after the changes in the International Code of Nomenclature for fungi, the name *Fusarium* was recognized as a unique name for all species including teleomorphs, which means that the name *Gibberella* and other names are not accepted anymore to indicate to the sexual stage of these pathogens (Geiser et al. 2013). The following scheme shows the taxonomical position of the genus *Fusarium* and *Microdochium* according to MycoBank 2019 (Figure 1).

3.1.2. *Fusarium* Species Involved in FHB

Fusarium graminearum is the main pathogen of FHB worldwide (Haile et al. 2019; McMullen et al. 2012; Summerell 2019; Torres et al. 2019). However, different studies showed that other *Fusarium* species may contribute significantly to this disease in different areas of the world with different climate conditions. For example, *F. graminearum*, *F. culmorum*, *F. avenaceum*, *F. poae*, *F. tricinctum*, and *M. majus* were the dominant species in Europe (Nielsen et al. 2014; Oerke et al. 2010; Spanic et al. 2010). In Canada, *F. avenaceum*, *F. equiseti*, *F. graminearum*, *F. poae*, and *F. sporotrichioides* were the most frequent species during the last two decades (Xue et al. 2019). Alkadri et al. (2013) recovered different *Fusarium* species from wheat in Syria. Table 1 shows the *Fusarium* species involved in FHB.

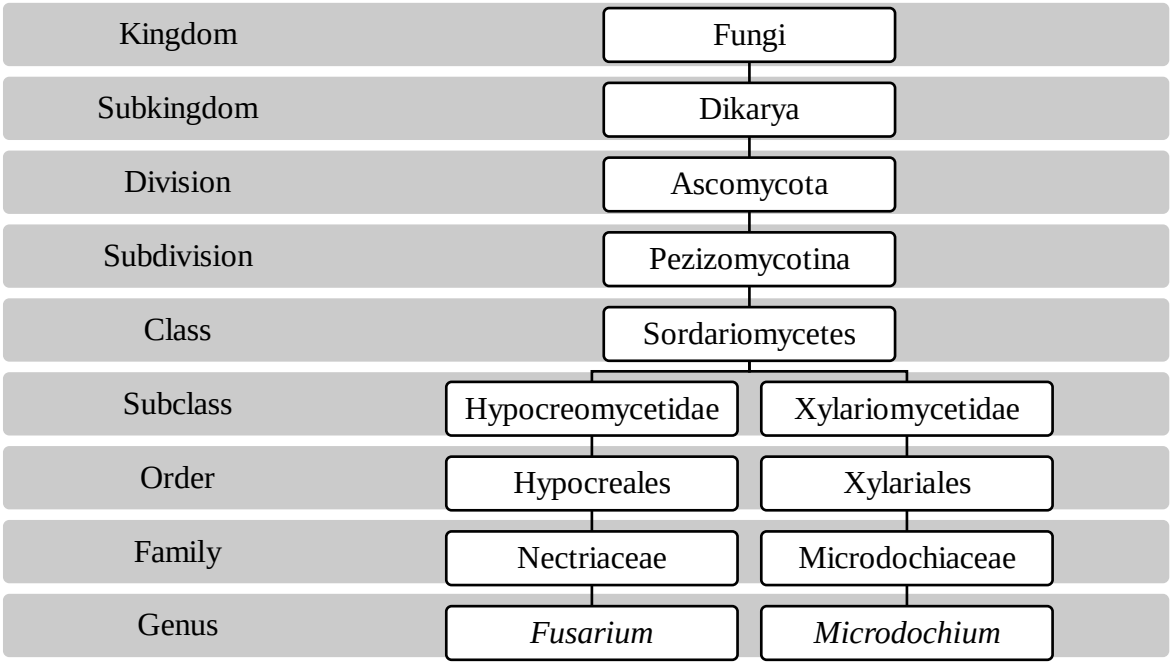

Figure 1. Taxonomical position of the genus *Fusarium* and *Microdochium* according to Mycobank database, 2019.

3.1.3. Life Cycle and Pathogenesis

Fusarium head blight is a monocyclic disease. The pathogen survives in the debris of the former crop as macroconidia or within sexual structures called perithecia as ascospores; or as asexual spores called macroconidia or microconidia for the species that have only anamorph stage. These spores are considered the primary inoculum of the disease. In addition, gramineous and non-gramineous weeds are not only a host range of *Fusarium* but also, they can serve as an alternative host and source of inoculum. At wheat anthesis which is the susceptible stage for infection, and in favorite weather conditions; the inoculum is blown by the wind or splashed by rain and lands on open spikelets (Figure 2). On the spikelet tissue, the spores germinate and produce germination tubes (Dong et al. 2020; McMullen et al. 2012; Mourelos et al. 2014; Suproniene et al. 2019; Torres et al. 2019; Trail 2009). After germination, the fungal hyphae spread on the surface of the ovary, palea, and lemma and start to produce mycotoxins without penetrating the spikelet tissue. Thereafter, the pathogen penetrates the host tissue starting a biotrophic infection with an intercellular growth in the spikelet and turns to the necrotrophic stage with inter- and intracellular growth laterally and vertically within the spike. During this stage of pathogenicity, mycotoxins accumulate in the spike tissue as well as in the kernels reducing the crop yield and quality (Brown et al. 2010; Divon et al. 2019; Kang and Buchenauer 1999).

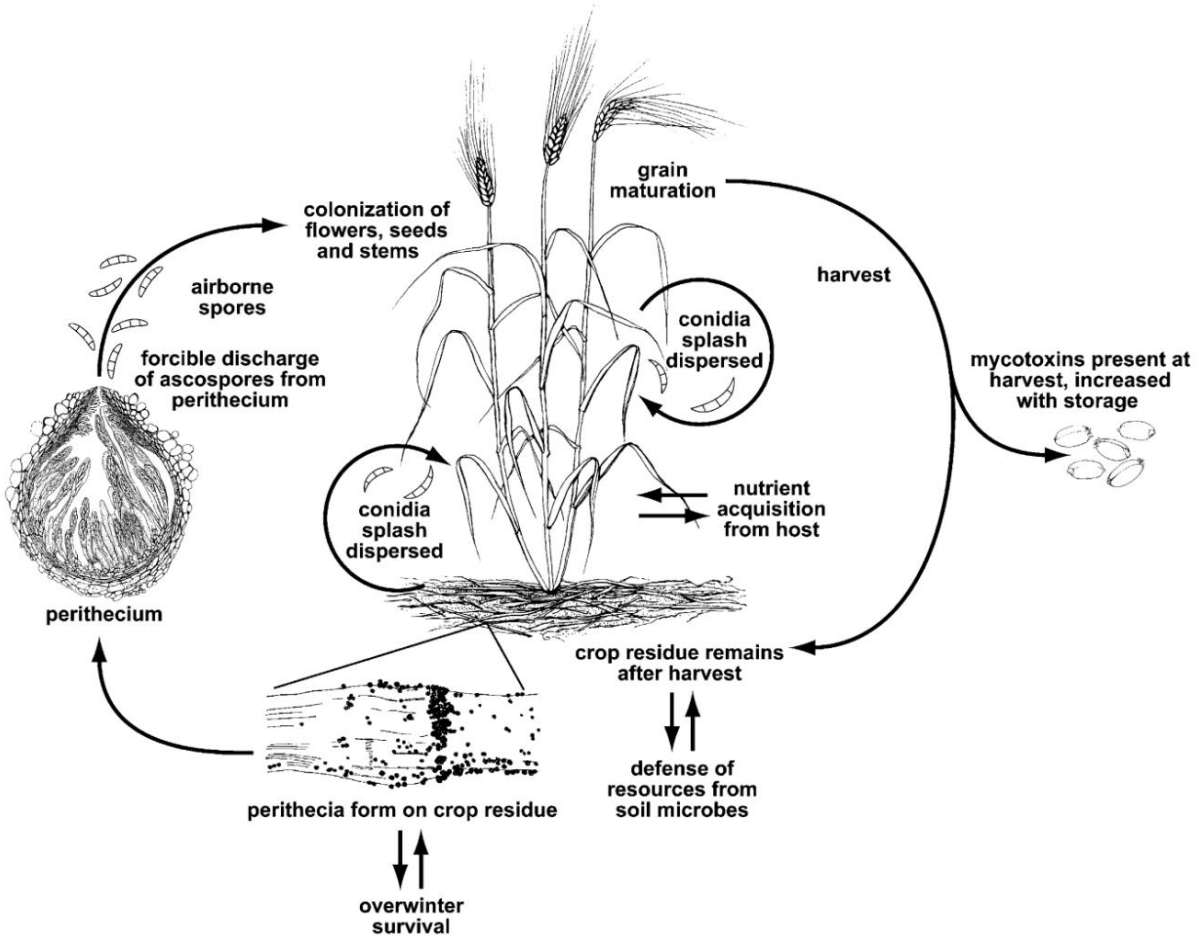

Figure 2. Disease cycle and survival of *Fusarium* head blight causal agents on wheat (Trail 2009).

3.1.4. Symptoms

The first symptoms appear as water-soaked spots on the infected spikelets; these symptoms develop to necrosis and in an advanced stage, the infected spikelets become bleached. The bleaching spreads to cover the entire spike resulting in premature whiten wheat heads. Under warm and humid weather conditions pinkish-red mycelium appears on the infected tissue. The kernels resulted from the infected spikes are known as tombstones because they are light in weight, shriveled, discolored with a pinkish or chalky appearance, and poor quality (Dweba et al. 2017; McMullen et al. 1997; 2012, Scherm et al. 2013; Trail 2009). However, some less virulent pathogens like *F. poae* may cause infection and result in high levels of mycotoxin contamination in the infected kernels without detectable symptoms on the spikelets or the (Stenglein 2009; Stenglein et al. 2014).

Table 1. *Fusarium* and *Microdochium* species involved in *Fusarium* head blight on wheat with their teleomorph and mycotoxin profile.

Pathogen	Teleomorph	Mycotoxin profile																		Reference
		Trichothecenes														Emerging Toxins				
		Trichothecenes A							Trichothecenes B											
		T-2 toxin	HT-2 toxin	DAS	MAS	NEO	NX-2	NX-3	DON	3-ADON	15-ADON	NIV	4-ANIV	Zearalenone	Fusaric Acid	Fumonisins	Enniatins	Beauvericin	Fusaproliferin	Moniliformin	
F. acuminatum Ellis & Everh.	+	+				+			+				+				+			+	(Beccari et al. 2019; Bottalico and Perrone 2002; Marín et al. 2012)
F. avenaceum (Fr.) Sacc.	+																+	+		+	(Beccari et al. 2018a; Beccari et al. 2019; Bottalico and Perrone 2002; Glenn 2007)
F. crookwellense L.W. Burgess, P.E. Nelson & Toussoun synonym *F. cerealis* (Cooke) Sacc.	-											+	+	+							(Bottalico and Perrone 2002; Chandler et al. 2003; Glenn 2007; Vesonder et al. 1991)
F. culmorum (W.G. Sm.) Sacc.	-								+	+	+	+	+	+							(Alisaac et al. 2019; Alkadri et al. 2013; Basler 2016; Kang and Buchenauer 1999; Pasquali et al. 2016; Siou et al. 2015a)
F. equiseti (Corda) Sacc.	+			+		+			+			+	+	+			+				(Alkadri et al. 2013; Covarelli et al. 2015a; Marín et al. 2012)
F. graminearum Schwabe	+						+	+	+	+	+	+	+	+							(Alisaac et al. 2019; Alkadri et al. 2013; Beccari et al. 2019; Crippin et al. 2019; Lofgren et al. 2018; Siou et al. 2015a; Varga et al. 2015)
F. lateritium Nees	+																+				(Jestoi 2008; Stanciu et al. 2017a)
F. oxysporum Schltdl.	-														+					+	(Ferrigo et al. 2016; Shi et al. 2017)
F. poae (Peck) Wollenw.	-	+	+	+	+							+	+				+	+			(Beccari et al. 2018a; Beccari et al. 2019; Covarelli et al. 2015a; Covarelli et al. 2015b; Ferrigo et al. 2016)

Pathogen	Teleomorph	Mycotoxin profile																		Reference
		Trichothecenes														Emerging Toxins				
		Trichothecenes A							Trichothecenes B											
		T-2 toxin	HT-2 toxin	DAS	MAS	NEO	NX-2	NX-3	DON	3-ADON	15-ADON	NIV	4-ANIV	Zearalenone	Fusaric Acid	Fumonisins	Enniatins	Beauvericin	Fusaproliferin	Moniliformin	
F. proliferatum (Matsush.) Nirenberg	+														+	+	+	+	+	+	(Beccari et al. 2018a; Guo et al. 2014, 2018)
F. sambucinum Fuckel	+	+	+	+	+	+						+					+	+		+	(Beccari et al. 2018a; Fraeyman et al. 2017; Jestoi 2008)
F. semitectum Berk. & Ravenel	-											+		+							(Barros et al. 2012; Ezekiel et al. 2008)
F. sporotrichioides Sherb.	-	+	+	+	+	+						+		+			+	+			(Beccari et al. 2018a; Covarelli et al. 2015a; Nazari et al. 2014)
F. subglutinans (Wollenw. & Reinking) P.E. Nelson, Toussoun & Marasas	+																+	+	+	+	(Ferrigo et al. 2016; Igor et al. 2019; Jestoi 2008)
F. tricinctum (Corda) Sacc.	+																+			+	(Beccari et al. 2018a)
F. verticillioides (Sacc.) Nirenberg synonym *F. moniliforme* J. Sheld.	+															+				+	(Ferrigo et al. 2016; Mylona et al. 2019)
Microdochium nivale var. nivale (Fr.) Samuels & I.C. Hallett	+																				(Xu et al. 2008)
Microdochium nivale var. majus (Wollenw.) Samuels & I.C. Hallett	+																				(Xu et al. 2008)

diacetoxy-scirpenol (DAS); monoacetoxy-scirpenol (MAS); neosolaniol (NEO); deoxynivalenol (DON); 3-acetyl-deoxynivalenol (3-ADON); 15-acetyl-deoxynivalenol (15-ADON); nivalenol (NIV); 4-acetyl-nivalenol (4-ANIV); zearalenone (ZEA); fusaric acid (FA); fumonisins (FUMs); enniatins (ENs); beauvericin (BEA); fusaproliferin (FP); moniliformin (MON)

3.1.5. Mycotoxins

Mycotoxins are secondary metabolites produced by mold fungi like *Alternaria*, *Aspergillus*, *Claviceps*, *Fusarium*, and *Penicillium*. *Fusarium* species involved in FHB produce a wide range of mycotoxins, mainly, trichothecenes, zearalenone, fusaric acid, fumonisins, and emerging toxins i.e. enniatins, beauvericin, moniliformin, and fusaproliferin.

3.1.5.1. Trichothecenes

Trichothecenes are the most dominant group of *Fusarium* mycotoxins accompanying FHB infection on wheat worldwide (Foroud et al. 2019). This group is split based on its chemical structure into four subgroups A, B, C, and D (Chen et al. 2019). However, trichothecenes produced by *Fusarium* spp. are A and B. The main difference between these two groups is the presence of ketone (=O) at C_8 of trichothecenes backbone in trichothecenes B while it is absent in trichothecenes A (Foroud et al. 2019). In general, trichothecenes A are more toxic *in Animalia* compared with trichothecenes B, however, *in Planta*, trichothecenes B are more toxic (McCormick et al. 2011). Trichothecenes A include T-2 toxin, HT-2 toxin, diacetoxy-scirpenol (DAS), monoacetoxy-scirpenol (MAS), neosolaniol (NEO), NX-2 and NX-3. This group is mainly produced by *F. acuminatum*, *F. equiseti*, *F. graminearum*, *F. poae*, *F. sambucinum*, and *F. sporotrichioides*. Trichothecenes B include nivalenol (NIV), 4-acetyl-nivalenol (4-ANIV), deoxynivalenol (DON), 3-acetyl-deoxynivalenol (3-ADON) and 15-acetyl-deoxynivalenol (15-ADON). *Fusarium* species that produce trichothecenes B are *F. acuminatum*, *F. crookwellense*, *F. culmorum*, *F. equiseti*, *F. graminearum*, *F. poae*, *F. sambucinum*, *F. semitectum*, and *F. sporotrichioides* (Table 1). Trichothecenes B are known as a virulence factor of *Fusarium* spp. against wheat (Goswami and Kistler 2005; Spanic et al. 2019). However, DON is more poisonous *in Planta* while NIV is more poisonous *in Animalia* (Ferrigo et al. 2016). The toxic effect of trichothecenes is inhibition of protein synthesis in eukaryote by binding with 60S ribosomes (Chen et al. 2019; Foroud et al. 2019; McCormick et al. 2011).

3.1.5.2. Zearalenone

Zearalenone is also one of the dominant *Fusarium* mycotoxins on wheat worldwide, it is normally found in the same climate regions of trichothecenes (Kuzdraliński et al. 2013; Stanciu et al. 2019; Tralamazza et al. 2016; Vogelgsang et al. 2019). Zearalenone derivatives, mainly, zearalanone, α- and β-zearalenol, and α- and β-zearalanol could be naturally produced by *Fusarium* spp. (Ferrigo et al. 2016). The main difference is the presence of ketone (=O) at C_{12}

in zearalenone and zearalanone while it is hydroxyl (-OH) in α- and β- derivatives (Li et al. 2019). Zearalenone is of low acute toxicity either *in Planta* or *in Animalia* compared with trichothecenes (Ferrigo et al. 2016; McLean 1995). *Fusaria* involved in zearalenone production are *F. crookwellense*, *F. culmorum*, *F. equiseti*, *F. graminearum*, *F. semitectum*, and *F. sporotrichioides* (Table 1). *In Animalia*, zearalenone has an estrogenic effect by binding to estrogen receptors which affect the sexual activities of animals (Bertero et al. 2018).

3.1.5.3. Fusaric Acid

Fusaric acid is one of the first identified *Fusarium* mycotoxins; it is produced by a wide range of *Fusarium* species, and interestingly, by both trichothecenes and fumonisins producers (Shi et al. 2017). It is considered as a virulence factor for different *Fusaria*. Fusaric acid has virulent toxicity *in Planta*; however, its toxicity *in Animalia* is low to moderate. The toxic effects of fusaric acid include modifying the potential of the cell membrane and inhibiting ATP synthesis (López-Díaz et al. 2018).

3.1.5.4. Fumonisins

Fumonisins were first identified in South Africa in 1988. They can be found mainly in maize products in the warm condition regions. However, they can also be detected in other cereals especially wheat, barley and sorghum, and other plants like soybean, asparagus, tea, and medical plants (Alshannaq and Yu 2017; Dall'Asta and Battilani 2016). Fumonisins are polyketide hydrophilic mycotoxins and they contain a large number of derivatives. Therefore, they are classified in four main groups A, B, C, and P. Fumonisins B is the most widespread group and it contains the FB1 which is of high concern regarding human and animal toxicity (Alshannaq and Yu 2017; Braun and Wink 2018; Ferrigo et al. 2016). Exposure to fumonisins causes esophageal cancer and embryonal neural tube defects in humans, leuko-encephalomalacia in equine and pulmonary edema in pigs (Alshannaq and Yu 2017; Braun and Wink 2018; Scott 2012). A large number of *Fusarium* species are involved in fumonisins production, however, *F. verticillioides* and *F. proliferatum* are the main producers of these toxins (Braun and Wink 2018).

3.1.5.5. Emerging Toxins

The emerging toxins of *Fusarium* are enniatins, beauvericin, fusaproliferin, and moniliformin (Jestoi 2008). The presence of emerging toxins is accompanied by traditional *Fusarium* toxins in cereals particularly maize, wheat, barley, and oat worldwide (Fraeyman et al. 2017; Igor et al. 2019; Kovalsky et al. 2016; Stanciu et al. 2017a,b).

3.1.5.5.1. Enniatins and Beauvericin

Enniatins and beauvericin are cyclohexadepsipeptides with lipophilic nature (Jestoi 2008). The main chemical derivatives of enniatins that can be detected in cereals are ENA, ENA1, ENB, and ENB1 (Prosperini et al. 2017). Besides their antibacterial, antifungal, insecticidal activities (Prosperini et al. 2017), they showed cytotoxic effect for different cell cultures *in vitro*, however, toxicity *in vivo* is limited to poultry especially in liver (Fraeyman et al. 2017; Ivanova et al. 2014). In addition, they exhibited cytotoxicity against cancer cell lines suggesting them as pharmacological candidates to fight cancer (Tedjiotsop Feudjio et al. 2010). Enniatins and beauvericin are produced by a wide spectrum of *Fusarium* species (Fraeyman et al. 2017), however, on wheat, they were recorded for *F. acuminatum*, *F. avenaceum*, *F. equiseti*, *F. lateritium*, *F. poae*, *F. proliferatum*, *F. sambucinum*, *F. sporotrichioides*, *F. subglutinans*, and *F. tricinctum* (Table 1).

3.1.5.5.2. Fusaproliferin

Fusaproliferin is a bicyclic sesterterpene which was later discovered in 1993 from *F. proliferatum* isolate. It can be produced simultaneously with deacetylated form in a 3:1 ratio (Jestoi 2008). Fusaproliferin shows toxicity on insect and mammalian cells in addition to poultry embryos (Ferrigo et al. 2016). On wheat, fusaproliferin production was reported for *F. proliferatum* and *F. subglutinans* (Table 1).

3.1.5.5.3. Moniliformin

Moniliformin is a small molecule with high polarity, it can be found in nature as a sodium or potassium salt. Moniliformin was first identified as a mycotoxin of *F. moniliforme* which was renamed as *F. verticillioides* (Jestoi 2008). The toxic effect of moniliformin is by disrupting thiamine enzymes which affect cellular energy supply. This leads to an acute heart failure, pulmonary and immunity disruption of animals (Fraeyman et al. 2017). On wheat, moniliformin accompanied FHB infect with *F. acuminatum*, *F. avenaceum*, *F. oxysporum*, *F. proliferatum*, *F. sambucinum*, *F. subglutinans*, *F. tricinctum*, and *F. verticillioides* (Table 1).

3.1.5.6. Masked Mycotoxins

The term “masked mycotoxin” indicates to the biologically modified mycotoxin by conjugation reaction by plants as a detoxification mechanism. This was suggested to differentiate them from other types of biological modification of mycotoxins e.g. by animals, fungi, and microbiota of animals and humans. In addition, to discriminate them from chemically modified mycotoxins (i.e. thermally and non-thermally) and matrix-associated

mycotoxins (Rychlik et al. 2014). The main concern regarding masked mycotoxins is that they are not detectable by traditional analysis, and they are hydrolyzed through digestion into their parental mycotoxins or even more or less toxic compounds (Rychlik et al. 2014). Different masked mycotoxins were reported in cereal grains. DON-3-glucoside (DON-3-G), NIV-3-glucoside (NIV-3-G), 4-ANIV-glucoside (4-ANIV-G), T-2-3-glucoside (T-2-3-G), HT-2-3-glucoside (HT-2-3-G), and ZEA-14-glucoside (ZEA-14-G) were reported to occur in wheat (Berthiller et al. 2013).

3.1.6. *Fusarium* Head Blight Epidemics on Wheat

The frequency of FHB epidemics increased in the last decades due to the changes in agricultural practices mainly zero tillage regime in wheat fields (Dill-Macky and Jones 2000; Miller et al. 1998). The incidence of FHB epidemics is highly correlated with weather conditions especially rainy days with warm temperatures at anthesis and abundance of primary inoculum (Dill-Macky and Jones 2000; Miller et al. 1998; Obanor et al. 2013; Shah et al. 2019; Torres et al. 2019). Several studies showed that FHB epidemics on wheat take place sporadically. In Europe, yield losses caused by FHB epidemics ranged between 40-50% in Romania and Hungary during the 1970s-1980s (Parry et al. 1995). Seven severe epidemics and 14 medium epidemics occurred during the second half of the last century in China. In 2012, more than 9.9 million hectares were affected in the main producing areas in China (Zhu et al. 2019). In Canada which is a major wheat producer, FHB epidemics were recorded during the 1940s and 1980s (Aboukhaddour et al. 2020). In the last two decades, epidemics were reported in 11 out of 17 surveyed years with disease severity of 1.5-57.8% (Xue et al. 2019). In the 20th century, five severe epidemics were described in the USA from the 1910s until the 1930s. However, FHB re-emerged from 1991-1996 and causing yield dropping up to 25% and economic losses of $1 billion (McMullen et al. 1997). It continued to occur frequently from 1997-2010 in several states in the USA resulting in annual losses up to 54.2% in 2003 in different states (McMullen et al. 2012). In Latin America, seventeen epidemics have been reported in Argentina from 1960-2012 with losses up to 70% in some years (Palazzini et al. 2015). Furthermore, a model-based assessment study analyzed the weather data from 1957-2006 in Brazil. It showed an increased FHB risk index during the 1960s and higher frequency of high risk years starting from 1990 (Del Ponte et al. 2009). Information about FHB epidemics in Australia are rare due to their sporadic nature. However, a severe epidemic was reported in 2010 with a disease of 79% in some fields (Obanor et al. 2013).

3.1.7. *Fusarium* Head Blight Diagnosis on Wheat

There are different methods to diagnose the fungal pathogens involved in FHB on wheat. The classical method is the pathogen re-isolation on selective media and identifying the fungus based on the morphological characteristics of the spores or the colony. The immunological method uses specific antibodies against specific protein or protein complex produced by the fungus. However, the most specific method is the molecular method using specific primers that target a specific region in the DNA of the fungus.

3.1.7.1. Selective Media

Fusarium species can be diagnosed based on the visual and microscopical characteristics of the colony and the spores after re-isolating the fungus on selective medium. Different media showed selectivity to *Fusarium* spp. e.g. Czapek Dox iprodione dichloran agar (CZID), dichloran-chloramphenicol peptone agar (DCPA), malachite green agar (MGA 2.5), modified Czapek Dox agar (MCz), Nash and Snyder medium (NS), and potato dextrose iprodione dichloran agar (PDID). However, MGA 2.5 was recommended as a selective medium for *Fusarium* re-isolation from naturally infected kernels (Bragulat et al. 2004). Furthermore, differentiation between *Fusarium* species was possible based on their pigmentation on CZID (Thrane 1996). Recently, different media containing the bacterial toxin "toxoflavin" produced by the *Burkholderia glumae* showed selectivity to *Fusarium* species (Jung et al. 2013). However, this method is laborious and time-consuming and it needs experts in fungal taxonomy to diagnose the disease on species scale.

3.1.7.2. Immunological Method

Enzyme-linked immunosorbent assay (ELISA) is used as a diagnostic method for *Fusarium* using poly- or monoclonal antibodies. These antibodies are obtained after immunization of animals or cell lines by exoantigens secreted by *Fusarium* (Gan et al. 1997; Hill et al. 2006). However, the main drawback of this method is that it is genus-specific (Brunner et al. 2012).

3.1.7.3. Molecular Method

Polymerase chain reaction (PCR) was invented in 1984 and became widely used in plant pathogen detection and quantification with high sensitivity and specificity (Henson and French 1993; Schaad and Frederick 2002). The PCR costs reduced with the introduction of DNA polymerase (Taq) of the high-temperature tolerant bacteria *Thermus aquaticus* in 1988. This allowed automated thermal cycling and abolished the need for enzyme refreshment after each cycle (Henson and French 1993). The PCR allows the detection of plant diseases before the

symptoms become visible. Moreover, it differentiates between fungal species scale even when they have morphological similarities. Different genomic regions are used to design species-specific primers e.g. internal transcribed spacers (ITS), intergenic spacer (IGS) regions, and protein-coding genes (Kuzdraliński et al. 2017). Different primers were developed to detect *Fusarium* species involved in FHB (Table 2). However, primers targeting *F. lateritium* and *F. semitectum* showed cross-hybridization with other *Fusarium* species (Hong et al. 2010).

Table 2. Forward and reverse primers sequences used to amplify specific fragments of fungal DNA of *Fusarium* species.

Pathogen	Primer name	Primer sequence (5´-3´)	Amplified fragment	Reference
F. acuminatum	FAC-F FAC-R	GGGATATCGGGCCTCA GGGATATCGGCAAGATCG	602 bp	(Williams et al. 2002)
F. avenaceum	Fave574 fwd Fave627 rev	TATGTTGTCACTGTCTCACACCACC AGAGGGATGTTAGCATGATGAAG	EF1α gene	(Nicolaisen et al. 2009)
F. crookwellense synonym *F. cerealis*	CRO-A F CRO-A R	CTCAGTGTCCACCGCGTTGCGTAG CTCAGTGTCCCAATCAAATAGTCC	842 bp	(Yoder and Christianson 1998)
F. culmorum	OPT18 F OPT18 R	GATGCCAGACCAAGACGAAG GATGCCAGACGCACTAAGAT	472 bp	(Schilling et al. 1996)
F. equiseti	Feq-F Feq-R	GGCCTGCCGATGCGTC CGATACTGAAACCGACCTC	990 bp	(Jurado et al. 2005)
F. graminearum	Fg16N F Fg16N R	ACAGATGACAAGATTCAGGCACA TTCTTTGACATCTGTTCAACCCA	280 bp	(Nicholson et al. 1998)
F. lateritium				
F. oxysporum	FOF1 FOR1	ACATACCACTTGTTGCCTCG CGCCAATCAATTTGAGGAACG	340 bp	(Mishra et al. 2003)
F. poae	Fp82 F Fp82 R	CAAGCAAACAGGCTCTTCACC TGTTCCACCTCAGTGACAGGTT	220 bp	(Parry and Nicholson 1996)
F. proliferatum	Fp3-F Fp4-R	CGGCCACCAGAGGATGTG CAACACGAATCGCTTCCTGAC	230 bp	(Jurado et al. 2006)
F. sambucinum	FSF1 FSR1	ACATACCTTTATGTTGCCTCG GGAGTGTCAGACGACAGCT	315 bp	(Mishra et al. 2003)
F. semitectum				
F. sporotrichioides	Fspor F1 Lanspo R1	CGCACAACGCAAACTCATC TACAAGAAGACGTGGCGATAT	332 bp	(Wilson et al. 2004)

Pathogen	Primer name	Primer sequence (5´-3´)	Amplified fragment	Reference
F. subglutinans	61-2F 61-2R	GGCCACTCAAGAGGCGAAAG GTCAGACCAGAGCAATGGGC	445 bp	(Möller et al. 1999)
F. tricinctum	Ftri573 fwd Ftri630 rev	TTGGTATGTTGTCACTGTCTCACACTAT TGACAGAGATGTTAGCATGATGCA	EF1α gene	(Nicolaisen et al. 2009)
F. verticillioides synonym *F. moniliforme*	VERT1 VERT2	GTCAGAATCCATGCCAGAACG CACCCGCAGCAATCCATCAG	800 bp	(Patiño et al. 2004)
Microdochium nivale var. nivale	Y13N F Y13N R	ACCAGCCGATTTGTGGTTATG GGTCACGAGGCAGAGTTCG	300 bp	(Nicholson et al. 1996)
Microdochium nivale var. majus	Y13M F Y13M R	CTTGAGGCGGAAGATCGC ATCCCTTTTCCGGGGTTG	220 bp	(Nicholson et al. 1996)

3.1.8. Integrated Management of *Fusarium* Head Blight

The effective management of FHB is challenging due to several factors. Firstly, maize intensification and reduced tillage increased the frequency of FHB epidemics during the last decades. This is because maize is the main host of *Fusarium* species which serves as a source of the inoculum and the reduced tillage helps to keep this source available during wheat vegetation. Secondly, the visible FHB symptoms appear on wheat spikes at a later stage of pathogenicity, and during this stage, it is too late for fungicides application because the kernels have been contaminated with *Fusarium* mycotoxins. In addition, traditional disease control using fungicides encloses different disadvantages mainly costs, bio- and eco-hazards, relatively short lifetime due to fungicide resistance, and low availability for smallholder farmers. Moreover, the environment and health protection measures lead to continuous regulatory changes regarding fungicides availability and applicability (Nelson 2020). This shows the need for an integrated management strategy incorporates cultural practices, resistant varieties, and bio- and chemical measures to control the disease.

3.1.8.1. Cultural Practices

Adopting moderately resistant varieties combined with variety rotation and using varieties with different maturities in addition to spreading anthesis times by disseminating planting dates showed efficiency in FHB control (Cowger et al. 2020; Salgado et al. 2014). In addition, the reduction of inoculum pressure during wheat anthesis can play a significant role in disease management. This can be achieved by plowing the soil and burying the residues of the previous crop especially if this crop is one of the main hosts of *Fusarium* species like maize and barley. This practice prohibits perithecia formation and ascospores discharge during wheat spike development (Blandino et al. 2012; Torres et al. 2019). Another practice to reduce inoculum pressure is avoiding FHB cultural hosts e.g. maize as a previous crop in wheat fields (McKee et al. 2019).

3.1.8.2. Host Plant Resistance to *Fusarium* Head Blight

Components of wheat resistance to FHB include passive resistance represented by morphological and phenological features and active resistance represented by physiological features (Mesterházy 1995). Morphological and phenological features that are involved in passive resistance are plant height, wheat awns, narrow and short floral opening, and the time of retained anthers. Plant height: tallness helps wheat spikes to stand away from splashed rain droplets that carry the inoculum from the soil surface and crop residues. Wheat awns: awns

trap the inoculum and increase natural infection while their absence reduces it (Mesterházy 1995). Narrow and short floral opening reduces the floret exposure to the inoculum and increases resistance while retained anthers and pollen might trap the inoculum and catalyze spore germination and fungal penetration (Steiner et al. 2017). Active resistance can be classified into the following types: resistance to initial penetration or infection (Type I resistance), resistance to fungal spread within the spike from the infected spikelet (Type II resistance) (Schroeder and Christensen 1963), resistance to kernel infection and tolerance against FHB (Type III and IV respectively) (Mesterházy et al. 1999), and resistance to trichothecenes (Type V) (Foroud et al. 2019).

Wheat resistance to FHB is a quantitative trait which means that many genes with cumulative effects are involved in this trait. Environmental conditions have a significant effect on this trait resulting in various resistance levels in different environments (Steiner et al. 2017). Durum wheat is known to be highly susceptible to FHB due to the scarcity of resistance sources in the tetraploid gene pool (Haile et al. 2019). Up to date, seven quantitative trait loci (QTLs) were officially given gene names most of them from Chinese hexaploid wheat (Table 3) (Bai et al. 2018). However, the direct introgression of these sources in breeding programs is still difficult due to undesirable agronomic traits (Bai et al. 2018). Steiner et al. (2017) suggested integrating genomic selection based on genome-wide prediction models with marker-assisted selection for QTL and classical phenotypic selection based on visible symptoms in breeding programs for FHB resistance.

Table 3. QTLs involved in wheat resistance to *Fusarium* head blight.

QTL	Location	Source	Resistance type	Reference
Fhb1	3BS	Sumai 3 and Nyubai	Type II	(Cuthbert et al. 2006)
Fhb2	6BS	Sumai 3	Type II	(Cuthbert et al. 2007)
Fhb3	7AS	*Leymus racemosus*	Type II	(Qi et al. 2008)
Fhb4	4BL	Wangshuibai	Type I	(Xue et al. 2010)
Fhb5	5AS	Wangshuibai and Sumai 3	Type I	(Xue et al. 2011)
Fhb6	1AS	*Elymus tsukushiensis*	Type II	(Cainong et al. 2015)
Fhb7	7D	*Thinopyrum ponticum*	Type II	(Guo et al. 2015)

3.1.8.3. Biological Control

Biological control uses antagonistic microorganisms to *Fusarium* species or biological secondary metabolites to control FHB on wheat. These microorganisms can be applied to the residues of the former crop to inhibit perithecia development or directly wheat spikes. For

example, bacteria from *Bacillus spp.*, *Lysobacter enzymogenes*, *Pseudomonas spp.* and *Streptomyces spp.*, and fungi from *Aureobasidium pullulans*, *Clonostachys rosea*, and *Trichoderma spp.* showed effectivity against *Fusarium* (Wegulo et al. 2015). The fungus *Clonostachys rosea* was applied on wheat residues infected with different *Fusarium* species under field conditions. *Fusarium* growth measured as fungal DNA reduced between 68-98% after 90 days of treatment and was undetectable after 180 days (Palazzini et al. 2013). Comby et al. (2017) reported three new fungal species namely *Aureobasidium proteae*, *Phoma glomerate*, and *Sarocladium kiliense* with high protection ratio between 75-100% on detached wheat spikelets. The basidiomycetous yeast *Cryptococcus nodaensis* OH 182.9 was isolated from wheat anthers (Khan et al. 2001). This isolate presented reduced disease severity between 45-60% under controlled and field conditions (Khan et al. 2004; Schisler et al. 2002). Zhang et al. (2019) isolated 113 endophytes from roots, stems, leaves, and spikelets of wheat and tested their antagonistic effect against *F. graminearum* on detached wheat spikes. Six isolates showed to inhibit *F. graminearum* growth while the strain XS-2 of *Bacillus amyloliquefaciens* reduced disease severity on detached wheat spikes significantly. *In vitro*, *B. subtilis* SG6 inhibited *F. graminearum* growth, sporulation, and DON concentration with ratios of 88, 96, and 100% respectively. While in the field, the same strain significantly reduced disease incidence, FHB index, and kernel DON contamination when it was applied from anthesis until soft dough (Zhao et al. 2014).

The usage of biochemical compounds proved to be effective in FHB control. Chitosan (the deacetylated derivative of chitin) inhibited the fungal growth and DON contamination in irradiated wheat kernels (Zachetti et al. 2019). It also reduced disease severity and DON contamination of ≥74% under greenhouse and field conditions (Khan and Doohan 2009). Drakopoulos et al. (2019) tested botanical aqueous extracts of white mustard (*Sinapis alba*) and Chinese galls (*Rhus chinensis*) against *F. graminearum in vitro*. All these compounds fully inhibited mycelium growth, conidial, and ascospore germination. Moreover, they reduced perithecia formation and ascospore discharge up to 50% and 6% respectively.

3.1.8.4. Chemical Control

Effective chemical control of FHB should be combined with other management practices (Blandino et al. 2012; Wegulo et al. 2011). The critical time for fungicides application is the susceptible stage i.e. anthesis stage and 10 days after anthesis. However, limited application period, anthesis heterogenicity, and weather conditions at this stage might be challenging for effective fungicides application, this may require multiple applications to achieve efficient

disease control (D'Angelo et al. 2014; Wegulo et al. 2015). Demethylation inhibitor (DMI) fungicides, namely metconazole, prothioconazole, tebuconazole, prothioconazole + tebuconazole showed to be more effective than propiconazole (McMullen et al. 2012; Paul et al. 2018). Another factor that affects fungicides efficiency is spike coverage during application which is affected by the nozzle type and spray angle. Lehoczki-Krsjak et al. (2015) showed that two sideward-spraying (90° and 120° for forward and backward streams respectively) increased fungicide content between 1.08-1.43 times in wheat spikes compared with vertically-spraying. Moreover, increasing spike coverage from 19 to 37% reduced FHB incidence and DON content significantly for all tested fungicides (Mesterházy et al. 2011).

3.1.8.5. Predicting and Detecting Disease Incidence

One of the prediction practices is risk assessment using disease prediction models based on weather conditions and the history of FHB epidemics in the growing region (McMullen et al. 2012). In addition, the effective monitoring of disease incidence in the field helps in early disease detection and supports the decision-making strategy to apply fungicides at a suitable time. Experts and prognosis models are based on information about the dominant *Fusarium* species, inoculum availability, resistance degree of the cultivated wheat variety, anthesis period, and the former crops in the surrounding area. In addition, information about favorable weather conditions (e.g. rainfall, temperature, and relative humidity) for FHB incidence during wheat vegetation are required as input data for these models. These two practices could be effective tools to prevent quantity and quality losses in wheat yield caused by FHB. These models can be supported or improved by innovative digital technology and remote sensing data to realize a knowledge-based plant protection management.

3.2. Remote Sensing for Monitoring and Phenotyping *Fusarium* Head Blight

Optical sensors are among remote sensing technology which have been widely investigated in monitoring plant diseases as well as in plant phenotyping. These sensors include RGB imaging (red, green, and blue bands), multi- and hyperspectral imaging in the visible-near infrared range and the shortwave infrared range, infrared thermography in the spectral range 7500-14000 nm and chlorophyll fluorescence imaging (Mahlein 2016).

3.2.1. Spectral Techniques

The spectral sensors acquire the spectral reflectance of the object. Based on the number of recorded wavebands, these sensors are classified as multispectral sensors and hyperspectral sensors. Multispectral sensors record the spectral reflectance of individual wavebands (e.g.

RGB wavebands or specific wavebands in the NIR range) (Mahlein 2016). While hyperspectral sensors record the spectral reflectance over a wide number of wavebands in the electromagnetic spectrum from 250-2500 nm. This information is correlated to the plant pigments, chemical compounds, and the water content of the plant (Mahlein et al. 2018).

The main flaw of using hyperspectral imaging sensors in plant disease detection is data complexity. To reduce data complexity, spectral vegetation indices can be derived from the spectral data based on a ratio between individual wavebands. Each of these indices can be used as an indicator of a specific compound of the plant which might be affected during the pathogenicity (e.g. chlorophyll, water content, or tissue structure). This data can be utilized in plant disease detection using supervised or unsupervised machine learning methods. Reducing data complexity reduces calculation time and improves the accuracy of the machine learning approach in plant disease detection (Behmann et al. 2015).

Bauriegel et al. (2011a) investigated the feasibility of HSI in the VIS and NIR ranges for the early detection of FHB using data from controlled and field conditions. They showed that the best time for disease detection is at the beginning of medium milk stage GS 71-85. Principal component analysis (PCA) to disclose the relevant wavelength of healthy and diseased wheat tissue. Based on this approach, the healthy and diseased areas of wheat spikes were correctly classified with an accuracy of 100% and 94% respectively. Spectral angle mapper (SAM) was also able to classify the diseased area with an accuracy of 87%. However, the main drawback of SAM is that it is time-consuming. Another study showed the superiority of HSI in FHB detection under controlled conditions compared with the field condition at the growth stage GS 71-73 (Menesatti et al. 2013). Ma et al. (2020) used the spectral reflectance in the VIS, NIR, and SWIR ranges to detect FHB under field conditions. Six feature bands correlated to FHB were extracted by continuous wavelet analysis (CWA). Afterward, these feature bands were utilized to establish a discrimination model using the Fisher linear discriminant analysis (FLDA). They reveal an accuracy of 89% using this model. Jin et al. (2018) used HSI in the VIS and NIR ranges to detect FHB on wheat under field conditions. They reached an accuracy of 85% using the neural network approach (NN).

In addition, HSI showed promising results as a fast, non-invasive, and non-destructive method for pre-screening *Fusarium* infection and mycotoxin contamination on the kernel scale. This can accelerate the kernel sorting procedure by replacing the laborious and cost-effective chemical methods (Femenias et al. 2020).

3.2.2. Infrared Thermography

Infrared thermography determines the plant temperature which reflects the water status of the plant. Plant pathogens influence the water balance in the plant tissue and this effect can be indirectly measured and visualized as a false-color image by IRT (Mahlein 2016). Maximum temperature difference (MTD) and average temperature difference (ΔT) are parameters derived from IRT and can be successfully used in plant disease detection. MTD represents the differences between the maximum and the minimum temperature within the object, while ΔT represents the difference between the average temperature of the ambient air and the average temperature of the object (Oerke et al. 2006). These parameters were implemented successfully using the support vector machine (SVM) approach to detect FHB on the spikelet scale (Mahlein et al. 2019).

3.2.3. Chlorophyll Fluorescence Imaging

Chlorophyll fluorescence imaging assesses the status of Photosystem II (PSII) of the plant (Murchie and Lawson 2013). The basic fluorescence (F_0) is the minimum value of fluorescence for dark-adapted PSII after excitation with low-intensity light but not enough for electron transport through PSII. The maximum fluorescence (Fm) is the maximum value of fluorescence for dark-adapted PSII after excitation with a saturating pulse. The variable fluorescence (Fv) represents the difference between Fm and F_0. While the ratio Fv/Fm represents the maximum quantum yield of PSII photochemistry with a constant value of ≈ 0.83 for the healthy plants (Baker 2008). FHB infection causes a significant reduction in photosynthetic activity of wheat spikes, this reduction can be detected by CFI (Bauriegel et al. 2011b; Bauriegel and Herppich 2014).

4. Publications

4.1. Comparison and Combination of Thermal, Fluorescence, and Hyperspectral Imaging for Monitoring *Fusarium* Head Blight of Wheat on Spikelet Scale

Anne-Katrin Mahlein, Elias Alisaac, Ali Al Masri, Jan Behmann, Heinz-Wilhelm Dehne, Erich-Christian Oerke. 2019. Sensors, 19, 2281. DOI: 10.3390/s19102281

Author Contributions

Elias Alisaac conceived the experiment (25%), E.A. performed the experiment (50%), E.A. analyzed the data (50%), E.A. wrote the paper (25%).

This text was not modified from the published version.

Abstract

Optical sensors have shown high capabilities to improve the detection and monitoring of plant disease development. This study was designed to compare the feasibility of different sensors to characterize *Fusarium* head blight (FHB) caused by *Fusarium graminearum* and *Fusarium culmorum*. Under controlled conditions, time-series measurements were performed with infrared thermography (IRT), chlorophyll fluorescence imaging (CFI), and hyperspectral imaging (HSI) starting 3 days after inoculation (dai). IRT allowed the visualization of temperature differences within the infected spikelets beginning 5 dai. At the same time, a disorder of the photosynthetic activity was confirmed by CFI via maximal fluorescence yields of spikelets (Fm) 5 dai. Pigment-specific simple ratio PSSRa and PSSRb derived from HSI allowed discrimination between *Fusarium*-infected and non-inoculated spikelets 3 dai. This effect on assimilation started earlier and was more pronounced with *F. graminearum*. Except the maximum temperature difference (MTD), all parameters derived from different sensors were significantly correlated with each other and with disease severity (DS). A support vector machine (SVM) classification of parameters derived from IRT, CFI, or HSI allowed the differentiation between non-inoculated and infected spikelets 3 dai with an accuracy of 78, 56, and 78%, respectively. Combining the IRT-HSI or CFI-HSI parameters improved the accuracy to 89% 30 dai.

4.1.1. Introduction

Fusarium head blight (FHB) is one of the most important diseases on small cereals since the beginning of the twentieth century (Stack 2003). In recent years, the frequency of FHB has increased because of intensive crop production systems such as intensified maize cultivations (Bauriegel and Herppich 2014). Due to the change in environmental conditions and its impact on pathogen appearance and distribution, improvements in FHB management have a high priority (Madgwick et al. 2011). The fungal pathogens *Fusarium graminearum* Schwabe [teleomorph *Gibberella zeae* (Schwein) Petch] and *Fusarium culmorum* (W.G. Smith) Sacc. are the most dominant pathogens in the FHB disease complex (Bottalico and Perrone 2002; Goswami and Kistler 2004; O'Donnell et al. 2004; Simpson et al. 2001). The high importance of FHB is mainly because of the contamination of infected kernels with mycotoxins, such as trichothecenes (e.g., deoxynivalenol and nivalenol) and zearalenones (Desjardins 2006). During the last decades, research efforts have promoted the resistance level of crop varieties to FHB. However, until now resistance cannot be the only solution to control FHB because of the long time needed to achieve this resistance (Mesterházy et al. 2011). Integrated management strategies, in which resistant varieties and fungicides application play a major role, are the best options to control FHB (Wegulo et al. 2011). However, the efficiency of the chemical control of FHB is limited (Amarasinghe et al. 2013). A critical aspect is scheduling the fungicide treatments during the vegetation period. Periods with a high risk of infection have to be evaluated by epidemiologic models and early infection sites have to be detected with high accuracy. Suitable techniques are a prerequisite for monitoring crop stands. Besides visible monitoring, optical sensor technologies have been introduced in plant disease monitoring, phenotyping, and precision agriculture (Alisaac et al. 2018; Mahlein et al. 2012a; Mahlein 2016; Oerke et al. 2014).

Infrared thermography (IRT) is a powerful technique for visualizing, diagnosing and quantifying plant stresses, resulting from biotic and abiotic stress factors. Thermographic cameras detect the infrared radiation in the range of 7.5-12 µm and display the temperature information in false-color images (Mahlein 2016). The suitability of IRT for early detection of plant diseases has been proved in different studies, e.g., in downy mildew of cucumber and grapevine (Lindenthal et al. 2005; Oerke et al. 2006; Stoll et al. 2008). The application of thermal imaging is a promising tool to study spatial patterns of soil-borne pathogens (Calderón et al. 2015; Joalland et al. 2017). Oerke and Steiner (2010) used IRT in the field to detect FHB on winter wheat. They reported a significantly higher temperature of infected spikes compared

to the healthy ones. Al Masri et al. (2017) used IRT to evaluate FHB development in wheat spikes under greenhouse conditions.

With respect to photosynthetic activity, chlorophyll fluorescence imaging (CFI) was used to detect differences resulting from biotic and abiotic stress. The study of plant diseases such as leaf rust and powdery mildew of wheat and barley have been successfully implemented (Brugger et al. 2018; Bürling 2011; Kuckenberg et al. 2009). CFI proved a high capability to assess plant stress, including plant diseases, objectively and non-destructively. However, the full capacity of CFI features in field application is difficult because of dark adaptation required prior to measurement, high and varying light intensity (Chaerle et al. 2003), and time between emission and detection of the measuring beam (Oerke et al. 2014).

Hyperspectral imaging (HSI) assesses the spectral information as reflectance or transmittance intensity in the visible (VIS, 400-700 nm), near-infrared (NIR, 700-1000 nm), and short-wave infrared (SWIR, 1000-2500 nm) ranges (Mahlein 2016). The resulting data consists of complex data matrices with three dimensions: two spatial dimensions x and y, and one spectral dimension z. Recently, there has been a remarkable increase in research and reports using hyperspectral imaging in plant disease studies, for example, FHB (Alisaac et al. 2018; Bauriegel et al. 2011b), yellow rust (Huang et al. 2007), powdery mildew of barley (Kuska et al. 2015), *Cercospora* leaf spot, rust and powdery mildew in sugar beet (Leucker et al. 2016; Mahlein et al. 2010, 2012b, 2013), and tomato late blight (Wang et al. 2008). These reports concluded that HSI is more objective than the traditional visual methods in characterizing plant diseases, however, these innovative techniques could be further improved (Bock et al. 2010).

CFI was used in combination with HSI to study FHB and both sensors proved suitable for disease detection after symptoms become visible but this was before senescence (Bauriegel et al. 2011b). IRT was used in combination with CFI and proved to be very useful for highlighting pre-symptomatic responses of viral diseases and powdery mildew on cucumber (Berdugo et al. 2014).

These non-destructive sensors have enabled the accurate and reliable detection of plant diseases and provided new insights into plant-pathogen interactions on different scales (Mahlein 2016). FHB symptoms could be detected by using imaging sensors of thermography, chlorophyll fluorescence, and hyperspectral reflectance after symptoms become visible (Al Masri et al. 2017; Bauriegel and Herppich 2014; Oerke et al. 2014).

A deeper understanding of FHB using data from multiple sensors is important to optimize risk estimations and management strategies. The aim of the study was to compare IRT, CFI, and HSI for the monitoring of FHB caused by *F. graminearum* and *F. culmorum* under controlled conditions. This individual and multi-sensor data were used as input for the support vector machine (SVM) classifier to investigate the potential of each combination for early detection of FHB and different stages of pathogenesis.

4.1.2. Materials and Methods

4.1.2.1. Experimental Plants

A variety of spring wheat (*Triticum aestivum* L.) moderately resistant to FHB (Anonymous 2013), Passat (KWS, Einbeck, Germany) was used in this study. The spikes of this variety are awnless and light green with 18-22 spikelets in each spike. Pots (12×12×20 cm) were filled with a mixed substrate (sand, subsoil C, potting substrate ED 73) at a 1:3:6 ratio [v/v/v]). Two seedlings were sown per pot. The plants were supported by sticks and wires to avoid lodging. The plants were cultivated at 20 ± 2°C and 50-70% relative humidity (RH) in a greenhouse. Artificial light (> 300 µmol $m^{-2}s^{-1}$, Philips SGR 140, Hamburg, Germany) was used to obtain a photoperiod of 16/08 h day/night.

4.1.2.2. Inoculum and Inoculation

Fusarium graminearum, isolate S.19, and *F. culmorum,* isolate 3.37, were obtained in 2011 and 2004, respectively from infected wheat kernels in Klein-Altendorf, Germany. They were stored at -80°C in the culture collection of the Institute of Crop Science and Resource Conservation (INRES), University of Bonn. The inoculum was produced on potato dextrose agar (PDA, 39 gL^{-1}), potato dextrose broth (PDB, 24 gL^{-1}), and low strength potato dextrose agar (LSPDA, 12.5 gL^{-1} and agar-agar, 19.5 gL^{-1}) according to Moradi (2008). The conidial suspension was adjusted to 10^5 conidia mL^{-1} using a Fuchs-Rosenthal hemocytometer.

Wheat spikes were inoculated on the same day with each *Fusarium* species separately at GS 61-65 (Lancashire et al. 1991). Four plants with 6 spikes similar in anthesis time were chosen for inoculation. The spikes were inoculated by spraying with 10^5 conidia mL^{-1} until run-off. Subsequently, plants of each treatment were incubated in separated plastic chambers at optimal conditions for infection (≥95% RH and 22-25°C), for 48 hours. After incubation, plants were grown at 50-70% RH, 16/08 photoperiod, 18/12°C day/night. Spikes were humidified for 1-2 h per day, using a hand sprayer. Non-inoculated control plants were grown under the same conditions. Six spikelets of each treatment were selected for data analysis.

4.1.2.3. Disease Severity of FHB

In this study, a rating system of FHB severity was established and used for a visual assessment of the disease severity (DS) within each individual spikelet (Figure 3). Disease severity was classified as follows: (i) from 1 to 5% represents early discoloration and small necrotic lesions on glumes, (ii) 10% early bleaching of spikelets which usually cover the typical floret, (iii) 20, 30 and 50% represent combinations of extended necrotic lesions and bleached florets at different levels, (iv) 70% bleached spikelets, but not completely dry, (v) 100 % bleached and dry spikelet.

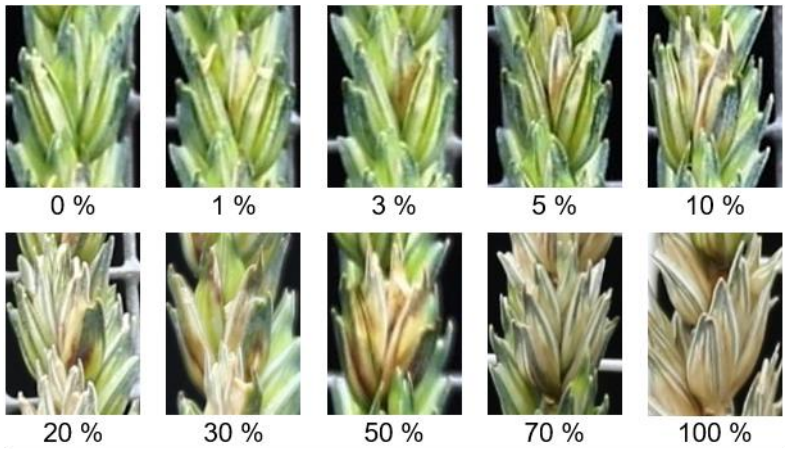

Figure 3. The rating system of disease severity of *Fusarium* head blight (FHB) within a single spikelet of the wheat spike.

4.1.2.4. Infrared Thermal Imaging (IRT)

Thermal imaging was performed in a greenhouse under controlled conditions at 50-70% RH and 17-24°C. The artificial supplementary light was reduced during measuring time to 20 ± 2 µmol m^{-2} s^{-1} (Hortilux Schréder, HPS 400W/230V, Monster, Netherland). Spikes were fixed vertically on metal grids (40×30 cm, grid size 12×12 mm) attached to supporting sticks in the pots. A digital thermocamera (VarioCAM High Definition, Jenoptik, Jena, Germany), sensitive to spectral range from 7.5 to 14 µm with uncooled microbolometer focal plane array was used. The camera has a thermal resolution of 0.03 K at 30°C, a geometric resolution of 1.024×768 IR-pixel, and 30 Hz IR-image frequency. The material emissivity was set to 1 for all measuring dates. The thermocamera was mounted on a tripod and placed at 40 cm distance from spikes and was controlled via the software package IRBIS 3 professional (InfraTec, Dresden, Germany). IR images were analyzed using the same software package by drawing polygons on the selected spikelets, thermal data of ambient air was used for normalization. The maximum

temperature difference (MTD) and the average temperature difference between air and spikelets (ΔT) were calculated. All parameters of sensor data are summarized in Table 4.

4.1.2.5. Chlorophyll Fluorescence Imaging (CFI)

An imaging pulse amplitude modulated chlorophyll fluorometer PAM, MAXI HEAD (Heinz Walz, Effeltrich, Germany) was used for chlorophyll fluorescence measurements under laboratory conditions. The measurement was conducted according to the saturation pulse method immediately after plants had been dark-adapted for 15 ± 2 min at room temperature. A standard distance of 18.5 cm between spikes and the camera for a 13×15 cm^2 imagery area was used with a black background. The CCD camera (1392×1040 pixel) recorded basic fluorescence F_0 after illumination of the horizontally laid spikes with blue light (470 nm) of 0.5 µmol quanta $m^{-2}s^{-1}$ PAR. Maximum fluorescence (Fm) was recorded after a saturation pulse of 2700 µmol quanta $m^{-2}s^{-1}$ PAR for 0.6 seconds. Based on F_0 and Fm, the maximal PSII quantum yield (Fv/Fm) was calculated (Table 4) which indicates the capacity of photosynthesis of the spikelets. Saturation pulses of 396 µmol quanta $m^{-2}s^{-1}$ PAR were produced at intervals of 20 s until the steady-state condition was reached and the efficient quantum yield Y [II] was estimated which indicates the stability of photosynthesis. The CCD camera was controlled via the software package ImagingWin professional (Heinz Walz, Effeltrich, Germany). Recorded false-color images of Fm, Fv/Fm, and Y [II] were analyzed by drawing polygons that fit the selected spikelets.

4.1.2.6. Hyperspectral Imaging (HSI)

For hyperspectral imaging, spikes were laid horizontally on a table with black background (68 cm distance from the cameras) in a light-proof room. Spikes were illuminated with an artificial light source (ASD-Pro-Lamps, Analytical Spectral Devices Inc., Boulder, CO, USA), 50 cm distance from the spikelets, and a vertical inclination of 45°. The hyperspectral camera ImSpector V10E (Spectral Imaging Ltd., Oulu, Finland) was used in the visible-near infrared (VIS-NIR) range from 400 to 1000 nm. A SWIR-camera (ImSpector N25E, Spectral Imaging Ltd., Oulu, Finland) was used in the SWIR from 1000 to 2500 nm. Measurements started after a runtime of 30 minutes of the entire system. The cameras were focused manually on a white barium sulfate calibration bar with black rhombi (Spectral Imaging Ltd., Oulu, Finland) placed at the same distance of the object. For more details about the imaging setup and image recording see Alisaac et al. (2018).

The software "Processing Imspector 3.1" (Geoscap, Cologne, Germany) was used to calculate the reflectance in relation to a white reference bar and the dark current image. The signals from hyperspectral images were smoothed by applying the Savitzky Golay filter (25 centered supporting points and a third-degree polynomial). All spikelets were masked with HSVaP ("Hyperspectral Visualization and Processing") (Alisaac et al. 2018), and the mean reflectance of each spikelet was extracted with MATLAB R2014a (MathWorks, Natick, Massachusetts, USA). Spectral vegetation indices, Normalized Differences Vegetation Index (NDVI), Photochemical Reflection Index (PRI), Pigment-Specific Simple Ratio (PSSRa, PSSRb, PSSRc) and Water Index (WI) (Table 4) were calculated as parameters in order to investigate the potential of specific bands in detecting FHB.

Table 4. Summary of parameters derived from multi-sensorial monitoring of Fusarium head blight on wheat.

Sensor	Index	Equation	Indicator
Thermography (IRT)	Maximum temperature difference (MTD)	MTD = maximum - minimum temperature within spikelets	Biotic stresses in early stage (Oerke et al. 2006)
	Average temperature difference (ΔT)	ΔT = average air temperature - average spikelets temperature	Biotic stresses in early and late stages (Oerke et al. 2006)
Chlorophyll fluorescence imaging (CFI)	Maximal fluorescence yields	Fm	Fast chlorophyll fluorescence kinetics (Kuckenberg et al. 2009)
	Maximal PSII quantum yield (Fv/Fm)	$Fv/Fm = (Fm - F_0)/Fm$	Maximal photochemical efficacy of photosynthesis II (Butler and Kitajima 1975)
	Effective PSII quantum yield (Y [II])	Y [II] = (Fm' - F)/Fm'	Photochemical quantum yields at steady state (Genty et al. 1989)
Hyperspectral imaging (HSI)	Normalized differences vegetation index (NDVI)	$NDVI = (R_{800} - R_{670})/(R_{800} + R_{670})$	Biomass, leaf area (Rouse et al. 1974)
	Photochemical reflection index (PRI)	$PRI = (R_{531} - R_{570})/(R_{531} + R_{570})$	Epoxidation state xanthophyll's cycle; pigments and photosynthetic radiation use efficiency (Gamon et al. 1992)
	Pigment-specific simple ratio (PSSR)	$PSSRa = R_{800}/R_{680}$	Chlorophyll a (Blackburn 1998a)
		$PSSRb = R_{800}/R_{635}$	Chlorophyll b (Blackburn 1998a)
		$PSSRc = R_{800}/R_{470}$	Carotenoid (Blackburn 1998a)
	Water index (WI)	$WI = R_{900}/R_{970}$	Water content (Penuelas et al. 1997)

4.1.2.7. Realization of Measurements

Measurements with the three sensors were performed subsequently on the same day. The thermal imaging was performed under greenhouse conditions from 8:00 to 9:30 am. CFI and HSI measurements took place in a laboratory. Time-series images were performed 3, 5, 7, 12, 17, 21, and 30 days after inoculation (dai). For data analysis, six spikelets were chosen from six spikes as experimental replications for each treatment.

4.1.2.8. Statistical Analysis

The Superior Performing Software System SPSS 24 (SPSS Inc., Chicago, IL, USA) was used for statistical analysis. A general linear model for repeated measurements was performed on DS (including the disease severity of infected spikelets and the senescence of non-inoculated control), MTD, ΔT, Fv/Fm, Y [II], Fm, NDVI, PRI, PSSRa, PSSRb, PSSRc, and WI. Mean comparisons of treatments were performed using Tukey's HSD test (significance level $P \leq 0.05$). A t-test on each single band of the electromagnetic spectrum was performed in Microsoft Excel 2010. A correlation matrix among all indices was applied using RStudio following Pearson's method (significance level $P \leq 0.05$). A support vector machine (SVM) classification was run in RStudio to classify non-inoculated and infected spikelets using the parameters derived from each sensor or a combination of different sensor parameters (Alisaac et al. 2018). Seven data sets were investigated: three from each sensor, three from combinations of two sensors (IRT-CFI, IRT-HSI, and CFI-HSI) and one using multi-sensor data (IRT-CFI-HSI). To train the model, half of the data was used as a training data with the radial basis function (RBF) kernel. Five-fold cross-validation was performed on the training data to optimize the parameters cost (C) and gamma (γ). The rest of the data was separated from the training data to evaluate the model.

4.1.3. Results

4.1.3.1. Disease Development

The first symptoms of FHB became visible 3 dai with small necrotic lesions (1%) on glumes of spikelets infected with *F. graminearum*. Starting 5 dai, *F. culmorum*-infected spikelets were associated with visible symptoms, not significantly different from those infected with *F. graminearum*. FHB symptoms of both pathogens increased significantly on 7 dai with no statistical difference between the two *Fusarium* species (Figure 4). Natural senescence started on 21 dai on non-inoculated spikelets, and could be monitored easily by visual assessment, the non-inoculated spikelets showed average bleaching of 56% 30 dai (GS 83) (Figure 4).

4.1.3.2. Effect of *Fusarium* Infection on Spikelet Temperature

Fusarium species affected the temperature of infected spikelets compared with non-inoculated control ones. The MTD (Figure 5a) indicates the temperature heterogeneity within individual spikelet. Significant increases in MTDs were observed starting 7 dai for infected spikelets of both *Fusarium* species compared with non-inoculated control (Figure 5a). Maximum MTDs were observed 12 dai, then the infected spikelets showed lower temperature heterogeneity. At

21 dai, MTDs of infected spikelets were not significantly different from the non-inoculated control (Figure 5a). A reduced ΔT of *Fusarium*-infected spikelets compared with non-inoculated control was observed 5 dai and was significant until 21 dai. In general, ΔTs of non-inoculated control were higher than those of infected spikelets with each pathogen even up until 30 dai (Figure 5b).

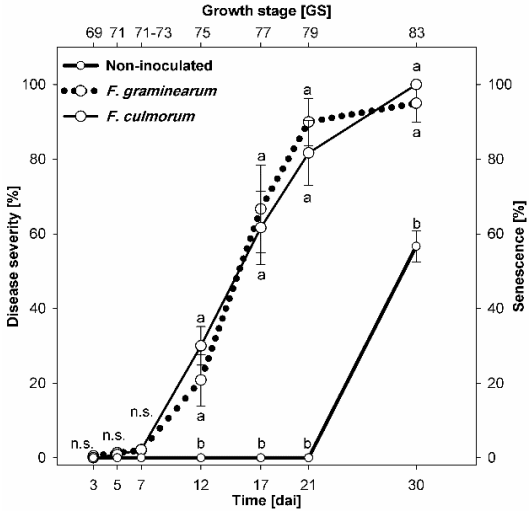

Figure 4. Progress curves of *Fusarium* head blight severity (% diseased spikelet area) due to *Fusarium graminearum* (dotted line) and *Fusarium culmorum* (solid line) on wheat spikelets after spray inoculation compared with non-inoculated control (bold solid line displaying the senescence of non-inoculated control). Spikes were inoculated at GS 61-65. Different letters at the same time point differ significantly according to Tukey's HSD, $P \leq 0.05$ (mean ± SE; n = 6). n.s., not significantly different.

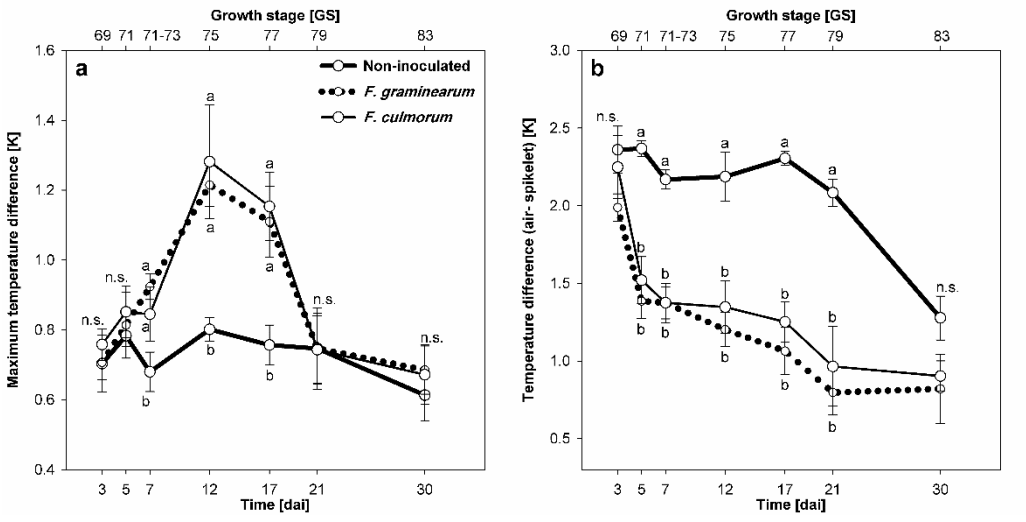

Figure 5. Effect of FHB caused by *F. graminearum* (dotted lines) and *F. culmorum* (solid lines) on the development of maximum temperature difference (a) and average temperature difference [ΔT = air - spikelet] (b) compared with non-inoculated control (bold solid lines). Spikes were spray-inoculated at GS 61-65. Different letters at the same date differ significantly according to Tukey's HSD, $P \leq 0.05$ (mean ± SE; n = 6). n.s., not significantly different.

4.1.3.3. Effect of *Fusarium* Infection on Chlorophyll Fluorescence

Fusarium infection caused by both *Fusarium* species was associated with reducing the photosynthetic activity of spikelet tissue in early stage of infection. In advanced stages (i.e. bleached symptoms stage), the photosynthetic apparatus was completely destroyed.

The Fm of dark-adapted spikelets was significantly reduced in *F. graminearum*-infected spikelets compared with *F. culmorum*-infected and non-inoculated control spikelets 7 dai (Figure 6a). The infection with each *Fusarium* species reduced Fm significantly after 7 dai compared with non-inoculated control. These differences were also pronounced 30 dai. Neither maximal photochemical efficacy of photosynthesis II [Fv/Fm] nor photochemical quantum yield Y [II] was suitable parameters to differentiate between infected spikelets and non-inoculated ones during the first week after inoculation (Figure 6b,c). Fv/Fm and Y [II] were significantly reduced only 12 dai as compared with non-inoculated control. At the last time point of the assessment, 30 dai, Fv/Fm of *F. culmorum*-infected spikelets was significantly different from *F. graminearum*-infected spikelets and those of the non-inoculated control (Figure 6b). In contrast, the Y [II] showed no significant differences among all treatments 30 dai (Figure 6c).

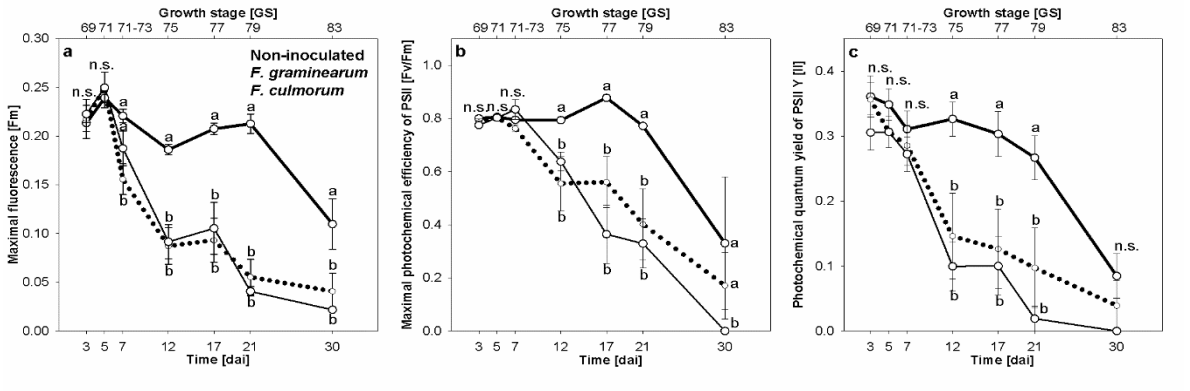

Figure 6. Effect of *Fusarium* head blight caused by *F. graminearum* (dotted lines) and *F. culmorum* (solid lines) on maximal fluorescence of dark-adapted spikelets [Fm] (a), maximal photochemical efficacy of photosynthesis II [Fv/Fm] (b), and photochemical quantum yield Y [II] (**c**) in comparison to non-inoculated control (bold solid lines). Spikes were spray inoculated at GS 61-65. Tukey's HSD, $P \leq 0.05$ (mean ± SE; $n = 6$). n.s., not significantly different.

4.1.3.4. Effect of *Fusarium* Infection on Spectral Signature of Spikelets

The spectral signatures of the non-inoculated control showed minor changes during the first 6 measuring times (until 21 dai). The senescence of the non-inoculated control increased the reflectance in the VIS and the SWIR ranges 30 dai (Figure 7a). A lower reflectance was observed in the NIR (Figure 7a). The spectral signatures of FHB infected spikelets changed

considerably in comparison with the non-inoculated control parallel to the development of infection (Figure 7). The reflectance of FHB spikelets showed gradual but low changes along the entire spectral signature until 7 dai for both *Fusarium* species (Figure 7b,c). More pronounced changes were shown for *F. culmorum*-infected spikelets in the SWIR range. From 12 dai onwards, the shape of spectra showed distinct changes compared with the earlier measurement times. Here, higher reflectance in the VIS and SWIR ranges and lower reflectance in the NIR range was pronounced. The largest changes in the shape of the spectral signatures were detected in the VIS range starting 17 dai. In the NIR range, the decrease in the spectral reflectance started 12 dai. At 30 dai, the strongest alteration was measured especially for spikelets infected with *F. culmorum* (Figure 7b,c).

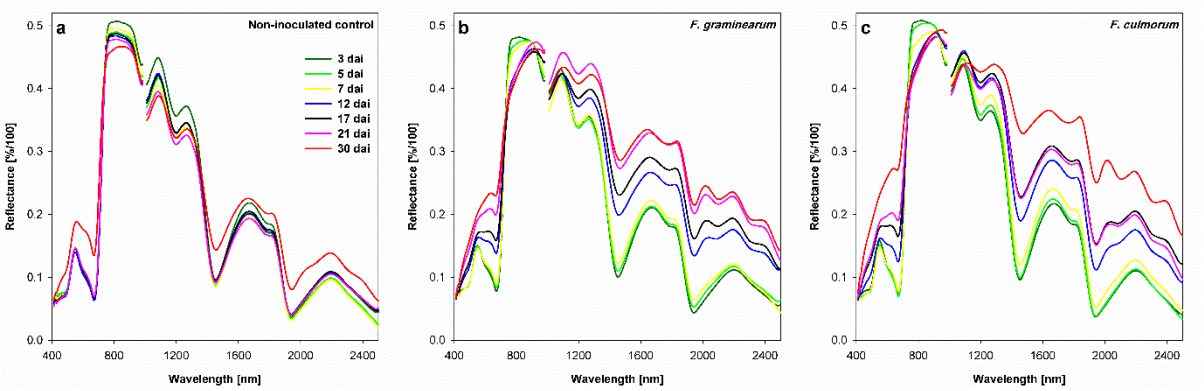

Figure 7. Effect of *Fusarium* head blight caused by *F. graminearum* (b) and *F. culmorum* (c) on spectral signatures of wheat spikelets compared with the non-inoculated control (a) at different time points after inoculation (3-30 days past inoculation, dai). Spikes were spray inoculated at GS 61-65. Means; $n = 6$.

Differences between non-inoculated control and *Fusarium*-infected spikelets were more obvious by plotting the differences of spectral reflectance (Figure 8). The comparison between the non-inoculated control and *F. graminearum*-infected spikelets (non-inoculated control - *F. graminearum*-infected spikelets) (Figure 8a) showed that the alteration in spectral signature started already at 3 dai. These differences were pronounced around 500 and 675 nm in the VIS range with two negative peaks, and at 760 nm in the NIR range with a positive peak. Wavelengths indicating water content in the SWIR showed clear differences with three negative peaks at 1440, 1880, and 2000 nm. Over time, the reflectance difference increased very clearly. *F. culmorum*-infected spikelets showed similar patterns of reflectance difference curves compared with that of *F. graminearum* (non-inoculated control - *F. culmorum*-infected spikelets) (Figure 8b). This indicates that the same wavelengths were affected by both *Fusarium* species. The differences between *Fusarium* species in terms of the spectral

reflectance (*F. culmorum* - *F. graminearum*) did not exceed ± 0.05% (Figure 8c). It showed that differentiation among causing pathogens of FHB was possible starting at 3 dai. The differences were shown along the spectrum over time. The significance of these differences among the spectral signatures of the treatments was confirmed by a t-test. The differences between spikelets of the non-inoculated control and *F. graminearum* or *F. culmorum*-infected spikelets were significant in the VIS and SWIR ranges starting from 7 and 5 dai, respectively. No significant differences could be detected between the spectral signatures of *F. graminearum* and *F. culmorum*-infected spikelets.

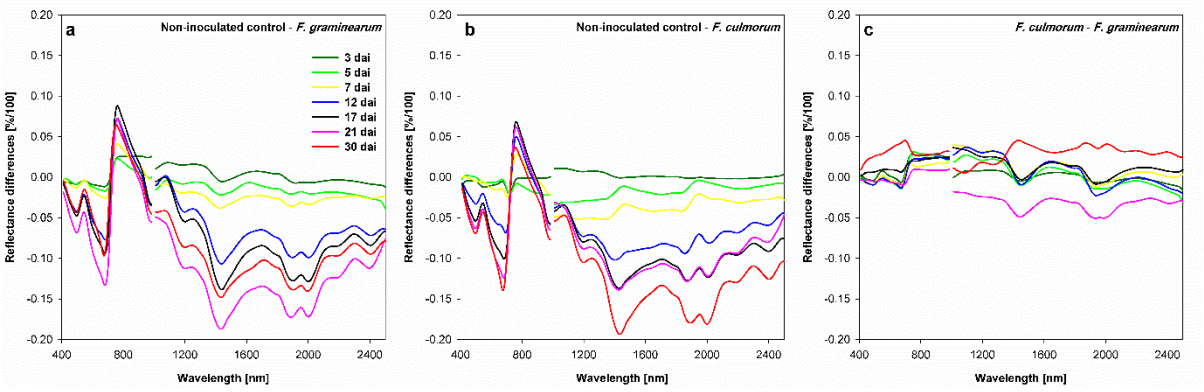

Figure 8. Difference spectra of *Fusarium* head blight caused by *F. graminearum* to non-inoculated control (a), FHB caused by *F. culmorum* to non-inoculated-control (b), and FHB caused by both *Fusarium* species separately (c) at different time points of assessment after inoculation. Spikes were spray inoculated at GS 61-65. Means; $n = 6$.

4.1.3.5. Correlation between Parameters Derived from Different Sensors

Parameters derived from different sensors showed a high significant correlation to each other and to the disease severity according to the Pearson's method (Figure 9). MTD was the only parameter that showed no significant correlation to the others. The correlation varied between strong (r from 0.60 to 0.79) and very strong ($r \geq 0.80$). The Pearson's correlation method confirmed a positive correlation among all selected parameters except MTD, and a negative correlation between DS and sensors data (the strongest, -0.88 to Fv/Fm and the weakest, -0.72 to ΔT).

4.1.3.6. Spatio-Temporal Dynamics of *Fusarium* Head Blight

Early and late symptoms of FHB compared with the non-inoculated control spikes are shown in Figure 10. The infection development can be visibly distinguished 3 dai with the help of the non-invasive sensors. The temperature of infected spikelets increased and reached values close to those of the ambient air 5 dai for the infection with both *Fusarium* species. At a late infection stage, 21 dai, infected spikelets were completely bleached and showed the temperature with

minimum differences to ambient air temperature. The chlorophyll fluorescence index Fm indicated to the spot where the infection started 3 dai, especially on *F. graminearum*-infected spikelets. Over time, Fm dropped to zero 21 dai. Early symptoms of FHB were detectable by the WI derived from hyperspectral images starting 3 dai (Figure 10).

Vegetation indices calculated from the spectral reflectance of different treatments are shown in Table 5. NDVI of non-inoculated control was in the range from 0.55-0.77 during the measuring period. Starting at 12 dai, the NDVI was significantly different from the infected spikelets. In contrast, the PRI was significantly different from infected spikelets at an earlier stage, 7 dai, but showed no significant difference to the non-inoculated control at late infection stages. PSSR a and b differed between non-inoculated control and *F. culmorum*-infected spikelets 3 dai. At 5 dai, these indices were significantly different between *Fusarium* infected spikelets. PSSRa, b, and c showed significant differences between non-inoculated control and *Fusarium* species infected spikelets 30 dai. WI was similar to PRI in differentiating between non-inoculated control and *Fusarium* infected spikelets, however, WI could differentiate between them even at 30 dai (Table 5).

DS	-0.05	-0.72	-0.86	-0.88	-0.83	-0.87	-0.82	-0.85	-0.85	-0.79	-0.83
	MTD	-0.10	-0.11	0.11	-0.03	-0.08	-0.15	-0.19	-0.16	-0.10	-0.23
		ΔT	0.74	0.69	0.64	0.67	0.69	0.73	0.72	0.65	0.73
			Fm	0.84	0.82	0.81	0.79	0.83	0.82	0.75	0.85
				Fv/ Fm	0.84	0.78	0.70	0.75	0.76	0.73	0.71
					Y [II]	0.76	0.72	0.79	0.79	0.73	0.74
						NDVI	0.80	0.95	0.96	0.95	0.89
							PRI	0.86	0.85	0.68	0.78
								PSSRa	1.00	0.95	0.89
									PSSRb	0.96	0.89
										PSSRc	0.85
											WI

Figure 9. Correlation between disease severity (DS: diseased spikelet area %) and data from different sensors: temperature difference between air and spikelet (ΔT), maximum temperature difference (MTD), maximal fluorescence yields of dark-adapted spikelets (Fm), photochemical quantum yield at steady state Y[II], maximal photochemical efficacy of photosynthesis II (Fv/Fm), normalized difference vegetative index (NDVI), photochemical reflectance index (PRI), pigment specific simple ratio (PSSRa, b, and c) and water index (WI). n = 126 pairs, Pearson's method.

Table 5. Effect of *Fusarium* head blight caused by *F. graminearum* and *F. culmorum* on spectral vegetation indices of wheat spikelets compared with the non-inoculated control.

Index	Treatment	Time [dai]						
		3	**5**	**7**	**12**	**17**	**21**	**30**
NDVI	Non-inoculated control	0.77 a	0.76 a	0.77 a	0.77 a	0.76 a	0.74 a	0.55 a
	F. graminearum	0.72 a	0.70 a	0.68 a	0.52 b	0.47 b	0.38 b	0.30 b
	F. culmorum	0.75 a	0.75 a	0.72 a	0.55 b	0.46 b	0.40 b	0.24 b
PRI	Non-inoculated control	-0.01 a	-0.01 a	-0.02 a	-0.02 a	-0.02 a	-0.03 a	-0.06 a
	F. graminearum	-0.02 a	-0.02 a	-0.03 b	-0.04 b	-0.05 b	-0.06 b	-0.06 a
	F. culmorum	-0.02 a	-0.02 a	-0.03 b	-0.04 b	-0.05 b	-0.06 b	-0.06 a
PSSRa	Non-inoculated control	7.10 a	6.72 a	7.21 a	6.99 a	6.63 a	6.29 a	3.50 a
	F. graminearum	5.85 b	5.29 b	4.96 b	3.29 b	2.81 b	2.28 b	1.86 b
	F. culmorum	6.46 ab	6.56 a	5.81 b	3.48 b	2.73 b	2.39 b	1.57 b
PSSRb	Non-inoculated control	5.53 a	5.27 a	5.58 a	5.44 a	5.19 a	4.94 a	2.99 a
	F. graminearum	4.74 b	4.42 b	4.24 b	3.03 b	2.67 b	2.23 b	1.90 b
	F. culmorum	5.02 ab	5.11 a	4.65 b	3.16 b	2.59 b	2.33 b	1.64 b
PSSRc	Non-inoculated control	6.85 a	6.47 a	6.96 a	7.18 a	6.95 a	6.94 a	4.96 a
	F. graminearum	5.88 a	5.76 a	5.68 b	4.53 b	4.22 b	3.67 b	3.31 b
	F. culmorum	6.39 a	6.75 a	6.50 a	4.91 b	4.18 b	3.96 b	2.83 b
WI	Non-inoculated control	1.14 a	1.14 a	1.15 a	1.16 a	1.15 a	1.15 a	1.12 a
	F. graminearum	1.14 a	1.13 a	1.11 b	1.05 b	1.03 b	1.02 b	1.01 b
	F. culmorum	1.14 a	1.13 a	1.10 b	1.05 b	1.03 b	1.02 b	1.00 b

NDVI, normalized difference vegetation index; PRI, Photochemical reflection index; PSSRa, Pigment-specific simple ratio chlorophyll a; PSSRb, Pigment-specific simple ratio chlorophyll b; PSSRc, Pigment-specific simple ratio carotenoid; WI, Water index. Within one column, lowercase letters indicate significant differences between the parameters (Tukey's HSD; $P \leq 0.05$, $n = 6$).

4.1.3.7. Support Vector Machine Classification of Infected and Non-Infected Spikelets at Different Pathogenesis Stages

Sensor data (i.e., MTD and ΔT from IRT; Fm, Fv/Fm, and Y [II] from CFI; and NDVI, PRI, PSSRa, PSSRb, PSSRc, and WI from HSI) were used as input parameters in a two-class classification (non-inoculated/infected spikelets) using an SVM approach (Table 7). An accuracy of 78% was obtained 3 dai using the parameters derived from IRT or HSI. This accuracy varied between 78 and 100% depending on the disease stage and decreased to 67% 30 dai using the IRT parameters. The accuracy increased to 100% 12, 17, and 21 dai and decreased to 78% on 30 dai using HSI parameters. Lower accuracy has been obtained when using the CFI parameters as an input of SVM. An accuracy of 56% was observed 3 dai and the maximum accuracy was 89% 7, 12, 17, and 21 dai, then it decreased to 78% 30 dai (Table 7).

Fusing parameters from two sensors showed no improvement in the classifier accuracy in all combinations along the time of the experiment until 21 dai. However, fusing IRT or CFI with HSI parameters increased the accuracy to 89% 30 dai. The best performance of the combinations was achieved using the combination of IRT with HSI with a mean accuracy of

90% over the time of the experiment. Multi-sensor data (i.e, IRT, CFI, and HSI) did not improve the accuracy of the classifier, and the mean accuracy of multi-sensor data was 87% over the time of the experiment (Table 7).

Table 4. Accuracy of two-class classification (non-inoculated/infected spikelets) using support vector machine (SVM) for each assessment date using the defined parameters derived from each sensor and combinations of different sensors.

Time	Accuracy [%] of Two-Class Classification						
[dai]	IRT [1]	CFI [2]	HSI [3]	IRT-CFI	IRT-HSI	CFI-HSI	Multi-Sensor (IRT-CFI-HSI)
3	78	56	78	67	67	56	56
5	100	67	78	67	100	78	100
7	78	89	89	78	78	78	78
12	78	89	100	100	100	100	100
17	100	89	100	100	100	100	100
21	78	89	100	89	100	100	100
30	67	78	78	67	89	89	78
Mean	82	79	89	81	90	86	87

[1] IRT, infrared thermography; [2] CFI, chlorophyll fluorescence imaging; [3] HSI, hyperspectral imaging

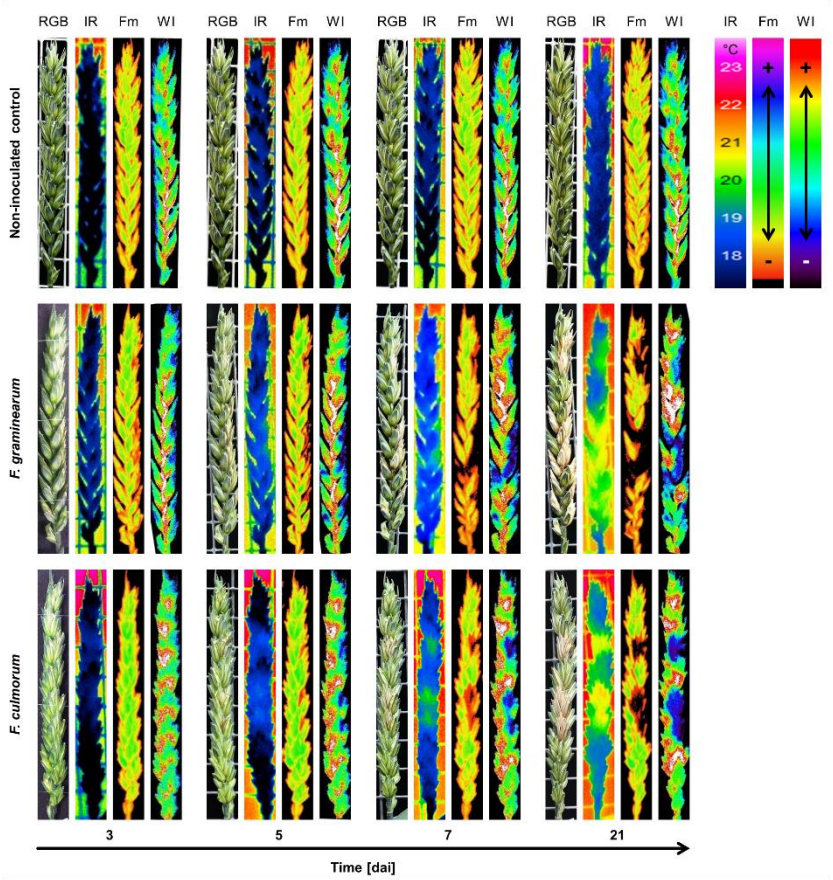

Figure 10. Spatio-temporal dynamics of *Fusarium* head blight caused by *F. graminearum* and *F. culmorum* compared with non-inoculated control visualized by digital images (RGB), thermograms (IR), maximum chlorophyll fluorescence false-color image (Fm), and water index false-color image (WI) derived from spectral reflectance.

4.1.4. Discussion

Optical sensors and non-invasive methods have recently attracted an increasing interest (Gebbers and Adamchuk 2010; Mahlein et al. 2018). They are expected to play a major role in detecting and monitoring plant diseases in the coming years (Lucas 2011). An application of these technologies to monitor FHB might contribute significantly to secure cereal production systems. Early detection and objective monitoring of FHB using proximal sensors such as IRT, CFI, and HSI, individually or in combination enhance our knowledge to improve disease management.

FHB symptoms are normally associated with a relatively low water content of infected spikelets. This reduction in water content causes an increased temperature of the infected spikelets compared with the non-inoculated control. This can be attributed to reduced transpiration due to reduced water supply (Al Masri et al. 2017). IRT was successfully used in detecting and monitoring FHB under field and controlled conditions (Al Masri et al. 2017; Oerke et al. 2014). In the current study, *Fusarium*-infected spikelets showed higher temperatures compared with non-inoculated control. This is in accordance with (Al Masri et al. 2017; Oerke et al. 2014), where thermal images were analyzed considering the entire spikes. Impeding the movement of assimilates above the preliminary site of infection leads to a reduction in transpiration in the upper part of the spike. Additionally, the "plug of" of the rachilla when the *Fusarium* infection moves from floret to rachilla can have a similar effect (Lemmens et al. 2004). This reduction leads to a higher temperature in that part of the spike (Al Masri et al. 2017). The higher temperature of infected spikelets allowed detection of FHB at the early stages at 5 and 7 dai based on ΔT and MTD, respectively, as it was shown by Al Masri et al. (2017).

Oerke et al. (2011) reported the possibility to detect apple scab infection due to (*Venturia inaequalis*) before the symptoms become visible by IRT. The same was reported for downy mildew of cucumber and grapevine leaves (Oerke et al. 2006; Stoll et al. 2008). In contrast, the early detection of other pathosystems was associated with higher temperatures. Gomez (2014) reported higher temperatures of rose leaves infected with downy mildew (*Peronospora sparsa*) two days before symptoms become visible. The infection with *Tobacco mosaic virus* (TMV) caused an increase in leaf temperature of tobacco. This is due to the closure of stomatal cells because of the accumulation of salicylic acid after infection (Chaerle et al. 1999). The higher sensitivity of IRT to detect leaf diseases pre-symptomatically compared with FHB could be

attributed to the differences between the spikelet and the leaf structures. This results in differences between the transpiration systems and leads to a higher temperature of spikes compared with that of leaves (Ayeneh et al. 2002). IRT proved high potential not only in the early detection but it also provided a more accurate assessment of FHB severity than the visual assessment.

Biotic and abiotic stresses in plants have been widely studied using CFI during the last decade (Bauriegel et al. 2011b; Chaerle et al. 2007; Cséfalvay et al. 2009; Scholes and Rolfe 2009). It provides a direct, non-invasive measurement of the photosynthetic apparatus and information about the impacts of fungal pathogens on host metabolism (Scholes and Rolfe 2009). The most sensitive parameters, indicating downy mildew infection on the grapevine (*Plasmopara viticola*) were Fv/Fm and Y [II] of PSII. It was possible to detect the infection 3 days before symptoms become visible (Cséfalvay et al. 2009). Kuckenberg et al. (2009) used Fm and Fv/F_0 for early and precise detection of brown rust (*Puccinia recondita*) and powdery mildew (*Blumeria graminis*) on wheat. They reported that Fv/F_0 was the most sensitive parameter responsive to both diseases. They were able to detect the infection before symptoms became visible or significant changes in the NDVI become pronounced. In the current study, Fv/Fm and Y [II] in addition to Fm showed also high sensitivity to monitor FHB. The potential of CFI to characterize FHB on wheat was investigated first by (Bauriegel et al. 2010). They proved the possibility of Fv/Fm to discriminate between healthy and infected spikes first at BBCH 75. Using CFI, FHB was already detectable from 5 dai onwards which is in accordance with Bauriegel et al. (2010, 2011b). However, the very early infection could be distinguished through a few pixels with lower Fm values (Figure 10). As already discussed, the plugging of the rachis has a side effect on water movement upwards, detectable by IRT, but not by CFI. In contrast, CFI is sensitive to detect the local *Fusarium* infection at early stages ($\leq$ 5%) when symptoms on glumes are difficult to be captured by IRT.

Hyperspectral imaging provides new insights in studying FHB compared with the other two sensors by investigating a broader spectral range from 400-2500 nm in narrow bands per pixel. This was pronounced in the spectral difference between infected spikelets and non-inoculated control along the electromagnetic spectrum. The high sensitivity of HSI has been proved for early detection of *Fusarium* infection before the symptoms become visible to the human eye (Bauriegel et al. 2011a). Furthermore, HSI was used to quantify wheat resistance to FHB (Alisaac et al. 2018). It was shown that the assessment of lesion phenotypes of *Cercospora* leaf spot by HSI can be a good reporter of sugar beet variety resistance (Leucker et al. 2016, 2017).

Kuska et al. (2015, 2017) investigated the resistance reaction of different barley genotypes to powdery mildew (*Blumeria graminis* f.sp. *hordei*). They proved the potential of HSI to characterize this pathosystem depending on the resistance/susceptibility of the infected barley genotype.

The wavelength near 700 nm had the most pronounced response to *Cercospora* leaf spot of sugar beet. This response is due to the correlation between this wavelength and chlorophyll content (Mahlein et al. 2010). In the current study, the effect of FHB infection was most pronounced for the wavelengths 500, 675, and 760 nm in the VIS-NIR range, and for wavelengths 1440, 1884, and 2000 nm in the SWIR range.

Spectral vegetation indices (SVIs) indicate specific parameters of plant functions. This reduces the data dimensionality and the computation time as well instead of considering the entire spectrum, (Delalieux et al. 2009; Mahlein et al. 2010). However, a single vegetation index is not specific enough to differentiate between plant diseases or stress factors (Mahlein et al. 2010). Huang et al. (2007) correlated the DS to PRI and proved the potential of PRI to quantify yellow rust severity in winter wheat.

Out of the six vegetative indices used in this study, NDVI, PRI, PSSR (a, b and c), and WI (Blackburn 1998a; Gamon et al. 1992; Penuelas et al. 1997; Rouse et al. 1974), PSSRa and PSSRb had the highest sensitivity for early detection of *Fusarium* infection. This is in accordance with the study of (Alisaac et al. 2018), which proved a high correlation between these indices and FHB infection on the spike scale. In the case of apple scab infection, Delalieux et al. (2009) claimed that the performance of SVIs depends on disease development and leaf age. The presence of plant pigments including chlorophyll a and chlorophyll b plays a key role affecting spectral reflectance (Moroni et al. 2013). These pigments are controlled by the chemical and the biological activity of the host plant (Sims and Gamon 2002). The second role affecting the spectral reflectance is the physical structure and the water content of the plant tissue (Fourty and Baret 1997). Mahlein et al. (2010) used PSSRa and PSSRb in combination with other SVIs to characterize *Cercospora beticola*, *Erysiphe beticola*, and *Uromyces betae* on sugar beet. They proved the possibility to differentiate between the three diseases using at least two indices in combination. As shown in this study, SVIs can be good indicators when they are correlated to each other and the parameters derived from CFI and IRT (Figure 9). This correlation can help to substitute one sensor by the other according to the application conditions in the field or the greenhouse.

An evaluation of the sensor's feasibility to monitor plant diseases depends on the individual parameters of each sensor. Previous studies showed that HSI imaging technologies are more sensitive compared with non-imaging technologies (Mahlein et al. 2012a). A further factor influencing the data quality is the distance between the object and the sensor. It is therefore of high importance to identify a proper measuring setup for each individual sensor. In the current approach, optical sensors with different technical parameters were compared with each other based on their data.

A support vector machine (SVM) approach was applied by Alisaac et al. (2018) to classify healthy and *Fusarium*-infected spikes using SVIs derived from HSI. They showed an increased accuracy starting from 79% at 4 dai to 95% at 17 dai. This is in accordance with the results of the current study that proved increasing accuracy from 78% at 3 dai to 100% at 12, 17, and 21 dai. The decrease in classification accuracy 30 dai is due to the senescence in the non-inoculated control spikelets.

In the current study, the highest classification accuracy of 89% was achieved based on the spectral vegetation indices of the spikelets derived from HSI. This was followed by parameters derived from IRT and CFI with classification accuracies of 82 and 79%, respectively. This confirms the results of Moshou et al. (2005) who compared HSI with CFI to discriminate wheat leaves infected with yellow rust from healthy leaves. They showed that the classification accuracy using three bands from HSI was higher than using CFI parameters.

In the current approach, combining parameters from IRT and HSI gave the best improvement in the classification accuracy especially at 30 dai. Other combinations (i.e., IRT-CFI, CFI-HSI) gave no improvement if the classification accuracy compared with the individual sensor. This is in contrast with the results of Chaerle et al. (2007) and Moshou et al. (2005). They proved that IRT provides a higher potential of non-invasive measurement when combined with CFI to characterize plant diseases. In addition, combining CFI with HSI parameters improved the accuracy of quadratic discriminant analysis (QDA) to 94.5% compared with the individual sensor when they were used to classify *Puccinia striiformis* infection. These results are due to the differences in the host plant and the pathogen in these studies.

Berdugo et al. (2014) applied a discriminant analysis approach using multi-sensor data (IRT-CFI-HSI) on cucumber diseases. They proved the possibility of early discrimination of symptoms of *Cucumber mosaic virus* (CMV), *Cucumber green mottle mosaic virus* (CGMMV), and powdery mildew due to *Sphaerotheca fuliginea* on cucumber. In the current

study, multi-sensor data of IRT-CFI-HSI did not improve the accuracy compared with the other combinations. This shows that the combination of IRT-HSI was superior not only to the other combinations but also to multi-sensor data (IRT-CFI-HSI) in monitoring FHB on wheat.

4.1.5. Conclusions

The present study showed that the use of different sensors allows to detect FHB infection on wheat spikelets and to monitor the damage of *Fusarium* species on wheat spikes. This can improve resistance phenotyping of wheat to FHB. Sensors data derived from IRT, CFI, and HSI showed a high correlation, and combined, they are describing the development of disease severity. Data derived from HSI was most sensitive to identify the early response of wheat plants to FHB infestation followed by IRT and CFI. The combination of data derived from HSI-IRT gave superior accuracy over the time of the experiment, and it seems to be most promising. Sensor data can contribute substantially to the monitoring of FHB but the suitability of multi-sensor application under field conditions and on canopies of cereal will be the next step of investigations.

4.2. Hyperspectral Quantification of Wheat Resistance to *Fusarium* Head Blight: Comparison of Two *Fusarium* Species

Elias Alisaac, Jan Behmann, Matheus T. Kuska, Heinz-Wilhelm Dehne, Anne-Katrin Mahlein. 2018. European Journal of Plant Pathology, 152:869-884. DOI: 10.1007/s10658-018-1505-9

Author Contributions

Elias Alisaac conceived the experiment (50%), E.A. performed the experiment (100%), E.A. analyzed the data (75%), E.A. wrote the paper (75%).

This text was not modified from the published version.

Abstract

Interactions of *Fusarium* species with different wheat varieties differ in their temporal dynamics and symptom appearance. Reliable and objective approaches for monitoring processes during infection are demanded for plant phenotyping and disease rating. This study presents an automated method to phenotype wheat varieties to *Fusarium* head blight (FHB) using hyperspectral sensors. In time-series experiments, the optical properties of spikes infected with *F. graminearum* or *F. culmorum* were recorded. Two hyperspectral cameras, in visible and near-infrared (VIS-NIR, 400-1000 nm) and shortwave-infrared (SWIR, 1000-2500 nm) captured the most relevant bands for pigments, cell structure, water, and further compounds. Correlations between disease severity (DS), spike weight, spectral bands and vegetation indices were investigated. Following, the detectability of infections was assessed by the Support Vector Machine (SVM) classifier. A variety ranking based on AUDPC was performed and compared to a fully-automated approach using Non-metric Multi-Dimensional Scaling (NMDS). A high correlation was found between the spectral signature and DS in 430-525 nm, 560-710 nm and 1115-2500 nm. All indices from the VIS-NIR showed a high correlation with DS and, for the first time, this was also confirmed for three indices from the SWIR: NDNI, CAI and MSI. Using SVM, differentiation between healthy and infected spikes was possible (acc. > 0.76). Furthermore, the possibility to differentiate between *F. graminearum* and *F. culmorum*-infected spikes has been verified. The NMDS approach was able to reproduce accurately the variety ranking and outlines the potential of hyperspectral imaging to phenotype the variety susceptibility for improved breeding processes.

4.2.1. Introduction

Fusarium head blight (FHB) is considered as one of the most important fungal diseases of wheat because it causes high crop losses and can lead to high economic losses (Johnson et al. 2003; McMullen et al. 2012; Salgado et al. 2015). In addition, kernels of infected spikes are small, shrunken, discolored and light in weight and the technological quality is also affected (Kreuzberger et al. 2015; McMullen et al. 2012). The most important *Fusarium* species inducing FHB are *Fusarium graminearum*, *F. culmorum*, *F. poae*, *F. avenaceum*, *F. sporotrichioides*, *F. equiseti* (Aoki et al. 2014; O'Donnell et al. 2004; Parry et al. 1995).

In wheat, FHB infection is initiated by airborne spores resulting from the mycelium and from the debris of the former crop. Infection may take place during flowering, preferably at warm temperature > 25°C with 100% relative humidity (RH). The germ tubes of conidia enter the spikelet tissue through the natural openings in the spikelet and the degrading anther tissue (Bushnell et al. 2003; Osborne and Stein 2007). First symptoms appear on infected spikelets as water-soaked spots. With ongoing disease development, the chlorophyll decomposes and the whole spikelet becomes bleached. In warm humid weather, pinkish-red mycelium and conidia develop in the infected spikelets (Trail 2009). The infection spreads to adjacent spikelets horizontally and vertically, up and down through the entire spike (Figure 11) (Al Masri et al. 2017; Brown et al. 2010; Ribichich et al. 2000). The main reason to focus on FHB is its ability to produce mycotoxins. Mycotoxins secreted by *Fusarium* species are toxic and detrimental to humans and animal nutrition (McCormick 2003; Pestka 2010). The main mycotoxins produced by these species are trichothecenes, mainly deoxynivalenol (DON) and its derivatives as well as zearalenone, fusaric acid, fusarenon or enniatins (Birzele et al. 2002; Ferrigo et al. 2016).

In order to achieve effective management of FHB, different control strategies must be combined. Integrated crop protection strategies include cultural practices such as crop rotation, biological control or fungicides application (Gilbert and Haber 2013). Thereby, breeding of resistant wheat varieties contributes to the integrated control of FHB (Dweba et al. 2017). These varieties should combine both types of FHB resistance (Mesterházy et al. 2007), i.e. Type I resistance (resistance to the initial infection (penetration)), and Type II resistance (resistance against pathogen spread from the point of infection) (Schroeder and Christensen 1963). Effective resistance breeding needs interdisciplinary research, integrating plant breeding, phytopathology, informatics and long investigation time. To achieve resistant

varieties, an important step in breeding programs after generating a new genetic variation is phenotyping. This approach relies on precise visual assessment of the disease severity after artificial inoculation (Steiner et al. 2017). According to Furbank and Tester (2011), precise and innovative methods for identifying and characterizing disease symptoms in an early stage of infection are needed. Until today, the phenotyping process is still a limiting factor in plant breeding, because it is time-consuming, and cost-intensive (Mahlein 2016). In the case of FHB, this process is especially challenging as *Fusarium* species can infest the wheat spike and produce mycotoxins without developing visual symptoms. Within this context, optical sensors beyond the capability of the human eye are beneficial to improve phenotyping (Kuska and Mahlein 2018).

Various sensors are applied for the detection, identification, and quantification of plant diseases like thermography, fluorescence, and hyperspectral sensors (Mahlein 2016). Recently hyperspectral imaging has shown to be useful as a precise and non-destructive tool in characterizing resistance to powdery mildew in barley, and in lesion characterization in *Cercospora beticola*-sugar beet interaction (Kuska et al. 2017; Leucker et al. 2016; Thomas et al. 2017). One of the challenges in hyperspectral imaging is the high dimensionality and massive amount of data (Behmann et al. 2015; Fahlgren et al. 2015; Thomas et al. 2018). Spectral vegetation indices (SVIs) are a straightforward approach to reduce the data dimensionality relying on only a few specific wavelengths. Qualitative and quantitative information concerning the plant pigments, biomass, tissue structure, water content and plant chemicals can be obtained using these indices (Xue and Su 2017). SVIs showed a good capability to detect FHB on wheat and to discriminate sugar beet diseases caused by *Cercospora* leaf spot, powdery mildew and leaf rust (Bauriegel et al. 2011a; Mahlein et al. 2012b). Moreover, they have been used as features in the support vector machine (SVM) approach to classify sugar beet leaves infected with different pathogens (Rumpf et al. 2010).

The hypothesis of this study is, that wheat varieties differ in their susceptibility to FHB and that these differences can be determined and assessed by hyperspectral imaging. Therefore, hyperspectral images of different wheat varieties inoculated with *F. graminearum* or *F. culmorum* were taken in the spectral range from 400-2500 nm during the pathogenesis. A set of fifteen SVIs were used in SVM classification to discriminate healthy, *F. graminearum* and *F. culmorum*-infected spikes. Furthermore, a selection of SVIs was used in non-metric multidimensional scaling (NMDS) to rank wheat varieties according to their susceptibility to FHB.

This study is designed to improve non-destructive and non-invasive screening methods for FHB resistance using the application of hyperspectral imaging technique.

4.2.2. Material and Methods

4.2.2.1. Plant Cultivation

Greenhouse experiments were performed using seven varieties of spring wheat (*Triticum aestivum* L.) with different resistant degrees to FHB (ranging from 1-9 scale where 1 is highly resistant and 9 is highly susceptible): Thasos (3) (Strube, Söllingen, Germany), Triso (4) (DSV, Lippstadt, Germany), Passat (4), Scirocco (4), Chamsin (5), Taifun (6) (KWS, Einbeck, Germany) and Sonett (6) (Syngenta, Basel Switzerland) (Anonymous 2017). Pots of 12×12×20 cm size were filled with a mixed substrate 1:3:6 of sand, horizon C and potting substrate ED 73 (Einheitserde, Sinntal-Altengronau, Germany). Five seeds per pot were cultivated at 20 ± 2°C and 50-70% RH (two pots for each variety). Pots were randomized in the greenhouse and supplemental artificial light (> 300 µmol m^{-2} s^{-1}, Philips SGR 140, Hamburg, Germany) was used to obtain a photoperiod of 16/8 h (day/night). After germination, two seedlings were left per pot and were supported by sticks to avoid lodging. Plants were watered as necessary.

4.2.2.2. *Fusarium* Inoculation and Disease Severity Assessment

Fusarium graminearum, isolate S.19, and *F. culmorum*, isolate 3.37 were used for inoculation (INRES-Plant Diseases and Plant Protection, University of Bonn, Germany). The isolates were obtained from infected wheat kernels from field experiments (Campus Klein-Altendorf, Rheinbach, Germany) in 2011 and 2004, respectively. They were stored as cryo culture at -80°C. The inoculum was produced according to the method of Moradi (2008) using potato dextrose agar (PDA, 39 gL^{-1}), potato dextrose broth (PDB, 24 gL^{-1}) and low strength potato dextrose agar (LSPDA, 12.5 gL^{-1} and agar-agar, 19.5 gL^{-1}). Conidia were harvested in water and the inoculum suspensions were adjusted to 10^5 conidia mL^{-1} using a Fuchs-Rosenthal chamber. Spikes of four plants of each variety were inoculated at plant growth stage (GS) 61-65 according to (Lancashire et al. 1991), with each *Fusarium* species separately by spraying the inoculum suspension until runoff. In addition, four control plants of each variety were mock-inoculated with water. For optimal infection, plants were incubated at 22-25°C and 95% RH for 48 h, by covering each treatment by a plastic bag according to Mesterházy et al. (2015). After incubation, six spikes of each treatment were fixed on a black metal grid in order to keep the spikes in the same orientation along the time of the experiment. Spikes were sprayed with

tap water until runoff every day, which kept the spikes wet for 1-2 h per day to provide appropriate conditions for disease development.

The disease severity (DS) was assessed according to the formula of Stack and McMullen (1998) 4, 6, 8, 10, 13, 17, 21 and 30 days after-inoculation (dai).

$$disease\ severity = \frac{symptomatic\ area\ of\ the\ spike}{whole\ \ area\ of\ the\ spike} * 100 \quad (1)$$

Reduction in spike weight was calculated as following:

$$spike\ weight\ reduction = \frac{spike\ weight_{control} - spike\ weight_{infected}}{spike\ weight_{control}} * 100 \quad (2)$$

Correlations and statistically significant differences between treatments in spike weight were calculated using RStudio. Spike Weight data were analyzed by standard analysis of variance (ANOVA) with a significance level $p \leq 0.05$, $n = 6$.

4.2.2.3. Hyperspectral Imaging

Hyperspectral imaging was performed with artificial illumination at 4, 6, 8, 10, 13, 17, 21, and 30 (dai). The reflectance of the spikes was recorded in the spectral range from 400 to 1000 nm using the hyperspectral camera ImSpector V10E (Spectral Imaging Ltd., Oulu, Finland) with a spectral resolution up to 2.8 nm and a sensor pixel size of 0.0074 mm which results in a spatial resolution of 0.219 mm per pixel. A spectral binning of 4 was used resulting in 211 hyperspectral bands. A SWIR-Camera (ImSpector N25E, Spectral Imaging Ltd., Oulu, Finland) with a spectral resolution up to 5.8 nm resulting in 256 hyperspectral bands was used to record hyperspectral images in the spectral range from 1000 to 2500 nm. The spatial resolution is 1.02 mm per pixel with 320 pixels per scan line. Both cameras and the illumination system were mounted on a motorized line scanner (Velmex BiSlide, Velmex Inc., Bloomfield, USA). Camera settings and the control of the motorized line scanner were adapted using the SpectralCube software (Spectral Imaging Ltd., Oulu, Finland). For hyperspectral imaging, spikes were laid horizontally with a homogeneous background. A homogeneous illumination was realized with six ASD-Pro-Lamps (Analytical Spectral Devices Inc., Boulder, Colorado, USA) at a distance of 665 mm and a 45° vertical slope to the spikes.

The whole setup was preheated for 30 minutes before image acquisition in order to get constant and reproducible illumination conditions. The cameras were focused manually and the exposure time was adjusted to the object. For image reflectance calculation four images were taken: A white reference bar (Spectral Imaging Ltd., Oulu, Finland) which reflects ~99% of

the radiated light. Subsequently, a dark current image was recorded by closing an internal shutter of the camera. Finally, the image of the spikes was taken with a subsequent second dark current image. The software "Processing Imspector 3.1" (Geoscap, Cologne, Germany) was used to calculate the reflectance from white reference and dark current measurements. The signals from hyperspectral images were smoothed by applying the Savitzky-Golay filter (25 centered supporting points and a third-degree polynomial). Masking and visualizing of image data was done using HSVaP ("Hyperspectral Visualization and Processing"), an Open Source software for supervised and unsupervised analysis of hyperspectral images. The program was initially developed in the IGG-Geoinformation, University of Bonn, and its development is continued in the INRES-Plant Diseases and Plant Protection department (available at http://www.ikg.uni-bonn.de/forschung/hsvap.html). It combines training data generation by active learning, clustering, classification and feature weighting in a uniform dataflow based on pure Java and established machine learning libraries. The calculation of mean spectral reflectance was done by MATLAB 2013a.

4.2.2.4. Spectral Vegetation Indices

In order to investigate the correlation between SVIs and FHB infection, fifteen vegetation indices related to different physiological parameters were calculated from the visible (VIS), the near-infrared (NIR) and the short-wave infrared (SWIR) ranges (Table 5). In the following text, the defined abbreviations for the indices are used. The full description can be found in Table 5. Pearson's correlation coefficient was calculated in RStudio to investigate the relationship between SVIs and DS.

4.2.2.5. Support Vector Machine Classification

Two class classification (healthy/infected) and multiclass classification (healthy/*F. graminearum*/*F. culmorum*) were performed both in RStudio using values of twelve calculated SVIs in VIS-NIR range and alternatively, using the whole spectral reflectance (432 bands). For the identification of FHB diseases, 1/3 of the data was selected randomly as training data to learn Support Vector Machine (SVM) classifier with Radial Basis Function (RBF) kernel (Cortes and Vapnik 1995). A grid-based approach was applied to optimize the parameter cost (C) and gamma (γ) to specify the best radial basis function. The test data was separated from the training data to evaluate the model by cross-validation. Important performance measures were the overall accuracy of the model and the sensitivity which gives the proportion of the correctly classified spikes of each class.

Table 5. Spectral vegetation indices used in this study: Equations, biological indicators, and the references are given.

Index	Equation	Indicator	Reference
modified Simple Ratio	$mSR = (R_{750} - R_{445}) / (R_{705} + R_{445})$	Green biomass	(Sims and Gamon 2002)
Normalized Differences Vegetation Index	$NDVI = (R_{800} - R_{670}) / (R_{800} + R_{670})$	Biomass, leaf area	(Rouse et al. 1974)
Photochemical Reflection Index	$PRI = (R_{531} - R_{570}) / (R_{531} + R_{570})$	Epoxidation state of xanthophyll cycle; pigments and photosynthetic radiation use efficiency	(Gamon et al. 1992)
Structure Insensitive Pigment Index	$SIPI = (R_{800} - R_{445}) / (R_{800} + R_{680})$	Carotenoid: chlorophyll a ratio	(Penuelas et al. 1995)
Pigment Specific Simple Ratio	$PSSRa = R_{800} / R_{680}$	Chlorophyll a	(Blackburn 1998a; Blackburn 1998b)
	$PSSRb = R_{800} / R_{635}$	Chlorophyll b	
	$PSSRc = R_{800} / R_{470}$	Carotenoids	
Pigment Specific Normalized Difference	$PSNDa = (R_{800} - R_{680}) / (R_{800} + R_{680})$	Chlorophyll a	(Blackburn 1998a; Blackburn 1998b)
	$PSNDb = (R_{800} - R_{635}) / (R_{800} + R_{635})$	Chlorophyll b	
	$PSNDc = (R_{800} - R_{470}) / (R_{800} + R_{470})$	Carotenoids	
Plant Senescence Reflectance Index	$PSRI = (R_{680} - R_{500}) / R_{750}$	Plant senescence	(Merzlyak et al. 1999)
Water Index	$WI = R_{900} / R_{970}$	Water content	(Penuelas et al. 1997)
Moisture Stress Index	$MSI = (R_{1599} / R_{819})$	Water stress	(Hunt and Rock 1989)
Cellulose Absorption Index	$CAI = 0.5 (R_{2000} + R_{2200}) - R_{2100}$	Cellulose	(Daughtry 2001; Nagler et al. 2003)
Normalized Difference Nitrogen Index	$NDNI = [\log(1/R_{1510}) - \log(1/R_{1680})] / [\log(1/R_{1510}) + \log(1/R_{1680})]$	Nitrogen	(Serrano et al. 2002)

4.2.2.6. Multi-Dimensional Scaling for Information Compression

A high number of suitable vegetation indices for the detection of plant stress, senescence, and bleaching from the VIS, NIR, and SWIR spectral reflectance were investigated in this study. Each of these mathematical formulas provides a slightly different view on parameters of interest from hyperspectral data. To extract an informative description of the plant's state or plant diseases, a single index is not enough but the comprehensive information of multiple indices needs to be combined (Behmann et al. 2015; Mahlein et al. 2010; Rumpf et al. 2010).

Non-metric multidimensional scaling (NMDS) is an unsupervised method to define a non-parametric transformation between an original space and a target space with defined dimensionality by minimizing the change in the inter-point Euclidean distances d_{ij}, measured by "Stress" (Kruskal 1964).

$$Stress_D(x_1, x_2, \ldots, x_N) = \left(\frac{\sum_{i,j} \left(d_{ij} - \|x_i - x_j\|\right)^2}{\sum_{i,j} d_{ij}^2} \right)^{1/2} \quad (3)$$

Based on a dissimilarity matrix *D*, the stress is minimized by a gradient descent approach leading to the transformed data points *x* in the target space with desired dimensionality (Borg and Groenen 2005). The resulting coordinates are not fixed with respect to rotation or translation as only the distances between the data points are regarded. Here, NMDS was used to compress the information of the seven most relevant vegetation indices in a one-dimensional ordinal scale representing the disease severity sensed by the hyperspectral camera. The rating of the respective variety control group was subtracted to remove the effect of natural senescence.

4.2.3. Results

4.2.3.1. Disease Severity

In all varieties, senescence started in healthy spikes from 21 dai. First FHB symptoms appeared on all inoculated varieties 4 dai (Figure 11). The disease severity of *F. graminearum* started < 20% in all varieties and developed gradually. In Scirocco, severe symptoms have been shown already 4 dai with a disease severity > 60% (Figure 12). The infection increased gradually in moderate resistant varieties until the end of the experiment, whereas the infection increased rapidly in susceptible varieties. The disease severity was > 50% in Scirocco, Taifun and Thasos from 8 dai. The disease severity of *F. culmorum* was lower than of *F. graminearum* in all tested varieties except Chamsin. The infection increased rapidly in Chamsin and Taifun and the

disease severity was > 50% 10 dai. Finally, the high susceptible varieties had completely bleached spikes 13 dai (Figure 11).

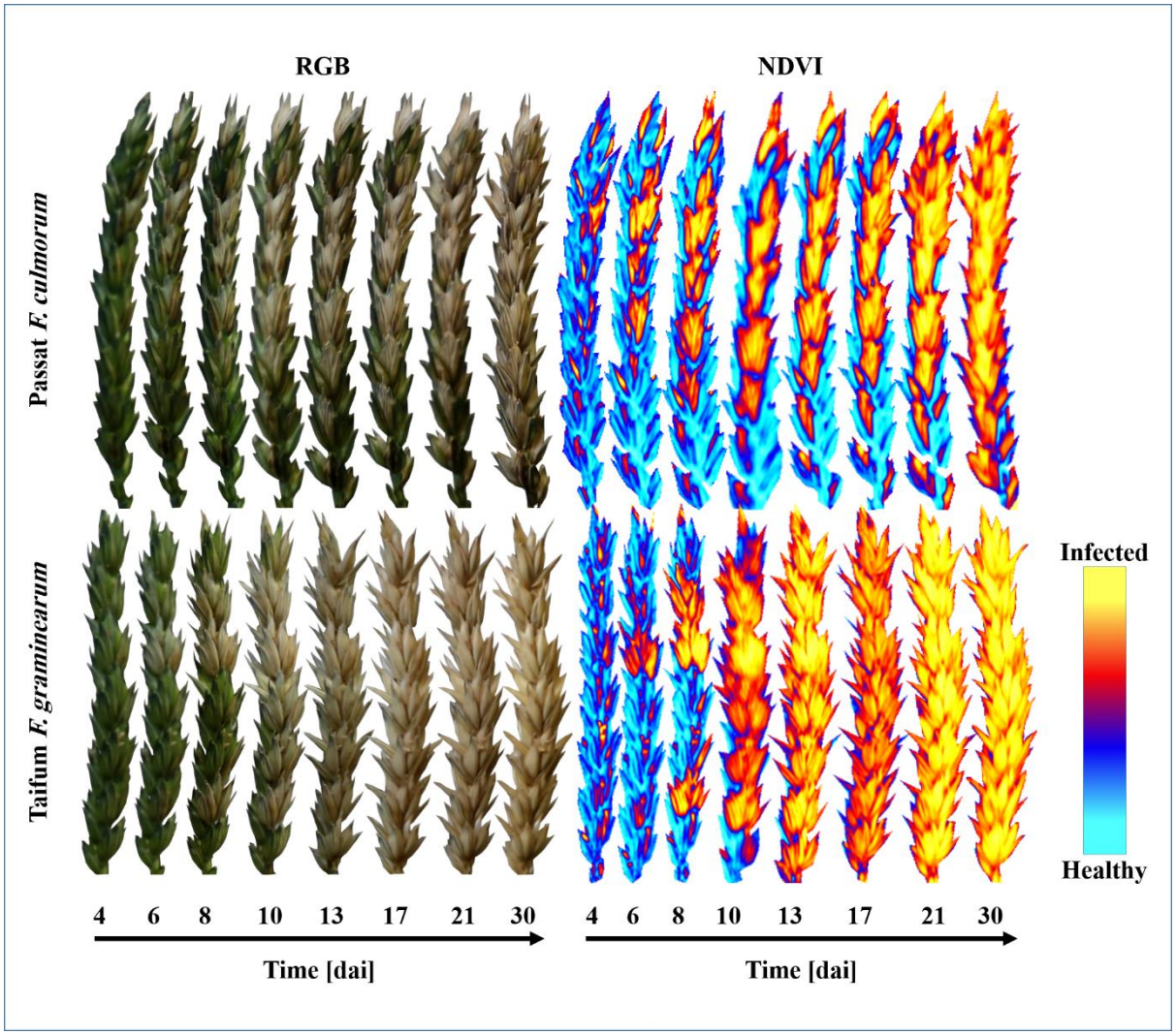

Figure 11. Visual symptoms of FHB on moderately resistant variety (Passat) and susceptible variety (Taifun) in different development stages of the disease, with NDVI visualization.

4.2.3.2. Progress of Spectral Signature of Control and FHB Infected Spikes

Mean spectral signatures of control spikes in all varieties were similar from 4-8 dai (Figure 13a). Taifun showed a slight increase in VIS and SWIR reflectance from 10 dai (Figure 13b). The similarity in the spectral signature of control spikes lasted until 21 dai (Figure 13c). Due to differences in senescence state, significant differences in spectral signatures can be shown 30 dai.

Changes in spectral signatures of *F. graminearum*-infected spikes appeared from 4 dai (Figure 14a). The susceptible variety Scirocco showed higher reflectance in the spectral range 460-670 nm and in the SWIR. With ongoing disease development, spectral signatures differed according

to the resistance of the varieties starting from 8 dai (Figure 14b). The highly susceptible varieties Scirocco and Taifun showed an increased reflectance along the whole spectral range. In contrast, a slight increase in reflectance intensity has been shown in the moderate resistant varieties Chamsin and Passat (Figure 14b).

Varieties infected with *F. culmorum* showed less differences in spectral signatures. The susceptible variety Taifun showed an increased reflectance from 550-670 nm and in the SWIR from 4 dai (Figure 14d). This reflectance pattern became more prominent 13 dai (Figure 14e). Passat showed an increased reflectance over the whole spectrum during the experimental period (Figure 14d,e,f). Whereas, moderate resistant varieties showed a later increase of the reflectance in VIS and SWIR and with a different spectral pattern.

All varieties infected with any of *Fusarium* species showed lower reflectance in the NIR range comparing to control spikes starting at 4 dai. The spectral signatures of infected spikes showed a non-vegetative pattern in the VIS-NIR range (Figure 14c,f).

4.2.3.3. Spectral Signature and Spectral Vegetation Indices Correlation with Disease Severity

To investigate the affected wavelengths by FHB, Pearson's coefficient between all spectral bands and disease severity was calculated (Figure 15). For this approach, hyperspectral signatures were separated to identify important time periods in the pathogenesis in groups for 4-10 dai, 13-30 dai, and 4-30 dai. A high positive correlation ($r > 0.75$) has been shown in the spectral ranges 430-525 nm, 560-710 nm and 1115-2500 nm in all time period groups. Negative correlation ($r < -0.6$) has been shown in the spectral range 740-810 nm using the measurement time points 4-10 dai. This correlation decreased using 4-30 dai and 13-30 dai as data sets.

The fifteen proved vegetation indices which correlated with physiological parameters (Table 5), showed a high correlation with disease severity (Figure 16a). The indices NDVI, SIPI, PSNDa and PSNDb showed the highest absolute correlation with the disease severity ($r > 0.81$) in the VIS-NIR range 4 dai. Whereas in the SWIR, MSI reached a peak correlation with disease severity of $r = 0.9$. During the experimental period, the absolute correlation between the calculated spectral indices and disease severity increased until 21 dai. In addition, mSR, PSSRa, PSSRb and CAI showed an increased absolute correlation until 30 dai.

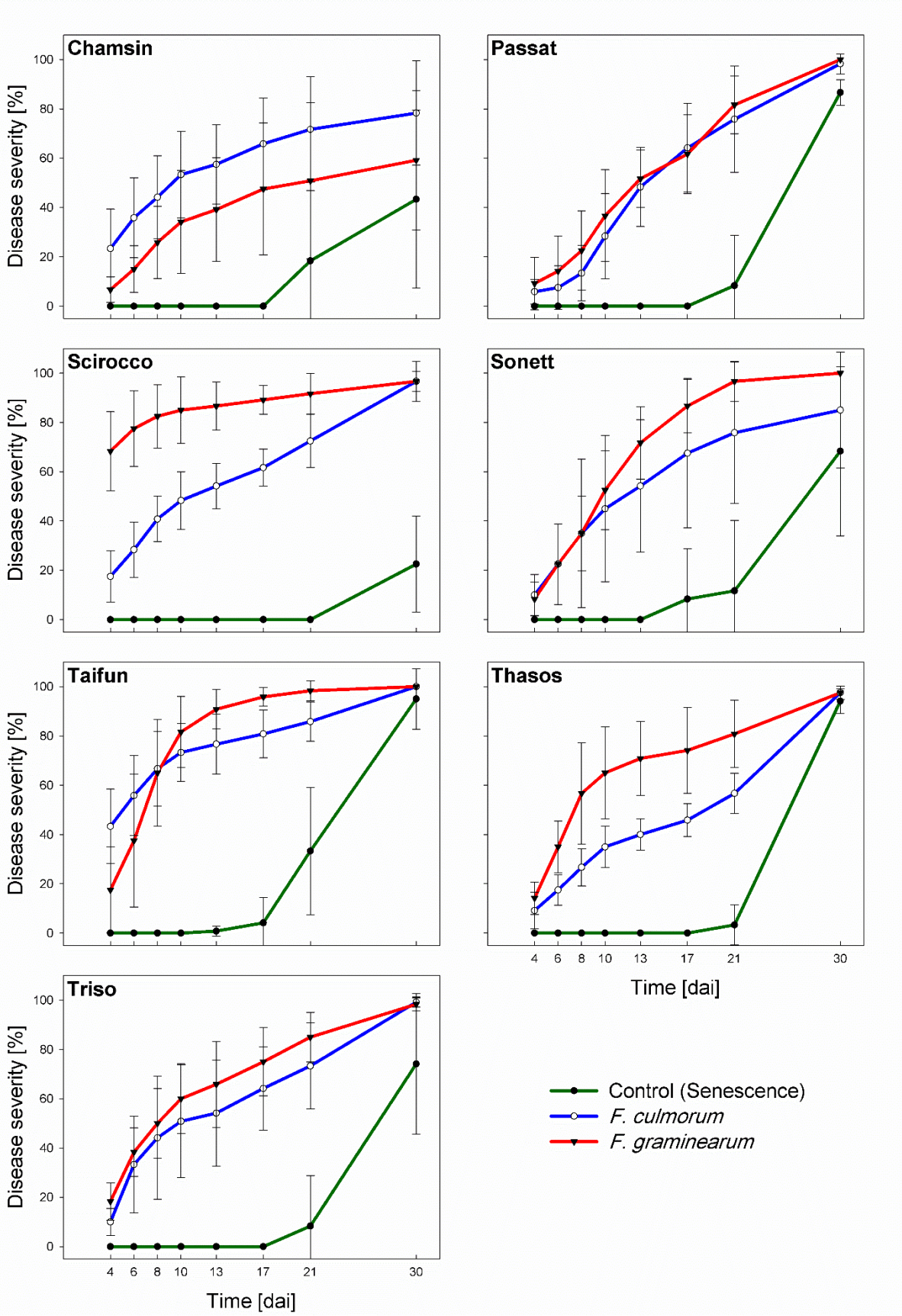

Figure 12. Disease progress curve of wheat varieties inoculated with mock inoculation (water), *F. graminearum*, and *F. culmorum* separately. (mean ± SD, *n* = 6).

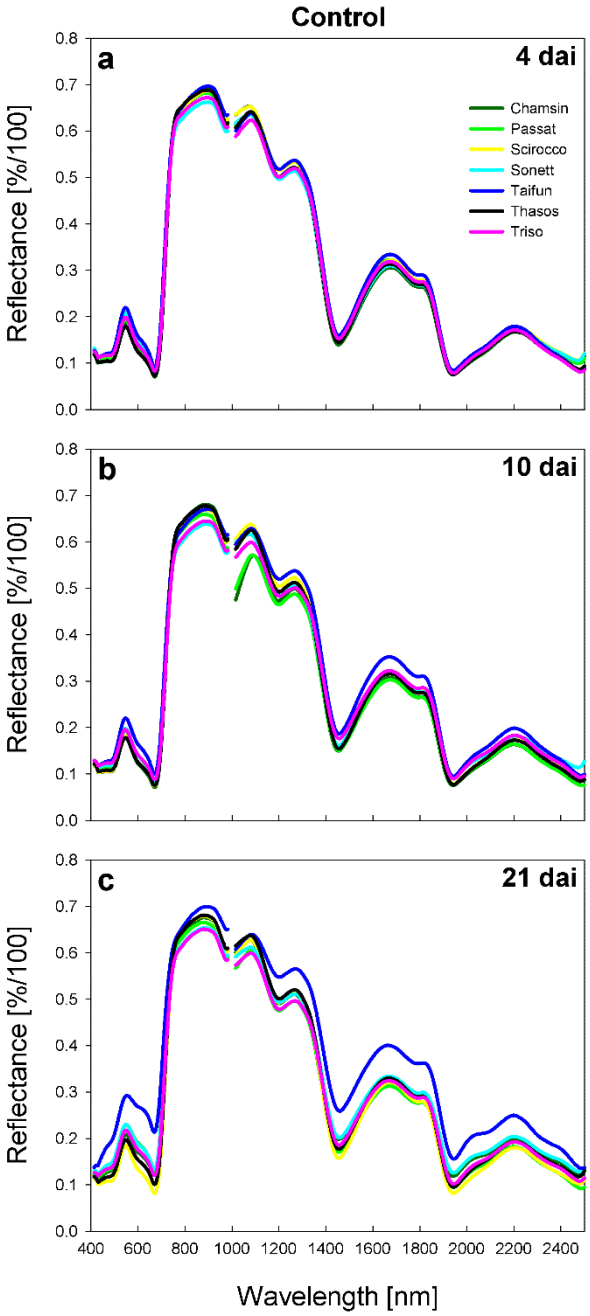

Figure 13. Progress of spectral signature of control spikes 4, 21, and 21 dai respectively.

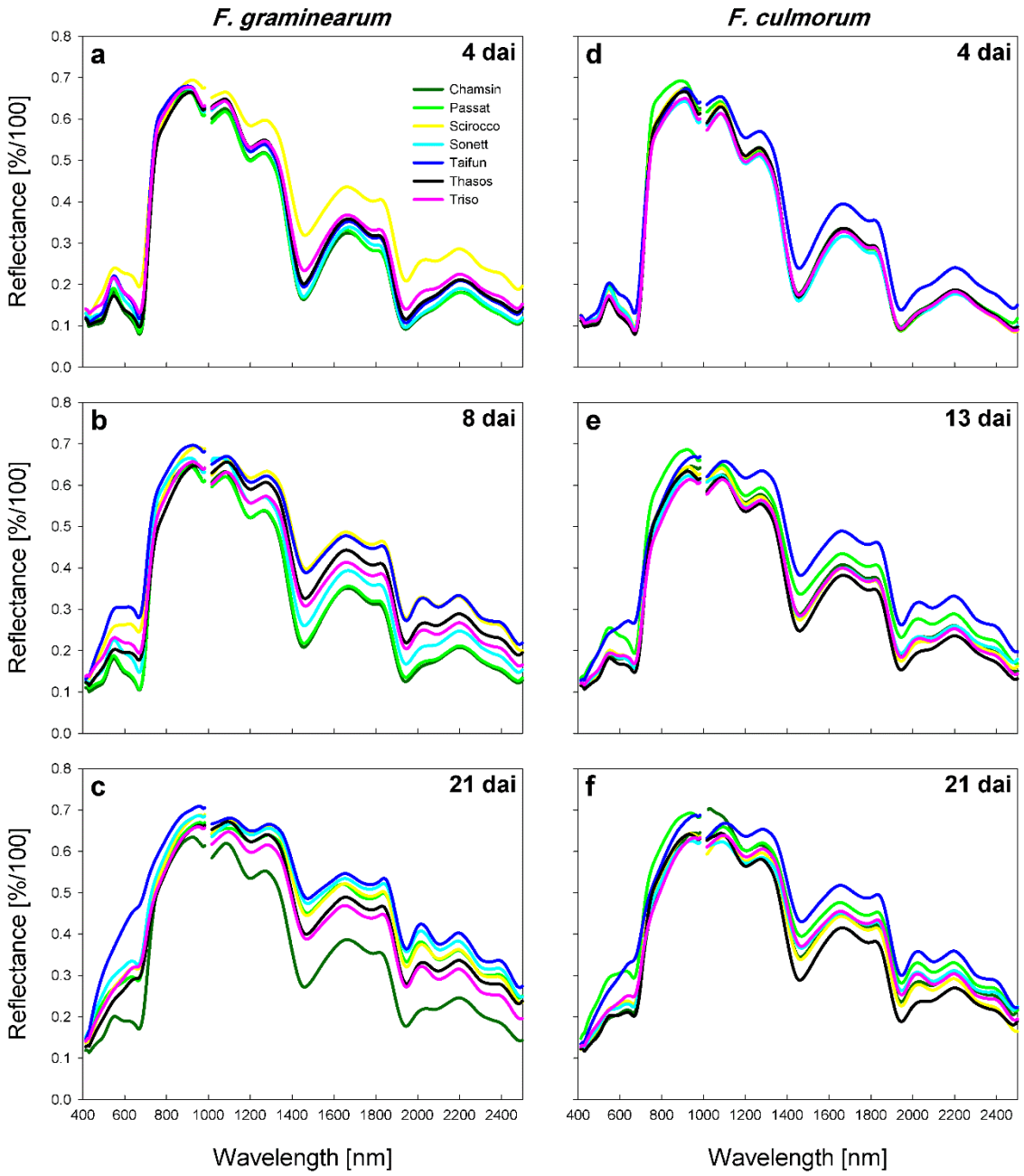

Figure 14. Spectral signatures of *F. graminearum*-infected spikes (a, b, c) 4, 8, and 21 dai respectively. *F. culmorum*-infected spikes (d, e, f) 4, 13, and 21 dai respectively.

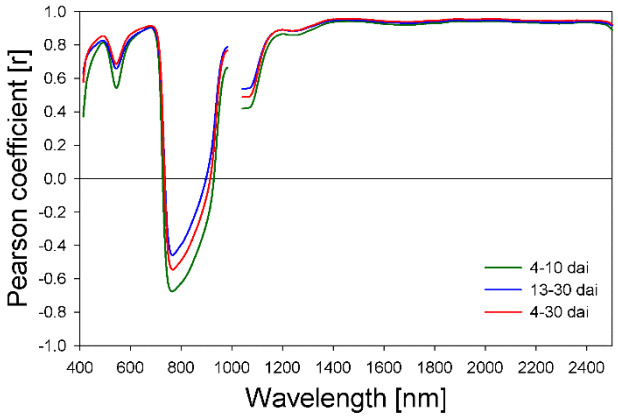

Figure 15. Correlation between spectral signature and disease severity using the data 4-10 dai, 13-30 dai, and 4-30 dai.

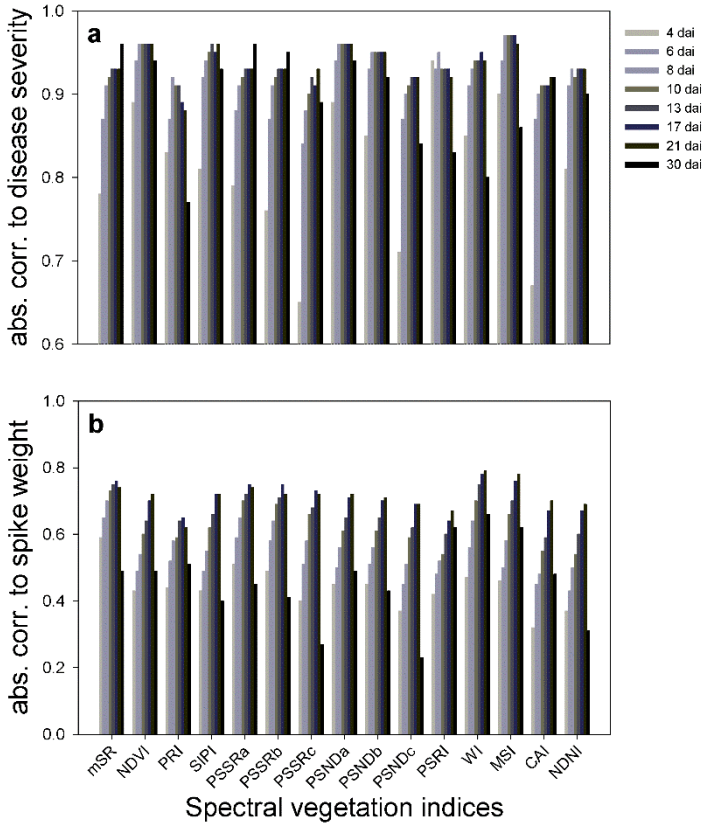

Figure 16. Correlation between spectral vegetation indices and disease severity (a), and correlation between spectral vegetation indices over time and spike weight at harvest of wheat varieties (b).

4.2.3.4. Effect of FHB on Spike Weight and Correlation with Spectral Vegetation Indices

The loss in spike weight depended on the variety and the inoculated *Fusarium* species (Figure 17). Reduction in spike weight caused by *F. graminearum* was higher than by *F. culmorum* in all varieties except Chamsin and Taifun. The spike weight reduction due to *F. graminearum*

ranged between 30.86% in Taifun and 67.30% in Passat. The effect of *F. culmorum* ranged between 28.63% in Sonett and 51.84% in Chamsin.

SVIs showed a gradual increased correlation over time with spike weight at harvest until 13 dai or 21 dai depending on the specific index (Figure 16b). For mSR the highest correlation was reached at 13 dai by $r = 0.75$. Afterward, WI had the highest correlation with the spike weight reduction until 21 dai ($r = 0.79$).

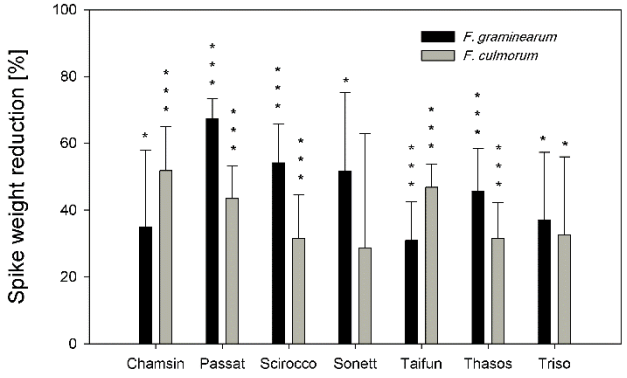

Figure 17. Normalized reduction in spike weight of wheat varieties caused by *Fusarium* species. Data were analyzed by standard analysis of variance (ANOVA, $n = 6$), marked by significance (*, $p \leq 0.05$) or high significance, (***, $p \leq 0.001$).

4.2.3.5. Two Class and Multiclass Classification of Control and FHB Infected Spikes

In the first step, SVM was used in two-class classification to differentiate between healthy spikes and FHB infected spikes. Classification results based on SVIs calculated from the VIS-NIR range were compared in their accuracies with the classification results based on spectral reflectance (Table 6). Both classification accuracies increased over time with increasing disease severity until 4-8 dai and 13-17 dai. Thereafter, accuracies started to decrease when the natural senescence started in control spikes (Table 6). Except for the first two measuring time points, the accuracy of spectral reflectance classification was higher than the accuracy of SVIs classification. In general, the accuracy was > 0.76 in both cases and reached 0.99 at 13 and 17 dai for the classification based spectral reflectance.

The multiclass classification has been implemented to investigate the capability of SVM to discriminate healthy, *F graminearum*, and *F. culmorum*-infected spikes. In the case of SVIs classification, the accuracy increased gradually until 13 dai and reached 0.76, then slight decrease has been shown until the end of the experiment (Table 6). Accuracy of spectral reflectance classification fluctuated during the experimental period. The highest accuracy of

0.77 has been reached 13 dai. Except for 6 dai, the accuracy was higher than > 0.61 for all measured time points.

Table 6. Accuracies of two-class and multiclass SVM classification based on hyperspectral data over time. Comparison between classification accuracies using twelve spectral vegetation indices (SVIs) and using the whole spectral reflectance 432 bands.

Time	Two class classification		Multiclass classification	
	SVIs	Reflectance	SVIs	Reflectance
4	0.79	0.76	0.49	0.65
6	0.87	0.86	0.61	0.51
8	0.93	0.94	0.67	0.67
10	0.89	0.96	0.71	0.61
13	0.94	0.99	0.76	0.77
17	0.95	0.99	0.70	0.70
21	0.87	0.96	0.74	0.68
30	0.90	0.93	0.58	0.61

The confusion matrix at 13 dai shows that discrimination between control and *Fusarium* spp. infected spikes using SVM classification is possible with a general accuracy of > 0.76 (Table 7). Control spikes are better predicted with a sensitivity of > 0.97. Whereas, the prediction between *F graminearum* and *F. culmorum*-infected spikes is possible in advances stages of infection with an average sensitivity of 0.65 (Table 7). Results of SVM multiclass classification based on hyperspectral data over the experimental period are indicated in Table 8.

Table 7. Confusion matrix of SVM multiclass classification 13 dai. Comparison between classification results using spectral vegetation indices (SVIs) (above), and using the whole spectral reflectance (below).

SVI				
		Ground truth		
		Control	*F. culmorum*	*F. graminearum*
Prediction	Control	29	1	2
	F. culmorum	1	14	4
	F. graminearum	0	12	21
	Sensitivity	0.97	0.52	0.78

Reflectance				
		Ground truth		
		Control	*F. culmorum*	*F. graminearum*
Prediction	Control	26	0	1
	F. culmorum	0	19	9
	F. graminearum	0	9	20
	Sensitivity	1	0.68	0.67

Table 8. Results of SVM multiclass classification based on hyperspectral data over time. Comparison between classification results using spectral vegetation indices (SVIs), and using the whole spectral reflectance.

Time [dai]	SVIs				Reflectance			
	Accuracy	Sensitivity			Accuracy	Sensitivity		
		Control	*F. culmorum*	*F. graminearum*		Control	*F. culmorum*	*F. graminearum*
4	0.49	0.70	0.45	0.31	0.65	0.89	0.48	0.60
6	0.61	0.74	0.52	0.54	0.51	0.87	0.62	0.16
8	0.67	1.00	0.23	0.86	0.67	1.00	0.70	0.35
10	0.71	0.84	0.64	0.63	0.61	0.73	0.37	0.70
13	0.76	0.97	0.52	0.78	0.77	1.00	0.68	0.67
17	0.70	0.89	0.37	0.88	0.70	0.90	0.71	0.52
21	0.74	0.94	0.54	0.71	0.68	0.87	0.32	0.84
30	0.58	1.00	0.64	0.21	0.61	1.00	0.74	0.10

4.2.3.6. Variety Ranking Based on Area under Disease Progress Curve and Non-Metric Multi-Dimensional Scaling

Spectral vegetation indices which are highly correlated to disease severity were selected due to their potential capability to differentiate between healthy and infected spikes. These SVIs were projected by NMDS onto a one-dimensional ordinal scale. This scale represents the disease severity sensed by the hyperspectral camera.

Figure 18 shows the variety ranking according to the area under disease progress curve (AUDPC) (Figure 18a,c), and non-metric multidimensional scaling (NMDS) (Figure 18b,d). The proved varieties showed different responses to the two investigated *Fusarium* species indicated in AUDPC (Figure 18a,c). The varieties Scirocco and Taifun infected with *F. graminearum* showed high susceptibility with an AUDPC > 2000 (Figure 18a). In contrast, Chamsin showed moderate infestation with an AUDPC > 1000. Most proved varieties revealed an AUDPC between 1300 and 1700 due to *F. culmorum* infection (Figure 18c). High susceptibility to *F. culmorum* was only indicated by Taifun with an AUDPC > 2000.

The results show that most proved varieties stayed in the same position in the ranking either using AUDPC or NMDS. Slight differences have been shown in variety order. The ranking of *F. graminearum*-infected varieties (Figure 18a,b) Thasos and Sonett differed two levels up and down using NMDS comparing to the AUDPC. *F. culmorum*-infected variety Chamsin differed two levels up (Figure 18c,d). Triso and Scirocco differed one-level down. Thasos and Passat exchanged their ranking using NMDS comparing to AUDPC.

4.2.4. Discussion

The main effects of FHB on wheat spikes are chlorosis, collapse in spikelet tissue, and disorder in the water system of the spikelets and the spike. The extent and the dynamic of symptom development depend on the host plant resistance (Al Masri et al. 2017; Ha et al. 2016; Trail 2009). Former studies showed the feasibility of hyperspectral imaging to assess visible and non-visible symptoms caused by fungal diseases (Bauriegel et al. 2011a; Delalieux et al. 2009; Mahlein et al. 2010). Characteristic spectral signatures in the VIS-NIR and SWIR are caused by alterations in pigment composition, tissue structure and plant water content (Mahlein 2016). In this study, the spectral reflectance was affected according to the susceptibility of wheat variety. The reflectance increased in VIS from 430-525 nm, 560-710 nm due to a rapid invasion of the pathogen which resulted in chlorophyll decomposition. The increase in reflectance intensity of susceptible varieties was higher compared to resistant varieties. Comparing

Fusarium species, the reflectance in *F. graminearum*-infected spikes was higher compared to *F. culmorum*-infected spikes. This is presumably attributed to the high virulence of *F. graminearum* isolate used in this study comparing with *F. culmorum* isolate.

The correlation between disease severity and the individual spectral signature differs according to the symptoms caused by the pathogen (Mahlein et al. 2010). Plant senescence and chlorophyll decomposition result in an increase in reflectance intensity in the spectral ranges 400-530 nm and 550-740 nm (Merzlyak et al. 1999). This is consistent with the high correlation between the wavelengths from 430-525 nm and 560-710 nm and FHB disease severity confirmed in this study. Likewise, a high correlation of SVIs derived from the VIS-NIR range and disease severity has been confirmed.

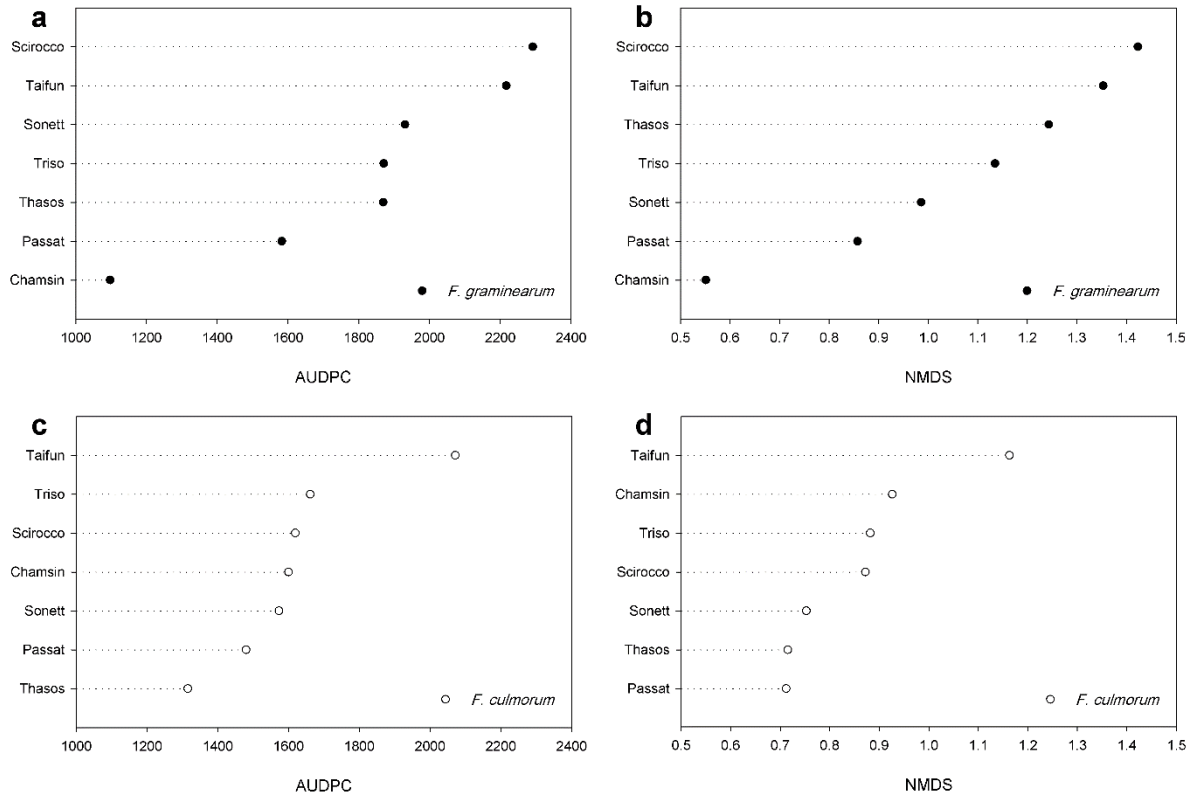

Figure 18. Varieties ranking according to their susceptibility to FHB using Area Under Disease Progress Curve (AUDPC) (a, c) and Non-metric multidimensional scaling (NMDS) (b, d).

Comparison between *Fusarium* spp. and *Cercospora beticola* shows that mycotoxins play a fundamental role in the pathogenicity resulting in the collapse of the tissue structure. *C. beticola* secretes cercosporin after penetrating the leaf through stomata (Daub and Ehrenshaft 2000). The main mycotoxins produced by *Fusarium* species is DON. A high correlation was observed between DON concentration produced by isolates of *Fusarium* species and isolate virulence, where *Fusarium* species use DON as protein synthesis inhibitor to overcome the

plant resistance (Beukes et al. 2018; Chetouhi et al. 2015; Kuhnem et al. 2015; Rotter et al. 1996).

In the NIR, Mahlein et al. (2010) proved a decrease in reflectance in the first stages of pathogenicity of *Cercospora beticola* on sugar beet leaves as a result of the collapse of the tissue structure. In advanced stages, the reflectance increased again in this range. According to Leucker et al. (2016), the spectral reflectance in NIR was higher in susceptible varieties than resistant varieties and accompanied with higher sporulation density in susceptible varieties of sugar beet. In the case of FHB infection, the NIR reflectance of spikelet invaded with red *F. culmorum* mycelium was higher than areas showing only bleached symptoms (Bauriegel et al. 2011a). Histological study of Ha et al. (2016) showed that dense growth of *F. graminearum* mycelium appeared more frequently and to a higher degree in the susceptible variety Milan than in the resistant variety Sumai-3. In the present study, the reflectance of spikes infected with both species was lower than the reflectance of non-infected spikes in the NIR. However, the correlation between varieties resistance and spectral reflectance in NIR could not be verified. The low correlation in NIR may be due to the three-dimensional structure of the wheat spike. Further investigations on the spikelet scale are still needed to correlate the reflectance in NIR with sporulation density, mycelium growth and variety resistance.

One of the main effects of FHB progress is early senescence (Trail 2009). The SWIR component of the electromagnetic spectrum was highly correlated to the water content, and might, therefore, serve as a proxy for early senescence and FHB progress. Following, a high correlation of DS with the spectral range in the SWIR was indicated. The reflectance in SWIR differed depending on the susceptibility of each variety. High susceptibility to FHB is related to early senescence and fast-draining in spike water and as a result, higher reflectance in SWIR. This is in accordance with the results presented by Iori et al. (2015). They proved the increase in reflectance in the SWIR over time in wheat varieties infected with *Stagonospora nodorum*. Comparing two apple varieties with different susceptibility to apple scab (*Venturia inaequalis*) showed higher reflectance in SWIR in susceptible variety than in resistant one, respectively (Delalieux et al. 2009).

Several studies showed a significant effect of *Fusarium* infection on the kernel protein content which is correlated to the kernel nitrogen concentration. The crude protein content increased due to *Fusarium* infection whereas the total glutenin and high-molecular-weight glutenin content decreased significantly in the wheat kernels resulted from *Fusarium* infected spikes

(Kreuzberger et al. 2015; Siuda et al. 2010; Wang et al. 2005). In this study, and for the first time, three indices derived from the SWIR range related to nitrogen (NDNI), cellulose (CAI) and water stress (MSI) showed a high correlation with FHB severity.

However, effective approaches for analyzing the obtained hyperspectral data with its high complexity are required. Machine learning approaches showed high capacities in hyperspectral data analysis and the potential to accelerate screening processes in plant resistance breeding (Behmann et al. 2015; Rumpf et al. 2010; Singh et al. 2016). In the present study, SVM classification was applied in multiple settings regarding time classes and features. The decrease in accuracy in later stages of FHB pathogenesis is due to the senescence in control spikes. The classification accuracy was lower using the SVIs than using the whole spectral reflectance which considered the water stresses detected in the SWIR caused by FHB. Interestingly, it was possible to differentiate between the infections of two *Fusarium* species by multiclass classification. This result could be due to the differences in the isolates' virulence more than differences in symptoms caused by both species.

The lack in FHB resistant varieties requires more efforts to investigate new resistance sources through wild and domesticated wheat germplasm diversity (Steiner et al. 2017). Due to the difficulties in Type I resistance assessment, most QTLs have been identified to be involved in Type II resistance (Buerstmayr et al. 2009; Steiner et al. 2017). Mesterházy et al. (2007) emphasized the necessity of including Type I resistance in breeding programs. The traditional rating of plant disease severity depends on AUDPC which is used to combine multiple observations of disease severity into a single value (Simko and Piepho 2012). It has been shown that the AUDPC can be reproduced with high accuracy by the combination of multiple SVIs transformed by NMDS. The differences in varieties ranking using the traditional AUDPC and NMDS could be attributed to two factors that were taken into account in the NMDS approach. The first, the data of control plants has been subtracted to omit the natural senescence. The second, the data of the first and the last measuring dates has been neglected to exclude the extreme values.

During the last decades, the FHB epidemics frequency increased in the main wheat production regions in the world. This could be attributed to the changes in the agricultural practices like reduced tillage, and the intensification of maize which is one of the main hosts of FHB in crop rotation (McMullen et al. 2012). Many studies monitored the geographic specificity in *F. graminearum* and *F. culmorum* chemotypes in wheat-producing countries (Alkadri et al. 2014;

van der Lee et al. 2015; Talas et al. 2011; Ward et al. 2008). They identified the changes in *Fusarium* dominant chemotypes during a short time. This emphasizes the need for continuous development of varieties with resistance to a wide range not only of *Fusarium* species but also of *Fusarium* chemotypes. Here, hyperspectral imaging and sophisticated machine learning approaches, as investigated in this study can improve the FHB resistance breeding process by an accelerated wheat resistance identification and characterization. New handheld hyperspectral cameras increase the flexibility and usability also by non-experts in the field (Behmann et al. 2018). These approaches assist e.g. the breeder for an improved determination of relevant wheat varieties.

4.2.5. Conclusions

Hyperspectral imaging is state-of-the-art technology and method for plant sciences and may be applied in plant resistance breeding. In addition to the assessment of the dynamics of FHB symptoms, it was feasible to differentiate not only between *Fusarium* infected spikes and healthy ones but also between spikes infected with different *Fusarium* species by an SVM classification. As an important outcome, an automated method to reproduce AUDPC depending on seven SVIs derived from the electromagnetic spectrum in VIS, NIR and SWIR was established. This will improve the automation in disease rating and will provide more objective information for the decision-making process in resistance breeding.

4.3. Assessment of *Fusarium* Infection and Mycotoxin Contamination of Wheat Kernels and Flour Using Hyperspectral Imaging

Elias Alisaac, Jan Behmann, Anna Rathgeb, Petr Karlovsky, Heinz-Wilhelm Dehne, Anne-Katrin Mahlein. 2019. Toxins, 11, 556. DOI: 10.3390/toxins11100556

Author Contributions

Elias Alisaac conceived the experiment (100%), E.A. performed the experiment (100%), E.A. analyzed the data (75%), E.A. wrote the paper (75%).

This text was not modified from the published version.

Abstract

Fusarium head blight (FHB) epidemics in wheat and contamination with *Fusarium* mycotoxins has become an increasing problem over the last decades. This prompted the need for non-invasive and non-destructive techniques to screen cereal grains for *Fusarium* infection, which is usually accompanied by mycotoxin contamination. This study tested the potential of hyperspectral imaging to monitor the infection of wheat kernels and flour with three *Fusarium* species. Kernels of two wheat varieties inoculated at anthesis with *F. graminearum*, *F. culmorum*, and *F. poae* were investigated. Hyperspectral images of kernels and flour were taken in the visible-near infrared (VIS-NIR) (400-1000 nm) and short-wave infrared (SWIR) (1000-2500 nm) ranges. The fungal DNA and mycotoxin contents were quantified. Spectral reflectance of *Fusarium*-damaged kernels (FDK) was significantly higher than non-inoculated ones. In contrast, spectral reflectance of flour from non-inoculated kernels was higher than that of FDK in the VIS and lower in the NIR and SWIR ranges. Spectral reflectance of kernels was positively correlated with fungal DNA and deoxynivalenol (DON) contents. In the case of the flour, this correlation exceeded r = -0.80 in the VIS range. Remarkable peaks of correlation appeared at 1193, 1231, 1446 to 1465, and 1742 to 2500 nm in the SWIR range.

4.3.1. Introduction

Changes in agricultural practices in particular intensification of maize production and the wide use of reduced tillage have resulted in an increased frequency of *Fusarium* head blight (FHB) epidemics worldwide (McMullen et al. 2012). Recent studies have demonstrated that the main causal agents, *Fusarium graminearum* and *F. culmorum* chemotypes, tend to show geographic specificity in the main wheat production areas (Alkadri et al. 2014; van der Lee et al. 2015; Pasquali et al. 2016; Talas et al. 2011). In Europe, the predominant *F. graminearum* chemotype is 15-acetyl-deoxynivalenol (15-ADON) whereas the predominant *F. culmorum* chemotype is 3-acetyl-deoxynivalenol (3-ADON) (Pasquali et al. 2016). However, drastic changes in *Fusarium* chemotypes were observed in some cereal-producing countries worldwide. For example, in Argentina, an increase in 3-ADON chemotypes was observed for four years (2001-2004). However, in Uruguay, this increase was shown in 15-ADON (Alvarez et al. 2009; Umpiérrez-Failache et al. 2013). Ward et al. (2008) reported a shift from the 15-ADON chemotype to the 3-ADON chemotype in Canada between 1998 and 2004. In North America, new strains of *F. graminearum* were isolated and these isolates showed type A trichothecene production, which is new for *F. graminearum* (Kelly et al. 2015; Varga et al. 2015). These results show the high ability of *Fusarium* species to adapt to variety resistance. Therefore, new varieties will be needed in the future with resistance to a wide range of *Fusarium* species and chemotypes. The first step to achieve these varieties is to screen a large number of wheat entries against FHB. For a better understanding of the host-pathogen interaction within the screening process, it should include not only disease symptoms but also the levels of fungal DNA and mycotoxins in the kernels.

The standard method for quantifying fungal DNA in infected kernels is by quantitative real-time polymerase chain reaction (qPCR) (Schaad and Frederick 2002), whereas the methods used to detect mycotoxin contents include immunochemical methods and analytical chemistry techniques (Krska et al. 2008; Meneely et al. 2011). However, these methods are laborious, time-consuming, and destructive. Therefore, there is a need for a fast, inexpensive, and reliable non-destructive method to pre-screen wheat kernels for FHB infection and mycotoxin contamination.

Recently, hyperspectral imaging has been introduced to identify and classify damage caused by different diseases and pests on cereal kernels. Del Fiore et al. (2010) used hyperspectral imaging in the visible near-infrared (VIS-NIR) (400-1000 nm) range for early identification of

toxigenic fungi, i.e., *Aspergillus* spp. and *Fusarium* spp., on commercial maize kernels. In another study, hyperspectral images in the VIS-NIR range were taken for maize kernels artificially contaminated with aflatoxin B1 (AFB1) (Wang et al. 2015). Principal component analysis (PCA) was then combined with stepwise factorial discriminant analysis (FDA) to discriminate control samples from samples artificially contaminated with different concentrations of AFB1. The authors were able to identify kernels contaminated with concentrations as low as 10 µg/kg of AFB1 (Wang et al. 2015). Similar results were achieved by Kimuli et al. (2017), who used hyperspectral imaging in the short-wave infrared range (SWIR) (1000-2500 nm) to classify AFB1 contamination in maize kernels by combining PCA with the Mahalanobis distance classifier. Additionally, AFB1 contents have been identified and classified in *Aspergillus flavus*-infected maize kernels by applying the support vector machine (SVM) classification approach on the PCA of the mean spectra of a single kernel in the SWIR (Chu et al. 2017).

Singh et al. (2008, 2009) used hyperspectral imaging in the NIR from 1000 to 1600 nm for the detection of insect-damaged kernels of wheat during storage. They classified healthy and insect-damaged kernels with an accuracy of 85% to 100% using different classification methods.

Peiris et al. (2009) applied NIR spectroscopy from 1000 to 2500 nm to differentiate between sound and *Fusarium*-damaged kernels (FDK) contaminated with different deoxynivalenol (DON) levels. They compared the spectral reflectance of the wheat kernels with that of the serial dilutions of pure DON in acetonitrile. Subsequently, commercial application of NIR spectroscopy was investigated to predict DON levels in a single wheat kernel and to sort sound kernels from FDK (Kautzman et al. 2015; Peiris et al. 2010). On the bulk scale, it was possible to differentiate between sample lots with different percentages of FDK using a combination of the spectral reflectance from 350 to 2500 nm and partial least square regression with an accuracy of 100% (Beyer et al. 2010). Using the mean spectral reflectance of a single wheat kernel in VIS-NIR from 400 to 1000 and 1000 to 1700 nm and linear discriminant analysis (LDA), it was possible to discriminate FDK from sound ones with an accuracy of 95% (Delwiche and Hareland 2004; Delwiche et al. 2011). Dowell et al. (1999) used VIS-NIR from 400 to 1700 nm spectroscopy in combination with a partial least squares (PLS) regression model to predict DON and ergosterol in single wheat kernels. The same model was used in the VIS-NIR range to detect FDK in Canadian wheat, with an overall accuracy of 90% (Shahin and Symons 2012). In the VIS range, RGB images or green and red light produced from the

high-power pulsed light-emitting diode (LED) were used in combination with LDA to classify FDK with an accuracy of > 85% (Delwiche 2009; Jirsa and Polišenská 2011). Barbedo et al. (2015) developed an algorithm for automatic detection of FDK in wheat kernels based on hyperspectral imaging in the spectral range 528-1785 nm.

All the above studies were performed to identify *Fusarium* infection in wheat kernels using one species of *Fusarium* taking the DON content into account. To expand that knowledge base, the present study was designed to investigate the feasibility of hyperspectral imaging to screen the infection of different *Fusarium* species with regard to fungal DNA and different mycotoxin levels in wheat kernels and produced flour.

4.3.2. Materials and Methods

4.3.2.1. Plant Material

Two varieties of spring wheat (*Triticum aestivum* L.) differing in their susceptibility to FHB were grown under greenhouse conditions: 'Triso' moderately resistant from DSV, Lippstadt, Germany, and 'Sonett' moderately susceptible from Syngenta, Basel, Switzerland (Anonymous 2017). The growth substrate was a mixture of 1 sand:3 horizon C:6 potting substrate ED 73 (Einheitserde, Sinntal-Altengronau, Sinntal, Germany). Three kernels per pot were planted in 12×12×20 cm-sized pots. After germination, the plants were thinned to two plants per pot and the plants were supported by wooden sticks. Environmental conditions in the greenhouse were: Photoperiod of 16/8 h (day/night) obtained from supplemental artificial light (>300 µmol m^{-2} s^{-1}, Philips SGR 140, Hamburg, Germany); a temperature of 20 ± 2°C; and 50-70% relative humidity. The plants were watered when necessary.

4.3.2.2. Plant Pathogens and Inoculation Techniques

Isolates of three *Fusarium* species stored at -80°C were used in this study: *Fusarium graminearum*, isolate S.19 produced 69% 15-ADON and 31% DON, and *F. culmorum*, isolate 3.37 produced 68% 3-ADON and 32% DON on rice culture. They were originally isolated from infected wheat kernels in an experimental field (Campus Klein-Altendorf, Rheinbach, Germany) in 2011 and 2004, respectively. *F. poae*, isolate EC15 was taken from the INRES (Plant Diseases and Plant Protection, University of Bonn, Germany) mycological collection. Pathogen cultivation and inoculum preparation were performed according to (Alisaac et al. 2018). The spore suspension was diluted to 1×10^6 spore/mL using a Fuchs-Rosenthal chamber. Spore densities of 1×10^4, 1×10^5, 2.5×10^5, 5×10^5, and 1×10^6 spore/mL were derived from the stock spore suspension and used in inoculation. Each treatment consisted of

one pot with two plants of each variety with more than 10 spikes per pot at the anthesis growth stage, GS 61-65 (Lancashire et al. 1991). Pots were randomly distributed on the table in the middle of the greenhouse in order to guarantee the homogeneity of the surrounding environment. Spray inoculation was done as described in (Alisaac et al. 2018). Control plants were mock-inoculated with water. At harvest, spikes were collected and threshed manually, and the resulting kernels prepared for hyperspectral measurement (Figure 19). After acquiring the hyperspectral images of the kernels, they were ground using a lab grinder (Retsch MM 200, Haan, Germany). The produced flour was measured using the same hyperspectral imaging setup with the same settings.

4.3.2.3. Hyperspectral Measurements

Hyperspectral measurements were done in a darkened room. The objects were illuminated using an artificial light produced from six ASD-Pro-Lamps (Analytical Spectral Devices Inc., Boulder, CO, USA) with a 45° vertical angle to the objects. The images were acquired in the visible-near infrared (VIS-NIR) range from 400 to 1000 nm using the hyperspectral camera ImSpector V10E (Spectral Imaging Ltd., Oulu, Finland). In total, 211 hyperspectral bands were recorded using a spectral binning of 4. In the short-wave infrared (SWIR) from 1000 to 2500 nm, a SWIR-Camera (ImSpector N25E, Spectral Imaging Ltd., Oulu, Finland) was used. In total, 256 hyperspectral bands were recorded using a spectral binning of 1. A motorized line scanner (Velmex BiSlide, Velmex Inc., Bloomfield, Ontario County, New York, USA) was used to move the cameras and the illumination system over the object. The software SpectralCube (Spectral Imaging Ltd., Oulu, Finland) was applied to adjust the settings of the camera and the motorized line scanner. To attain stable measuring conditions, the cameras and the illumination system were preheated for 30 min before the measurements. For more details about the imaging system and data processing, see Alisaac et al. (2018). To acquire the hyperspectral images, a black Petri dish (Brightic, Nagymaros, Hungary) was used as a background for the kernel and flour measurements. This Petri dish has low reflectance of < 5% in the spectral range of 400 to 2500 nm. For flour measurement, black rings of a 1 mm height were filled with the flour in order to obtain a homogeneous topography for the flour surface. Four images were made to calculate the reflectance of the object sample: (i) A white reference image using a white barium-sulfate bar (Spectral Imaging Ltd., Oulu, Finland), which reflects ~99% of the light; (ii) a dark current image by closing the shutter of the camera at the same exposure time of the white reference; (iii) the image of the object sample; and (iv) a second dark current image at the same exposure time of the object sample. The open-source software

HSVaP ("Hyperspectral Visualization and Processing") was used for masking and visualizing the image data (available at https://github.com/janBehmann/HSVAP). The mean spectral reflectance was calculated using MATLAB 2013a (MathWorks, Natick, MA, USA).

4.3.2.4. DNA Extraction and Fungal DNA Quantification

Total DNA was extracted from 20 mg of flour according to a cetyltrimethylammonium bromide method and precipitated with polyethylene glycol (Schilling et al. 1996). The pellets were washed twice with 80% (*v*/*v*) ethanol, dried in vacuum at 30°C, dissolved in 50 µL TE-buffer (10 mM Tris, 1 mM EDTA, pH 8.0), and diluted 100-fold in water for qPCR. Three-fold dilution series of pure fungal DNA from 0.3 to 100 pg per reaction were used as standards. A real-time PCR thermocycler CFX 384 (Biorad, Rüdigheim, Germany) was used for fungal DNA quantification using the primers listed in Table 9. The components of the reaction mixture were: Taq Polymerase with ThermoPol Buffer (20 mM Tris-HCl, 10 mM $(NH_4)_2SO_4$, 10 mM KCl, 2 mM $MgSO_4$, 0.1% Triton-X-100, pH 8.8 at 25°C); 0.15 mM of each dNTP; 2.5 mM $MgCl_2$ (Bioline, Lückenwalde, Germany); 0.3 µm of each primer; and SYBR Green I (Invitrogen, Karlsruhe, Germany). The PCR started with an initial denaturation at 95.0°C for 2 min, followed by 35 cycles according to Table 9. The final elongation was done at 68.0°C for 5 min. Melting curves were generated after amplification by heating PCR products to 95.0°C for 1 min, cooling to 55.0°C for 1 min, then tardily raising the temperature 0.5°C/10 s according to Table 9. The fluorescence was measured continuously. Because of the degradation of wheat DNA in infected kernels, the amount of fungal DNA per gram of dry flour rather than the ratio of fungal to wheat DNA was used as a measure of fungal colonization.

4.3.2.5. Mycotoxin Extraction and Quantification

Mycotoxins were extracted from 350 mg of flour per treatment in 3.5 mL of acetonitrile-water (84:16, *v*/*v*). The mixture was vortexed, shaken overnight, and centrifuged at 4500 min^{-1}. One mL of the supernatant was transferred to a 2-mL Eppendorf tube and dried at 40°C. The dry residue was re-suspended in 1 mL of methanol-1% formic acid in water (25:75, *v*/*v*), and sonicated in an ultrasonic bath until completely dissolved. Blank (control) samples of wheat flour were prepared in the same way. The following mycotoxin standards were used (Table 10): Nivalenol (NIV), deoxynivalenol (DON), 3-acetyl-deoxynivalenol (3-ADON) and 15-acetyl-deoxynivalenol (15-ADON), HT-2 toxin, T-2 toxin, zearalenone (ZEA), enniatin A1, and enniatin B1.

An Agilent (Waldbronn, Germany) 1290 Infinity II HPLC system linked to an Agilent 6460 Triple Quad was employed for toxin quantification. The separation was carried out on an Agilent Zorbax Eclipse C18 column with 1.8-µm particle size and 100 × 2.1 mm. Details concerning the mass transition, recoveries, and the limits of detection and quantification can be found in Table 10.

4.3.2.6. Statistical Analysis

All Pearson's correlation coefficients and statistical analysis were done using the open-source software RStudio. For significant statistical differences in the fungal DNA and mycotoxins contents, standard analysis of variance (ANOVA) was applied to the data. This analysis was followed by Tukey's honest significance test with a significance level of $p \leq 0.05$, $n = 3$ ("agricolae" package in RStudio).

4.3.3. Results

4.3.3.1. Effect of *Fusarium* Infection on the Spectral Signature of the Kernels

Fusarium-infected kernels of both varieties showed severe symptoms for all investigated *Fusarium* species and all spore densities (Figure 19). Non-inoculated kernels of both varieties had the same spectral signature patterns in the VIS-NIR and SWIR ranges (Figure 20). In contrast, *Fusarium*-infected kernels showed higher spectral reflectance along the whole spectrum compared with non-inoculated kernels.

The spectral signature of *Fusarium*-infected kernels differed according to the wheat variety, *Fusarium* species, and spore density of the inoculum (Figure 20). *F. culmorum*-infected kernels of 'Sonnet' from all spore densities showed identical spectral reflectance from 400 to 630 nm. Small differences among treatments appeared in the spectral range from 630 to 700 nm and from 750 to 1000 nm. In the SWIR range, these differences were pronounced from 1460 to 1850 nm (Figure 20). More obvious differences among treatments were shown in the case of 'Triso'. The highest reflectance of kernel samples resulted from the treatment of 1×10^4 spore/mL, whereas the lowest reflectance was for the kernels from the treatment of 5×10^5 spore/mL (Figure 20).

F. graminearum infection affected the same wavelengths that were affected by *F. culmorum* infection in the VIS-NIR range (i.e., from 400 to 630 nm and from 750 to 1000 nm), whereas the entire SWIR range was influenced by *F. graminearum* infection. The treatment of 1×10^5 spore/mL resulted in the lowest reflectance of infected kernels in both varieties. The highest reflectance appeared in the treatment of 5×10^5 spore/mL in 'Sonett' and 2.5×10^5 in 'Triso'.

F. poae infection influenced only the NIR and the SWIR ranges. The highest reflectance was found for the treatment of 2.5×10^5 spore/mL in both varieties, and the lowest levels were with the treatment of 5×10^5 in 'Sonett' and 1×10^6 in 'Triso' (Figure 20).

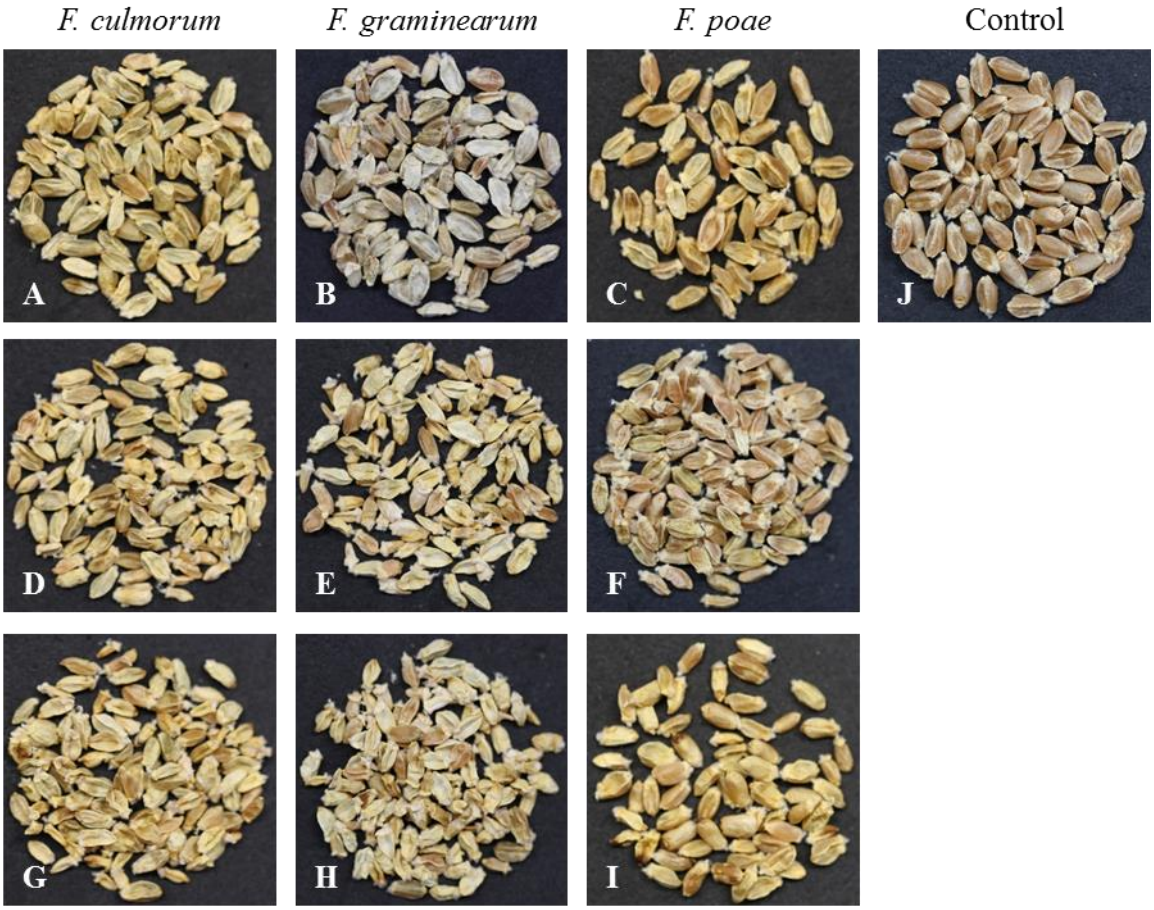

Figure 19. Summer wheat kernels cv. 'Sonett' inoculated with different spore densities (A–C): 1×10^4 spore/mL; (D–F): 2.5×10^5 spore/mL; (G–I): 1×10^6 spore/mL; (J): water treatment of three *Fusarium* species (A, D, and G: *F. culmorum*; B, E, and H: *F. graminearum*; **C**, **F,** and **I**: *F. poae*; **J**: Control).

4.3.3.2. Comparison between the Spectral Signatures of the Kernels and the Produced Flour

The spectral signature patterns of flour differed from those of kernels (Figures 20 and 21). The spectral reflectance of non-inoculated kernels was lower than that of infected kernels along the assessed waveband range. However, in the case of flour, the spectral reflectance of non-inoculated flour was significantly higher than that of infected flour in the VIS range (Figure 21). Obvious differences appeared from 630 to 670 nm in the spectral signatures of the flour produced from *F. culmorum*- and *F. graminearum*-infected kernels (Figure 21). Flour produced from *F. poae*-infected kernels showed no distinct differences in the spectral signatures in the VIS range. The treatment with the 2.5×10^5 spore/mL concentration, which resulted in the

highest spectral reflectance of the infected kernels, caused the lowest spectral reflectance of the flour in both varieties (Figure 21). The spectral reflectance of the flour produced from non-inoculated kernels had the lowest values in the spectral range from 870 to 1000 nm in all treatments. In the SWIR range, the infection altered the wavelengths from 1100 to 1300 and 1950 to 2500 nm. In general, flour produced from non-inoculated kernels had lower reflectance than infected ones in the SWIR range (Figure 21).

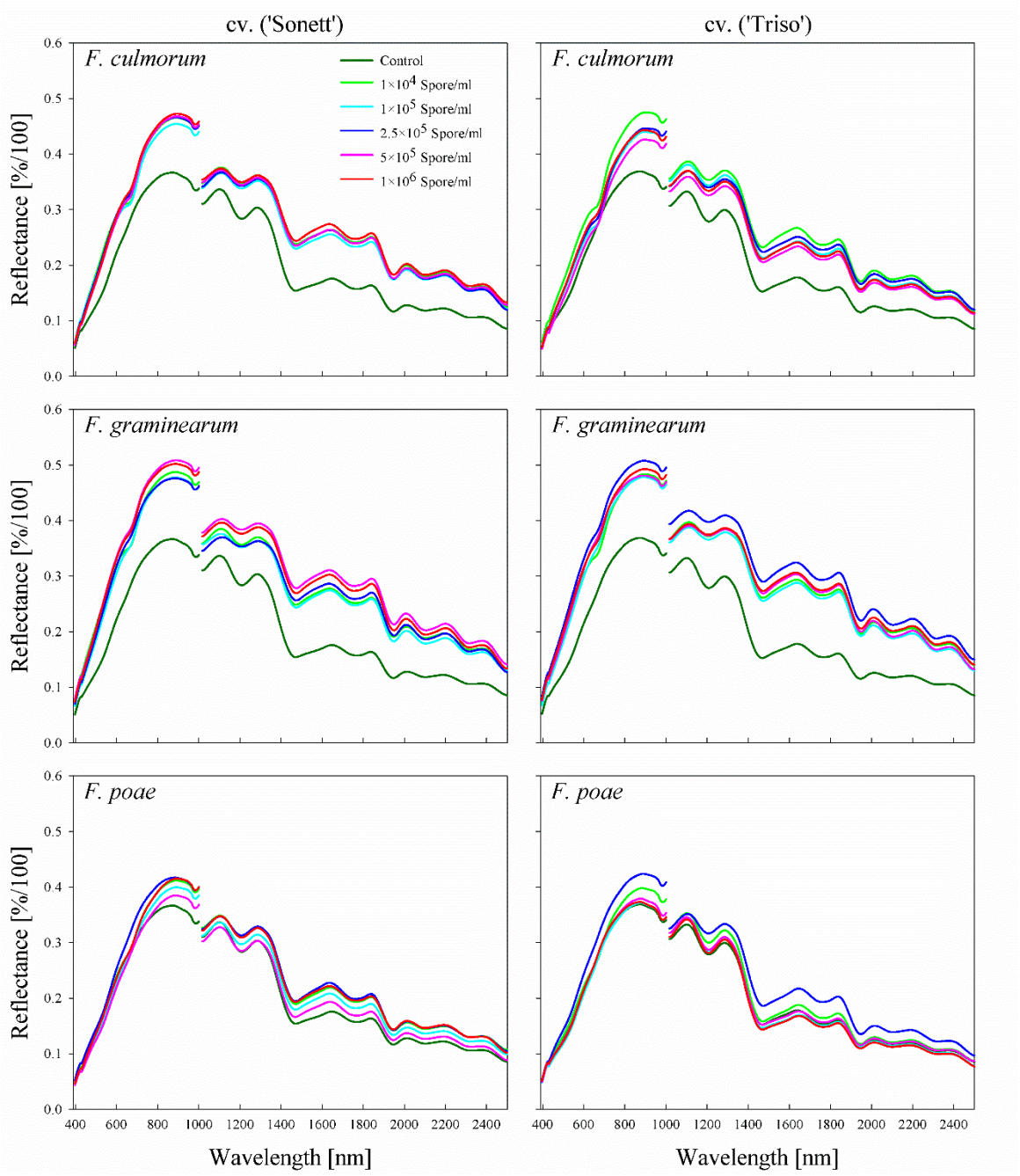

Figure 20. Spectral signature of wheat kernels cv. 'Sonett' and 'Triso' inoculated with different spore densities of three *Fusarium* species (*F. culmorum*, *F. graminearum*, and *F. poae*).

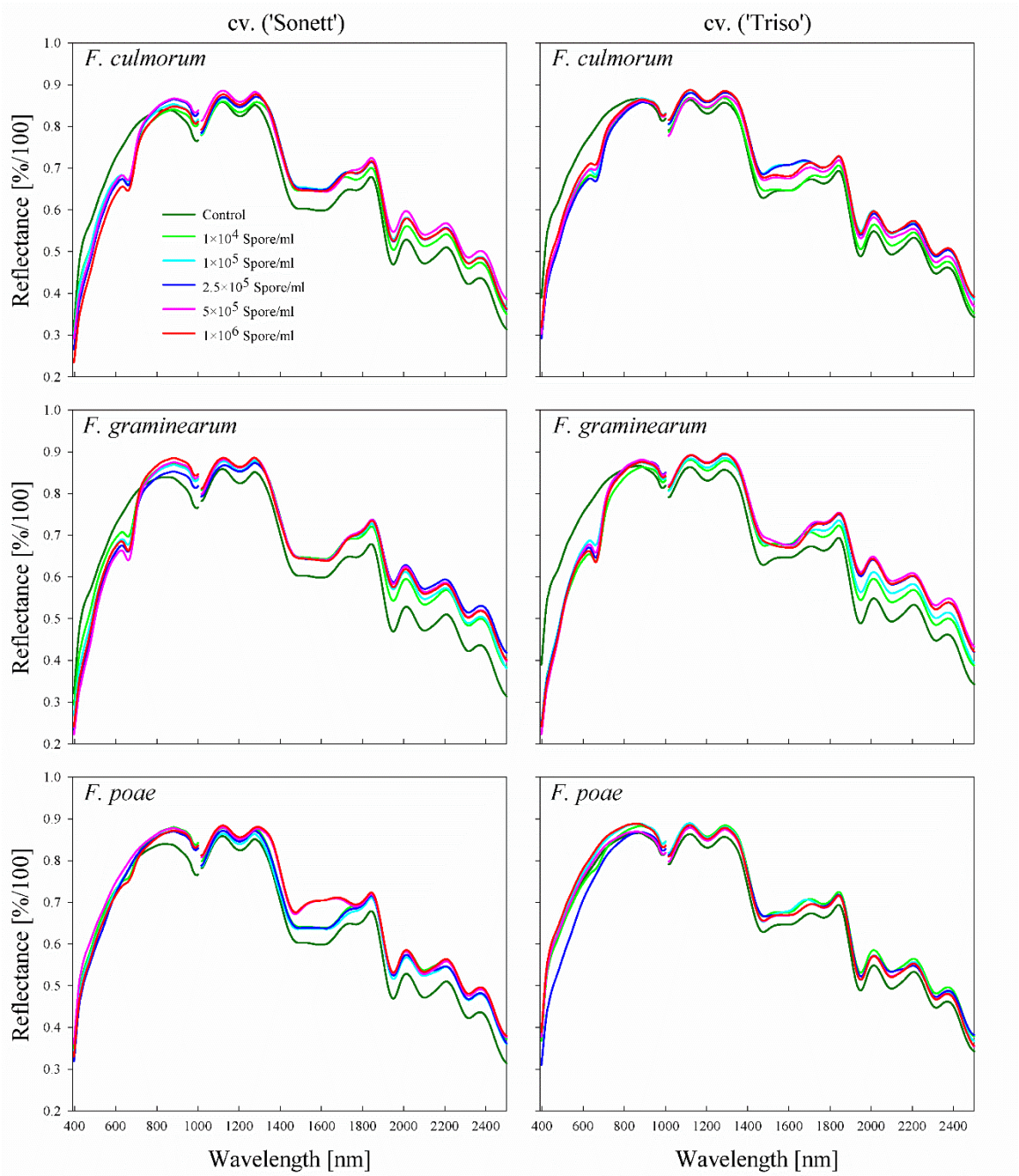

Figure 21. Spectral signature of the flour samples produced from wheat kernels cv. 'Sonett' and 'Triso' inoculated with different spore densities of three *Fusarium* species (*F. culmorum*, *F. graminearum*, and *F. poae*).

Table 9. Forward and reverse primers sequences; denaturation, annealing, elongation, and melting curve temperatures of the primer used to amplify specific fragments of the fungal DNA of *Fusarium culmorum*, *F. graminearum*, and *F. poae* on wheat kernels and in flour.

Pathogen	**Denaturation**		**Annealing**		**Elongation**		**Melt Curve**		**Primers**			
	°C	**min**	**°C**	**min**	**°C**	**min**	**°C**	**°C**	**Primer name**	**Primer sequence (5'-3')**	**Amplified fragment**	**Reference**
F. culmorum	94.0	0:20	62.0	0:40	68.0	0:45	65.0	95.0	OPT18 F OPT18 R	GATGCCAGACCAAGACGAAG GATGCCAGACGCACTAAGAT	472 bp	Schilling et al. 1996
F. graminearum	94.0	0:30	61.0	0:30	68.0	0:30	55.0	95.0	Fg16N F Fg16N R	ACAGATGACAAGATTCAGGCACA TTCTTTGACATCTGTTCAACCCA	280 bp	Nicholson et al. 1998
F. poae	94.0	0:35	62.5	0:30	68.0	0:35	55.0	95.0	Fp82 F Fp82 R	CAAGCAAACAGGCTCTTCACC TGTTCCACCTCAGTGACAGGTT	220 bp	Parry and Nicholson 1996

Table 10. Mass transitions, recoveries, and the limits of detection and quantification of mycotoxins in flour samples produced from wheat kernels cv. 'Sonett' and 'Triso' inoculated with different spore densities of three *Fusarium* species (*F. culmorum*, *F. graminearum*, and *F. poae*).

Toxin	Obtained From	Molecular Ion	Parent Ion	Collision Energy [V]	Product Ions	LOD * [mg/kg]	LOQ * [mg/kg]	Recovery *** %
NIV	Merck (Darmstadt, Germany)	$[M-H]^-$	357.1	10 10	311.1 281.1 **	0.007	0.025	89
DON	Merck (Darmstadt, Germany)	$[M+H]^+$	297.1	4 64	249.1 ** 91.2	0.006	0.018	113
3-ADON	Merck (Darmstadt, Germany)	$[M+H]^+$	339.2	8 8	231.1 ** 203.0	0.022	0.072	110
15-ADON	Merck (Darmstadt, Germany)	$[M+H]^+$	339.2	10 10	261.0 ** 203.0	0.070	0.230	111
HT-2	Enzo Life Sciences (Lörrach, Germany)	$[M+Na]^+$	447.0	17 17	345.1 ** 285.0	0.029	0.097	96
T-2	Enzo Life Sciences (Lörrach, Germany)	$[M+Na]^+$	489.2	98 142	128.1 115.1 **	0.029	0.092	119
ZEA	Romer Labs (Tulln, Austria)	$[M+H]^+$	319.2	12 12	301.1 283.0 **	0.098	0.322	76
Enniatin A1	Merck (Darmstadt, Germany)	$[M+H]^+$	668.4	20 20	228.2 210.2 **	0.029	0.095	68
Enniatin B1	Merck (Darmstadt, Germany)	$[M+H]^+$	654.4	23 23	228.2 210.2 **	0.046	0.151	80

* Limit of detection (LOD) and limit of quantification (LOQ) were estimated according to a procedure suggested by an EU guidance document by spiking 10 blank samples to 1.9 µg/L of each toxin. ** Product ion used as a quantifier. *** Spike level of 300 µg/L at the beginning of the extraction procedure.

4.3.3.3. Fungal DNA and Mycotoxin Content in Wheat Flour

Flour produced from non-inoculated kernels of both varieties showed neither fungal DNA nor mycotoxins for any of investigated *Fusarium* species.

F. culmorum produced a large amount of fungal DNA in both varieties amounting to 60 to 82 and 37 to 73 µg/g in 'Sonett' and 'Triso', respectively. Additionally, both varieties showed high DON content: 108 to 157 mg/kg in 'Sonett' and 44 to 81 mg/kg in 'Triso'. Fungal DNA and DON contents were not significantly different among treatments within the same variety. In addition, small amounts of 3-ADON (up to 10 and 2.7 mg/kg in 'Sonett' and 'Triso', respectively) were observed. Only in 'Sonett' were low levels of 15-ADON (0.5 mg/kg) and nivalenol (NIV) (up to 1.3 mg/kg) detected. The variety 'Sonett' showed higher levels of fungal DNA and mycotoxins than 'Triso' (Figure 22).

Comparing with *F. culmorum*, *F. graminearum* resulted in lower fungal DNA and 3-ADON and higher DON, 15-ADON and NIV content in all treatments. In contrast with *F. culmorum*, 'Sonett' showed lower fungal DNA amounts 20 to 48 µg/g comparing with 'Triso' 29 to 54 µg/g. DON contents ranged between 146 to 296 mg/kg in 'Sonett' and 176-304 mg/kg in 'Triso'. Maximum amounts of 2.4, 4.5 and 2.3 mg/kg have been observed for 3-ADON, 15-ADON and NIV, respectively, with no significant differences between treatments (Figure 22).

In contrast to *F. culmorum* and *F. graminearum* infections, *F. poae* induced very low amounts of fungal DNA that ranged between 0.1 and 0.5 µg/g, without significant differences among treatments. Maximum concentrations of 27, 2.3, and 2.1 mg/kg for DON, 3-ADON, and NIV, respectively, were observed in 'Sonett'. In contrast, in 'Triso', 2.8 and 0.1 mg/kg for DON and 3-ADON, respectively, were recorded. No 15-ADON contamination was observed in the two varieties (Figure 22).

4.3.3.4. Correlation between Fungal DNA and Mycotoxin Content

The data of all samples of both varieties inoculated with different spore densities was used to calculate the correlation between fungal DNA and mycotoxin content for each *Fusarium* species. Table 11 shows the correlation between fungal DNA and mycotoxins content and the correlation between different mycotoxins for each *Fusarium* species, separately. In the case of *F. poae* infection, the correlations between fungal DNA and mycotoxin contents, and individual mycotoxin content with the other mycotoxins were not significant since most of the samples showed no mycotoxin content (Table 11).

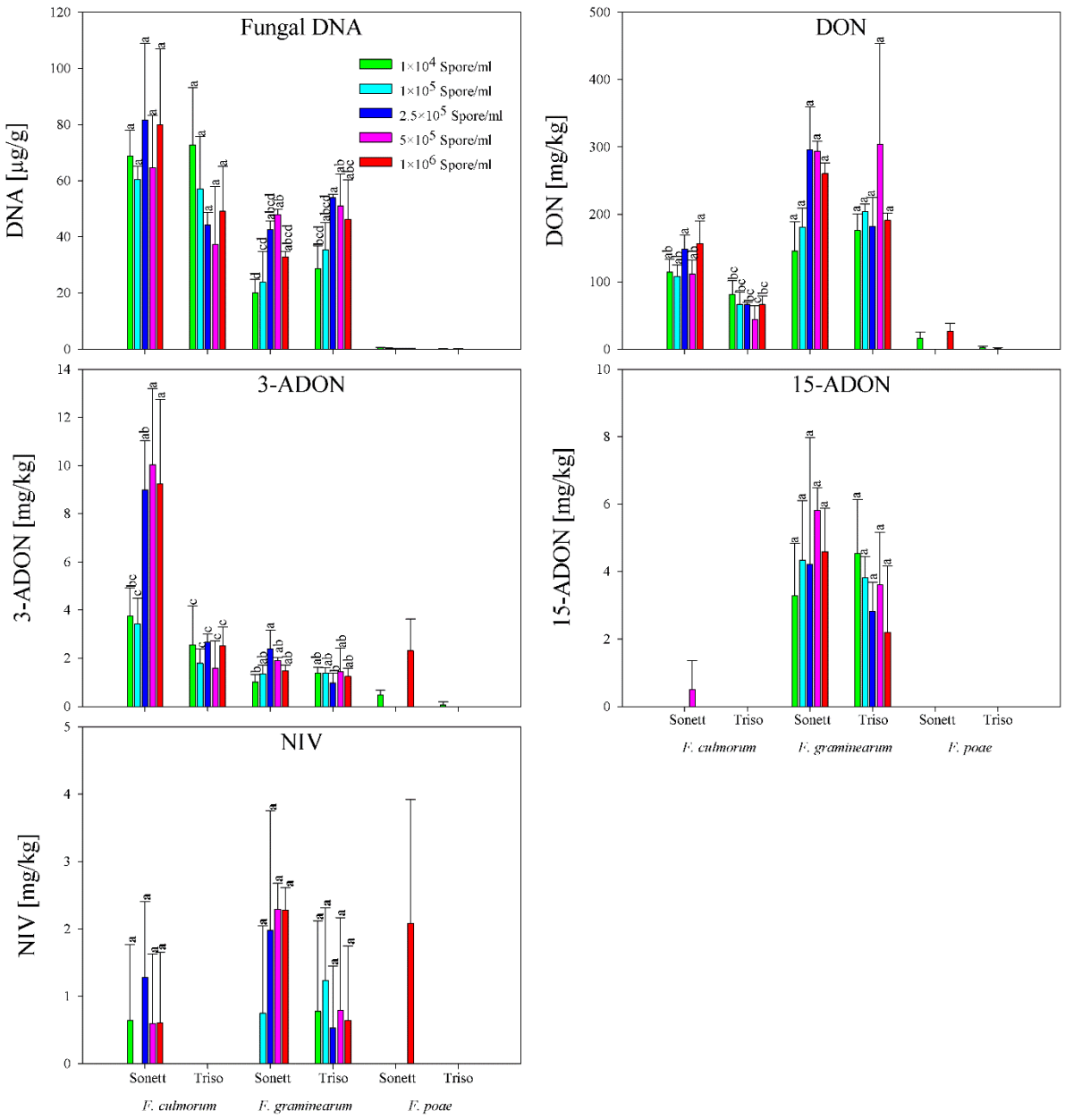

Figure 22. Fungal DNA and mycotoxin contents in the flour samples produced from wheat kernels cv. 'Sonett' and 'Triso' inoculated with different spore densities of three *Fusarium* species (*F. culmorum*, *F. graminearum*, and *F. poae*; Tukey's test; $n = 3$). On the species scale, treatments with the same letters are not significantly different.

Table 11. Pearson's correlation coefficient between fungal DNA and concentrations of different mycotoxins in the flour samples produced from wheat kernels cv. 'Sonett' and 'Triso' inoculated with different spore densities of three *Fusarium* species (*F. culmorum*, *F. graminearum*, and *F. poae*).

Fungal DNA-Mycotoxin	*F. culmorum*	*F. graminearum*	*F. poae*
Fungal DNA-DON	0.90	0.80	n.s.
Fungal DNA-3-DON	0.70	n.s.	n.s.
Fungal DNA-15-DON	n.s.*	0.51	n.s.
DON-3-ADON	0.85	n.s	n.s.
DON-15-ADON	n.s.	0.79	n.s.

The correlation was calculated from the data of all samples inoculated with different spore densities of each *Fusarium* species (n = 30). *n.s. the correlation was not significant at $p \leq 0.05$.

4.3.3.5. Correlation of Spectral Signature of Wheat Kernels to Fungal DNA and Mycotoxin Content

The spectral reflectance of *F. culmorum*-infected kernels showed a high correlation of $r > 0.80$ with the fungal DNA content in the spectral range 450-652 and 700-750 nm and along the SWIR range (Figure 23). This correlation reached $r = 0.90$ in the spectral range 750-1000 nm. The correlation of the spectral reflectance with DON content showed high values of $r > 0.80$ in the spectral range 441-1000 nm. This correlation was $r > 0.90$ in the spectral ranges from 505 to 655 and 695 to 843 nm. In the SWIR range, the correlation of $r > 0.80$ was shown in the spectral ranges from 1200 to 1212 and 1345 to 2500 nm, with a peak of $r > 0.90$ in the spectral range 1906-2018 nm. A lower correlation of $r > 0.60$ occurred for the 3-ADON content in the spectral ranges from 460 to 1000 and 1377 to 2500 nm, with a remarkable peak of $r > 0.80$ in the spectral range from 640 to 712 nm.

The correlation of the spectral reflectance of *F. graminearum*-infected kernels with the fungal DNA content was $r > 0.80$ in the spectral ranges 524-1000 and 1130-2500 nm (Figure 23). Similarly, the correlation with DON content resulted in the same values in the spectral ranges 558-814 and 1377-2031 nm. The correlation of the spectral reflectance with the DON derivative contents was lower compared with the DON content. This correlation ranged between r = 0.60-0.70 in the spectral ranges 474-1000 and 1358-2500 nm for the 3-ADON content, and between r = 0.62 and 0.76 along the electromagnetic spectrum for 15-ADON. No correlation between the spectral reflectance and NIV was observed.

The spectral reflectance of *F. poae*-infected kernels showed a lower correlation with the fungal DNA content compared with *F. culmorum* and *F graminearum* (Figure 23). A correlation of $r > 0.60$ in the spectral ranges 538-572 and 828-1000 nm was proven. In the SWIR range, the correlation ranged between r = 0.60 and 0.73 in the spectral range 1350-2500 nm.

4.3.3.6. Correlation of Spectral Signature of Wheat Flour to Fungal DNA and Mycotoxin Content

The spectral reflectance of the produced flour resulted in negative correlations with the fungal DNA and mycotoxin contents in the VIS range. In addition, a positive correlation in the SWIR range and no significant correlation in the NIR range were confirmed (Figure 23).

The spectral reflectance of flour produced from *F. culmorum*-infected kernels exhibited a high negative correlation of $r > 0.80$ with the fungal DNA content in the spectral ranges 427-494 and 601-692 nm. In the SWIR range, two remarkable peaks of $r > 0.45$ appeared in the spectral ranges 1193-1231 and 1446-1465 nm. The correlation increased to $r > 0.51$ in the spectral range 1742-2500 nm and reached $r = 0.61$ in 2050 to 2075 nm (Figure 23). The correlation with DON content was higher than the correlation with the fungal DNA in the VIS range, and lower in the SWIR range. The correlation reached $r > 0.85$ in the spectral ranges 427-494 and 655-675 nm; however, the highest value of $r = 0.52$ appeared in the range 2050-2075 nm. The correlation with 3-ADON content showed decreasing values with an increasing wavelength in the VIS range and ranged between 0.70 and 0.50, with no remarkable correlation in the SWIR range (Figure 23).

The spectral reflectance of flour produced from *F. graminearum*-infected kernels had a higher correlation with fungal DNA than that of *F. culmorum*. The highest negative correlation of $r > 0.85$ appeared in the spectral ranges 397-494 and 652-670 nm. Likewise, for *F. culmorum*, the same peaks appeared in the spectral ranges 1193-1231 and 1446-1465 nm, with a higher correlation of $r > 0.81$ and $r > 0.76$, respectively, and increased to $r > 0.86$ in the spectral range 1742-2500 nm (Figure 23). The correlation with DON content showed values of $r > 0.80$ and $r > 0.79$ in the spectral ranges 397-494 and 655-675 nm, respectively. In the SWIR range, the correlation reached $r > 0.64$, $r > 0.50$, and $r = 0.65$ in the spectral ranges 1193-1231, 1446-1465, and 1742-2500 nm, respectively. In the VIS range, the correlation with 3-ADON showed a decreasing value with an increasing wavelength, with a peak of 0.76 in the spectral range 422-435 nm. While, it showed the reverse with 15-ADON, with a peak of $r = 0.69$ in the spectral range 635-700 nm. The correlation with 3-ADON reached $r > 0.46$ and $r > 0.60$ in the spectral ranges 1193-1231 and 1800-2500 nm, respectively. In contrast, no correlation was observed with 15-ADON in the SWIR range. The NIV content showed no significant correlation with the spectral reflectance of the produced flour, and the highest negative correlation of $r = 0.53$ was achieved in the spectral range 475-497 nm (Figure 23).

The spectral reflectance of flour produced from *F. poae*-infected kernels had the highest correlations with fungal DNA of $r = 0.53$ and $r = 0.56$ in the spectral ranges 664-672 and 1912-1950 nm, respectively (Figure 23).

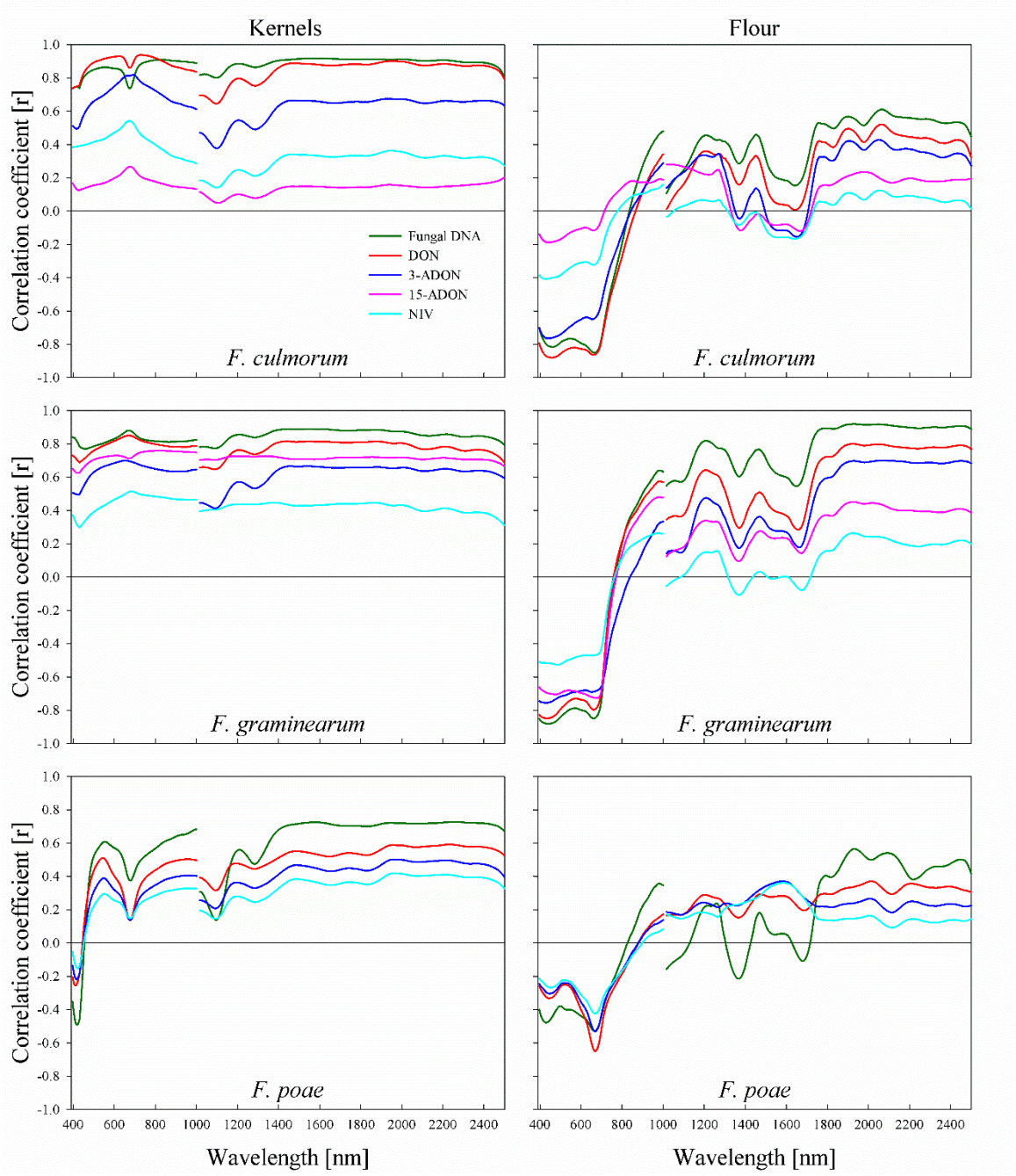

Figure 23. Pearson's correlation coefficient between the spectral signature of wheat kernels cv. 'Sonett' and 'Triso' (left) inoculated with different spore densities of three *Fusarium* species and wheat flour produced from these kernels (right) in relation to fungal DNA and various mycotoxin levels.

4.3.4. Discussion

The symptoms of *Fusarium* infection on infected kernels result in a reduction of the thousand kernel weight, shriveling, pinkish discoloration, and chalky appearance (McMullen et al. 1997, 2012). Several studies showed the applicability of hyperspectral imaging for the detection of *Fusarium*-damaged kernels or spikelets (Alisaac et al. 2018; Beyer et al. 2010; Delwiche and Hareland 2004; Delwiche et al. 2011; Kautzman et al. 2015; Mahlein et al. 2019; Peiris et al. 2009, 2010). The reflected light in the VIS range shows the tissue pigments; the NIR range represents the tissue structure, while the SWIR range characterizes the chemical compounds (Mahlein et al. 2018). In the current study, the reflectance of infected kernels was higher than that of non-infected ones in the VIS-NIR range. This is attributed to the discoloration of infected kernels compared with healthy ones, and to the changes in the kernel structure due to infection. This is in accordance with previous studies that proved a lower reflectance of healthy wheat kernels compared with *Fusarium*-damaged kernels in the VIS-NIR range (Beyer et al. 2010; Delwiche et al. 2011; Shahin and Symons 2012). Former studies demonstrated an increase in the protein, starch, starch lipids, and non-starch lipids in *Fusarium*-infected kernels (Hettiarachchy and Boyacioğlu 1995; Kreuzberger et al. 2015; Siuda et al. 2010). The reflectance of infected kernels was higher than of healthy ones in the SWIR range, which is consistent with the results of (Beyer et al. 2010; Delwiche and Hareland 2004; Delwiche et al. 2011). This is due to the changes in the chemical contents of the infected kernels due to *Fusarium* infection.

The quality of wheat flour depends strongly on gluten proteins (Wieser 2000). *Fusarium* infection leads to substantial changes in the storage contents of wheat kernels (Wang et al. 2005), and consequently, flour appearance. Histological investigation proved high degradation in the starch granules and the protein matrix of the endosperm of *Fusarium*-infected kernels (Nightingale et al. 1999). Gärtner et al. (2008) showed a positive correlation ($r = 0.93$) between the disease severity and ash content (minerals like potassium and calcium salts) of *F. culmorum*-infected kernels. This explains the lower reflectance of flour from infected kernels compared with that from non-infected kernels in the current study.

The study of Hellin et al. (2018) showed a high correlation between the spore density in the air above the canopy and DON concentration and disease incidence of *F. graminearum* under field conditions. In the current study, no significant differences were found between inoculum density and fungal DNA and mycotoxin concentrations in the infected kernels with all

Fusarium species. This is due to the differences in the experimental conditions of these studies. While the study of Hellin et al. (2018) was implemented under natural conditions in the field and without incubation, the current study was implemented under greenhouse conditions with incubation for 48 h after inoculation. Under these optimal conditions for the pathogens, the lowest number of spores was enough to induce infection with maximum disease severity, which could not be further increased using higher spore densities.

In this study, *F. culmorum* isolate produced DON and 3-ADON as secondary metabolites, while *F. graminearum* produced DON, 3-ADON, and 15-ADON. This is in accordance with the results that showed the ability of *F. graminearum* to produce DON, 3-ADON, and 15-ADON simultaneously (Castañares et al. 2014). Small amounts of NIV were detected in some samples. This is due to a side infection with NIV producer, since the isolates used in this study are DON producers. The results of the current study showed high correlations of $r = 0.90$, $r = 0.70$, and $r = 0.85$ between fungal DNA-DON, fungal DNA-3-ADON, and DON-3-ADON, respectively, for *F. culmorum*. In addition, correlations of $r = 0.80$, $r = 0.51$, and $r = 0.79$ between fungal DNA-DON, fungal DNA-15-ADON and DON-15-ADON, respectively, for *F. graminearum* were observed. This indicates that the major source of DON, 3-ADON, and 15-ADON in the samples resulted from the isolates used for inoculation, and not from a spontaneous infection. Moreover, it shows that these isolates produce trichothecenes in the same ratio *in vitro* and *in vivo*. In the case of *F. poae*, no significant correlation was seen because it was less effective in inducing infection in both wheat varieties. This corresponds to the results of previous studies that showed high correlations between the fungal DNA of *F. culmorum* and *F. graminearum* and the amount of DON in infected kernels of wheat and barley. In addition, a positive correlation between the fungal DNA of *F. poae* and NIV content was documented. However, on the species scale, it was shown previously that *F. poae* was less effective in term of fungal DNA and mycotoxin production (Beccari et al. 2019; Nielsen et al. 2014; Siou et al. 2014).

The results of the current study showed higher correlations in the NIR range compared with the VIS range between the spectral reflectance of wheat kernels and the fungal DNA and DON contents for all *Fusarium* species. This is in accordance with the results of Shahin and Symons (2012) that proved no specific wavelengths correlated to *Fusarium* infection in wheat kernels in the VIS-NIR ranges. The results of Delwiche et al. (2011) showed that the spectral ranges 502-678 nm, 1198-1496 nm, and 1420-1560 nm were affected by *Fusarium* infection. They showed that the NIR range was superior to the VIS range to identify *Fusarium*-infected kernels.

They attributed this to the transformation of the endosperm compound into fungal characteristic compounds, i.e., chitin and ergosterol. Delwiche (2003) showed that the wavelengths 1182 and 1242 nm gave the best results to discriminate sound kernels from *Fusarium*-damaged kernels. The study of Delwiche and Hareland (2004) showed that the spectral range 1130-1190 nm was strongly affected by *Fusarium* infection, with a peak at 1158 nm. In addition, the spectral range 1300-1450 nm was affected with a remarkable peak at 1400 nm. In the current study, the same peak of correlation between the spectral reflectance and the fungal DNA and DON contents appeared in the spectral range 1200-1212 nm. However, a higher correlation has been proven in the spectral range 1350-2500 nm for all *Fusarium* species.

In the current study, more pronounced peaks of correlations appeared between the spectral reflectance of wheat flour and fungal DNA and DON contents compared with wheat kernels. Dowell et al. (1999) showed that the wavelengths of 750 and 950 nm were characteristic bands in the VIS-NIR range for predicting *Fusarium*-damaged kernels. They attributed this to the effect of *Fusarium* infection on the starch and protein content of wheat kernels, which absorb the radiation of these bands. In the current study, two pronounced peaks between the flour spectral reflectance and fungal DNA and DON contents were shown in the spectral ranges 427-494 and 655-670 nm. No correlation was found in the NIR range, which indicates the tissue structure. This is attributed to the destruction of the kernel tissue structure during grinding.

In the SWIR, Peiris et al. (2009) showed that the absorption bands of different DON concentrations dissolved in acetonitrile were in 1390 to 1440 and 1880 to 1950 nm. They proved clear peaks at 1414 nm due to the -OH groups and 1906 nm due to the -C=O and R-OH groups of the DON molecule. Moreover, they proved that the bands 1195, 1208, 1365, 1445, 1700, 1905, and 2001 nm were characteristic bands for *Fusarium*-infected kernels. This is in accordance with the results of the current study, which showed two remarkable peaks of correlation between the spectral signature of the flour and fungal DNA and DON contents in the spectral ranges 1193-1231 and 1446-1465 nm, in addition to a high correlation along the spectral range 1742-2500 nm.

4.3.5. Conclusions

This study showed that *Fusarium* infection influences the spectral signatures of wheat kernels and flour produced from them. Correlations between the spectral data of infected kernels and corresponding flour, fungal DNA, and individual mycotoxins were documented. This shows the feasibility of hyperspectral imaging to screen wheat kernels and flour for *Fusarium* infection. Previous results showed the suitability of hyperspectral imaging to phenotype *Fusarium* head blight on wheat at the spike scale. Combined with the results of this study, hyperspectral imaging provides the breeder with an integrated tool to phenotype *Fusarium* infection on the spike scale and in harvested grain, accelerating the phenotyping process.

4.4. *Fusarium* Head Blight: Effect of Infection Timing on Spread of *Fusarium graminearum* and Spatial Distribution of Deoxynivalenol within Wheat Spikes

Elias Alisaac, Anna Rathgeb, Petr Karlovsky, Anne-Katrin Mahlein. 2021. Microorganisms, 9, 79. DOI: 10.3390/microorganisms9010079

Author Contributions

Elias Alisaac conceived the experiment (100%), E.A. performed the experiment (100%), E.A. analyzed the data (50%), E.A. wrote the paper (75%).

This text was not modified from the published version.

Abstract

Most studies of *Fusarium* head blight (FHB) focused on wheat infection at anthesis. Less is known about infections at later stages. In this study, the effect of infection timing on the development of FHB and the distribution of fungal biomass and deoxynivalenol (DON) along wheat spikes was investigated. Under greenhouse conditions, two wheat varieties were point inoculated with *Fusarium graminearum* starting from anthesis until 25 days after anthesis. The fungus and fungal DNA were isolated from the centers and the bases of all spikes but not from the tips for all inoculation times and both varieties. In each variety, the amount of fungal DNA and the content of DON and deoxynivalenol-3-glucoside (DON-3-G) were higher in the center than in the base for all inoculation times. A positive correlation was found between the content of fungal DNA and DON in the centers as well as the bases of both varieties. This study showed that *F. graminearum* grows downward within infected wheat spikes and that the accumulation of DON is largely confined to the colonized tissue. Moreover, *F. graminearum* was able to infect wheat kernels and cause contamination with mycotoxins even when inoculated 25 days after anthesis.

4.4.1. Introduction

Fusarium head blight (FHB) is a major threat to the yield and quality of wheat worldwide. This is because the kernels of infected plants are light in weight, deformed, and contaminated with a range of mycotoxins (McMullen et al. 2012). The most susceptible stage of wheat plants for infection with *Fusarium graminearum* is the anthesis stage GS65 (Siou et al. 2014). The pathogen can easily penetrate wheat spikes through open florets and extruded anthers. In addition, extruded anthers can trap *Fusarium* spores and stimulate fungal growth by providing nutrients required for germination and penetration (Kubo et al. 2013; Skinnes et al. 2010; Strange et al. 1974). Various studies have shown that anther extrusion contributed to wheat susceptibility to FHB (Lu et al. 2013; Xu et al. 2020).

Francl et al. (1999) showed a continuous daily release of *Fusarium* spores from the anthesis stage to kernels soft dough stage in wheat fields adjacent or distant to fields with wheat and maize residues. In fields with residues, the spore deposition on wheat spikes was highly correlated with rain periods. Wheat and maize residues thus represent a significant source of inoculum from anthesis to the later growth stages.

It is generally assumed that wheat spikes are susceptible to *F. graminearum* infection only during anthesis (Brown et al. 2010). Under greenhouse conditions, Beccari et al. (2019) investigated the effect of timing of *F. graminearum* infection on disease symptoms, fungal DNA, and secondary metabolites in wheat kernels. They concluded that the timing of infection from 0 to 9 days after anthesis (daa) did not affect disease symptoms but the infection pressure used in the experiment was too high to allow for this inference (disease severity was 100% in all varieties). Similarly, Siou et al. (2014) found the largest amount of fungal DNA and the highest toxin levels after inoculating *F. graminearum* at anthesis or 8 daa. Very low fungal biomass and toxin levels were found in spikes inoculated 18 daa. Under field conditions, Cowger and Arrellano (2010) reported comparable disease incidence and deoxynivalenol (DON) levels in wheat kernels resulted from wheat spikes inoculated with *F. graminearum* at anthesis and 10 daa in two experiments. In line with Siou et al. (2014), they found very little kernel damage and DON accumulation when *F. graminearum* was inoculated 20 daa. In contrast, Yoshida and Nakajima (2010) reported a high incidence of damaged kernels and high toxin levels after infection of susceptible wheat varieties with *F. graminearum* 20 daa. Importantly, late infections may lead to healthy-appearing kernels with high DON levels (Cowger and Arrellano 2010).

Weather conditions, particularly moisture, play an important role in FHB development and DON accumulation in infected kernels. Several researches showed that moisture in late stages after anthesis i.e. 10, 20, and 30 daa increased disease incidence, disease severity, and DON content (Cowger et al. 2009; Cowger and Arellano 2013).

Wheat shows several types of resistance to FHB. Resistance to the initial invasion of the spike and resistance to fungal spread from the infection site along the spike, they are called Type I and Type II resistance, respectively. DON is a major mycotoxin produced by *F. graminearum* and it is a virulence factor in FHB (Foroud et al. 2019). Wheat resistance to DON accumulation by preventing DON synthesis or by detoxification has been originally described as Type III resistance (Mesterházy et al. 1999) and later reclassified as Type V resistance (Foroud et al. 2019). Wheat detoxifies DON by glycosylation. DON-3-glucoside (DON-3-G) was reported for the first time in wheat suspension cultures by (Miller and Arnison 1986) and later found in naturally and artificially infected wheat kernels (Dall'Asta et al. 2005; Kluger et al. 2015; Winter et al. 2013). Lemmens et al. (2005) reported glycosylation of DON by wheat spikes and found that the genetic locus encoding this activity colocalized with a major quantitative trait locus for FHB resistance in wheat. In a comparison of a set of wheat varieties, the authors also showed that FHB resistance and the DON-3-G/DON ratio are closely related. In another study, Lemmens et al. (2016) reported that all wheat varieties are able to detoxify DON by glycosylation, which means that this trait has not been recently introduced by breeding for FHB resistance. Moreover, they suggested that increasing FHB resistance in wheat may increase DON-3-G/DON ratio in kernels.

In the studies of the effect of infection timing on FHB development reviewed above, the entire spikes were spray-inoculated, preventing the investigation of the spread of the pathogen within the spike. The aim of this research was to unravel the effect of the timing of *F. graminearum* infection of the wheat spike on fungal colonization along the spike and on the spatial distribution of DON and DON-3-G.

4.4.2. Materials and Methods

4.4.2.1. Plant Material and Experimental Conditions

In this experiment, two spring wheat varieties (*Triticum aestivum* L.) with different susceptibility to FHB were: the moderately resistant variety 'Triso' (DSV, Lippstadt, Germany) and the susceptible variety 'Sonett' (Syngenta, Basel, Switzerland) (Anonymous 2017). A mixture (1:3:6 v/v/v) of sand, horizon c of natural soil (Anonymous 2014), and potting

substrate ED 73 (Einheitserde, Sinntal-Altengronau, Sinntal, Germany) was used as a growth substrate. The experimental unit consisted of two plants per pot were grown in plastic pots of 12×12×20 cm in size. The greenhouse conditions were: 16/8 h (day/night) photoperiod obtained from an artificial light with a light intensity of >300 µmol m^{-2} s^{-1} (Philips SGR 140, Hamburg, Germany); 20 ± 2°C temperature, 50-70% relative humidity (RH) and water on demand (Alisaac et al., 2019).

4.4.2.2. *Fusarium* Inoculum and Inoculation

The isolate S.19 of *Fusarium graminearum* was used from the collection of the Institute of Crop Science and Resource Conservation (INRES), University of Bonn. . This isolate was used in previous studies and proved its virulence and its ability to produce high amounts of mycotoxins (Alisaac et al., 2019). Fungus culturing and inoculum production were performed according to Alisaac et al. (2018). A Fuchs-Rosenthal chamber was used to adjust the inoculum concentration to 1×10^5 conidia/mL. A fresh inoculum was produced for each inoculation time and used immediately after harvest to inoculate the two-central spikelets of the spike. The inoculation was done using a pipette by injecting 5 µl of inoculum and water as a control in the space between the palea and the lemma of the two-terminal florets of the spikelet.

At anthesis, six homogeneous secondary spikes per variety per pot were marked to be inoculated at different dates after anthesis. The inoculation at the anthesis stage GS61 to GS65 was considered 0 daa. Plants of both varieties were inoculated at six different dates (0, 5, 10, 15, 20, and 25 daa; six spikes per variety). Parallel controls of six spikes per expiremental unit were mock inoculated for each inoculation timing. After inoculation, the plants were incubated for 48 h at greenhouse conditions and 95% RH by covering them with plastic bags. At harvest, the spikes were collected, and each spike was divided equally into three parts: tip, center (which contains the inoculated spikelets) and base (Figure 24). Each part was threshed manually.

4.4.2.3. Pathogen Re-isolation

Twelve kernels of each part of the spike (two kernels per part and spike were selected randomly) were superficially sterilized for 2 min in 2% NaOCl and rinsed three times with sterilized distilled water for 2 min each time. The kernels of each part were placed on potato dextrose agar (PDA) (Merck, Darmstadt, Germany) in 9-cm Petri dishes and incubated at 22 ± 2°C for one week. After incubation, the re-isolation ratio was calculated.

4.4.2.4. DNA Extraction and qPCR

DNA was extracted from 20 mg flour using the cetyltrimethylammonium bromide method with polyethylene glycol precipitation (Brandfass and Karlovsky 2006) and dissolved in 50 µL TE-buffer (10 mM Tris, 1 mM EDTA, pH 8.0). DNA quality was checked by electrophoresis in 0.8% agarose gel. The DNA samples were diluted 100-fold in water and *F. graminearum* DNA was quantified by real-time PCR (qPCR) with species-specific primers (Nicholson et al. 1998) as described previously (Brandfass and Karlovsky 2006). Briefly, the PCR was performed with an initial denaturation at 95.0°C for 2 min, followed by 35 cycles of denaturation at 94.0°C for 0:30 s, annealing at 61.0°C for 0:30 s, and elongation at 68.0°C for 0:30 s. Final elongation was carried out at 68.0°C for 5 min. To generate melting curves, PCR products were heated to 95.0°C for 1 min and cooled to 55.0°C for 1 min; then the temperature was slowly raised at 0.5°C/10 s with continuous fluorescence monitoring. The standards were prepared as 3-fold dilutions of pure *F. graminearum* DNA.

4.4.2.5. Mycotoxin Extraction and HPLC-MS

For mycotoxin extraction, the flour of each part of the spike was weight, suspended in acetonitrile-water (84:16) at a ratio of 100 mg flour to 1 mL solvent, and shaken overnight. The mixture was centrifuged at 4,500 rpm and 1 mL of the supernatant was transferred to a 2-mL Eppendorf tube and dried under reduced pressure at 40°C. One mL methanol-1% formic acid in water (25:75, v/v) was used to re-suspend the dry residue. The samples were completely dissolved by sonication in an ultrasonic bath. For toxin quantification, an Agilent (Waldbronn, Germany) 1290 Infinity II HPLC system connected to an Agilent 6460 Triple Quad was used. An Agilent Zorbax Eclipse C18 column with 1.8-µm particle size and 100 × 2.1 mm diameter was used for separation (Beule et al. 2019). Briefly, the analytes were eluted by a gradient of 5% to 36% methanol in water containing 0.1% formic acid, ionized by electrospray in a positive mode, and detected by tandem mass spectrometry. DON was detected using a precursor ion m/z 297.1 $(M+H)^+$ and a product ion m/z 249.1. DON-3-G was detected after in-source fragmentation using the same transition. The limits of detection (LOD) and quantification (LOQ) for DON were 6 and 18 ng/g, respectively. The LOD and LOQ for DON-3-G were 0.11 and 0.36 µg/g, respectively.

4.4.2.6. Statistical Analysis

The statistical analysis was performed in the open-access software RStudio with the ‘agricola’ package (RStudio, Boston, USA). Kruskal-Wallis test was used to assess the significance of differences in fungal DNA, mycotoxin levels and DON-3-G/DON ratio at $p \leq 0.05$, $n = 6$.

Correlations between fungal DNA and mycotoxin levels were assessed using Pearson's correlation coefficient with the threshold of significance set at $p \leq 0.0001$, $n = 36$.

4.4.3. Results

4.4.3.1. Pathogen Movement and Re-isolation

The control spikes of both varieties showed no infection in all parts of the spike i.e. base, center, and tip. The pathogen grew in the inoculated plants from the inoculation site downward. At all inoculation times and in both varieties, the pathogen was never isolated in the tips of the spikes, but 100% from the centers and the bases of the spikes (Figure 24).

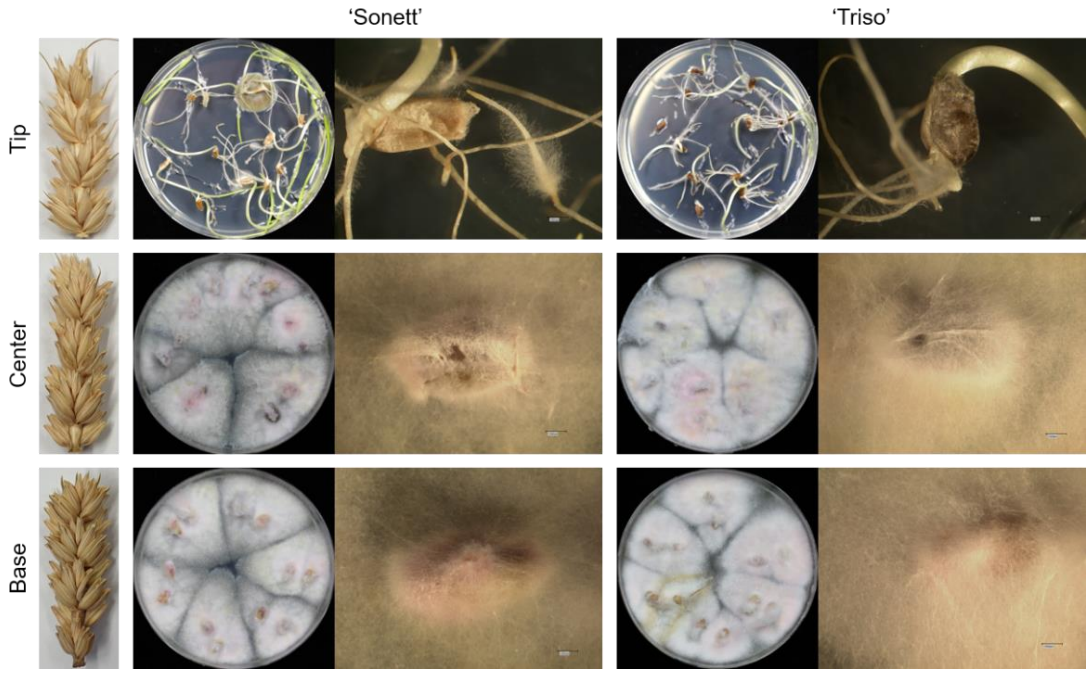

Figure 24. Sampling method and re-isolation of *Fusarium graminearum* from the tips (top row), centers (middle row), and bases (bottom row) of the spikes of spring wheat varieties 'Sonett' and 'Triso' after inoculation of the central spikelets of the spike ($n = 12$).

4.4.3.2. Effect of Infection Timing on Fungal DNA Content in Wheat Kernels

Neither variety contained any DNA of *F. graminearum* in any part of control spikes. In addition, no fungal DNA was detected in the tips of the spikes for all inoculation times in both varieties (Figure 25). The content of *F. graminearum* DNA in the centers of the spikes was higher than in the bases for all inoculation times (Figure 25). In the spike centers of both varieties, the greatest fungal DNA content was observed at the inoculation time 5 daa. The fungal DNA content decreased with inoculation timing till 25 daa. The bases of the spikes of both varieties showed the same trend, except for the maximum DNA level reached in 'Sonett' inoculated at anthesis.

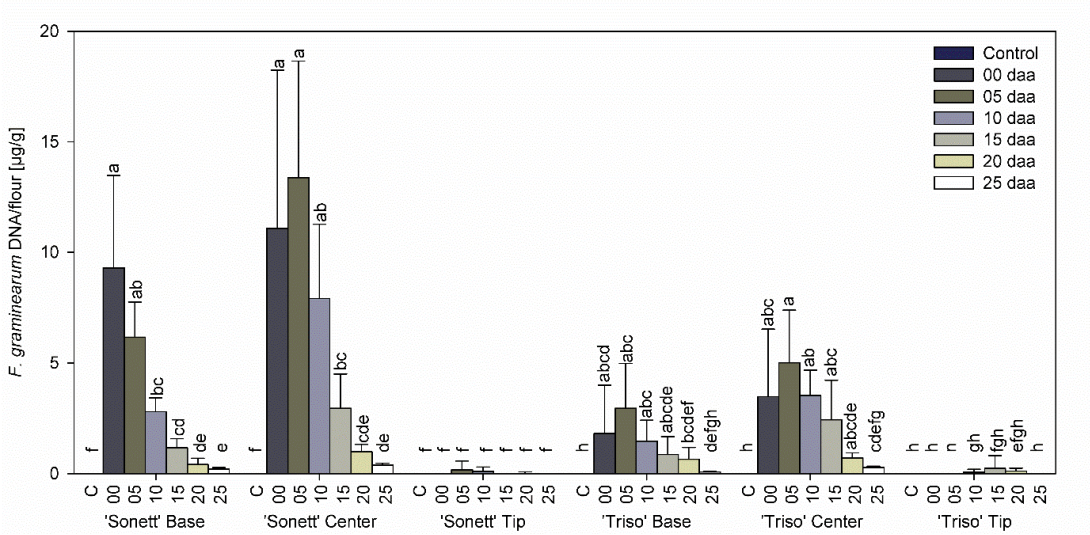

Figure 25. Fungal DNA content in the tips, centers, and bases of the spikes of spring wheat varieties 'Sonett' and 'Triso' after inoculation of the central spikelets of the spike with *Fusarium graminearum* at different days after anthesis (daa), Kruskal-Wallis test, ($p < 0.0001$), $n = 6$; treatments with the same letters at the level of the variety are not significantly different.

4.4.3.3. Effect of Infection Timing on DON, DON-3-G Content and Detoxification Ratio in Wheat Kernels

Neither DON nor DON-3-G was detected in any part of control spikes and the tips of inoculated spikes of both varieties at all inoculation times (Figure 26, 27). In both varieties, higher contents of DON and DON-3-G were shown in the centers compared with the bases at all inoculation times. The content of DON and DON-3-G in the centers and the bases of the spikes of 'Sonett' decreased with the inoculation timing from very high levels in spikes inoculated at anthesis to scarcely detectable amounts in spikes inoculated at 25 daa. In spike bases of 'Triso', the highest contents of DON and DON-3-G declined with the inoculation time in a similar way, except that the highest levels accumulated in spikes inoculated 5 daa. In spike centers of 'Triso', the values first rose before they decreased with the highest levels at 10 daa.

The ratio DON-3-G to DON, reflecting the detoxification activity, varied between 10 and 90% in the bases and the centers of the spikes in both varieties with a distinct trend (Figure 28). Very low levels or absence of DON and DON-3-G in the tips of spikes prevented the assessment of their detoxification activities.

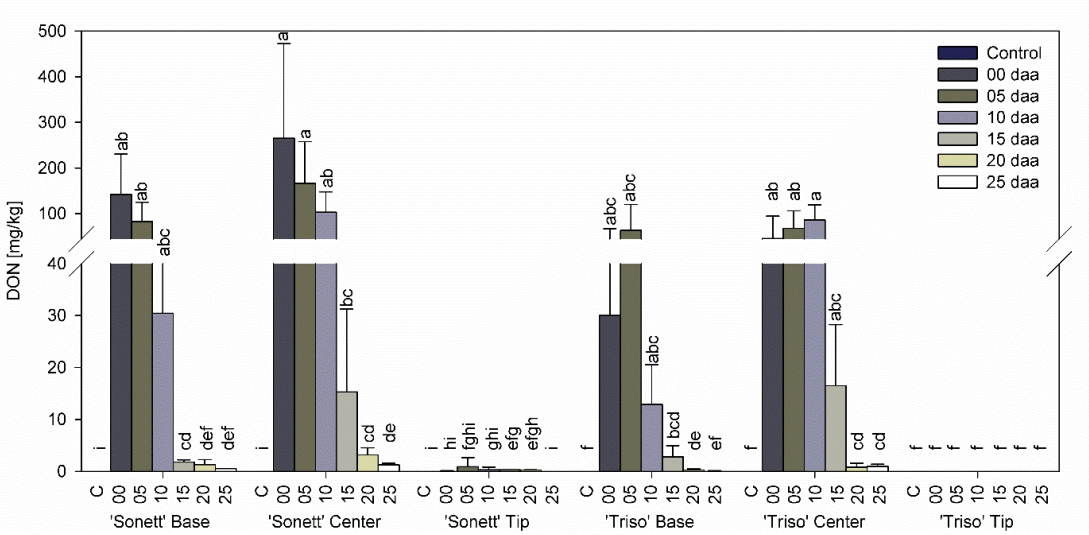

Figure 26. Deoxynivalenol content in the tips, centers, and bases of the spikes of spring wheat varieties 'Sonett' and 'Triso' after inoculation of the central spikelets of the spike with *Fusarium graminearum* at different days after anthesis (daa), Kruskal-Wallis test, ($p < 0.0001$), $n = 6$; treatments with the same letters at the level of the variety are not significantly different.

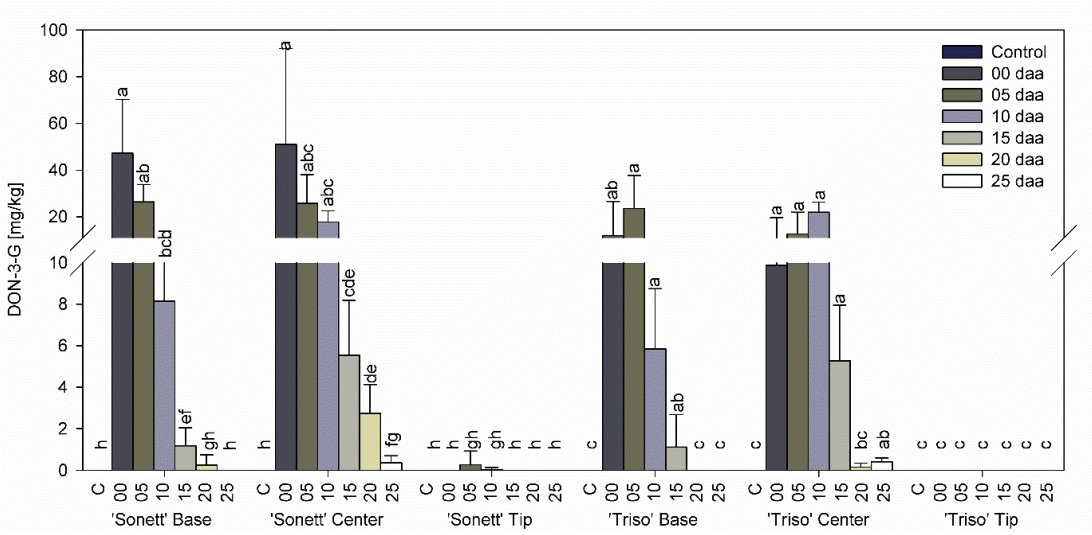

Figure 27. Deoxynivalenol-3-glucoside content in the tips, centers, and bases of the spikes of spring wheat varieties 'Sonett' and 'Triso' after inoculation of the central spikelets of the spike with *Fusarium graminearum* at different days after anthesis (daa), Kruskal-Wallis test, ($p < 0.0001$), $n = 6$; treatments with the same letters at the level of the variety are not significantly different.

4.4.3.4. Correlation between Mycotoxin Content and Fungal DNA

Pearson's correlation coefficient between fungal DNA and mycotoxin level was calculated using the data from all inoculation times. In general, a higher correlation was observed in the bases of the spikes than in the centers for both varieties (Figure 29). The susceptible variety 'Sonett' showed a higher correlation than the resistant 'Triso' for the same parts of the spike (Figure 29).

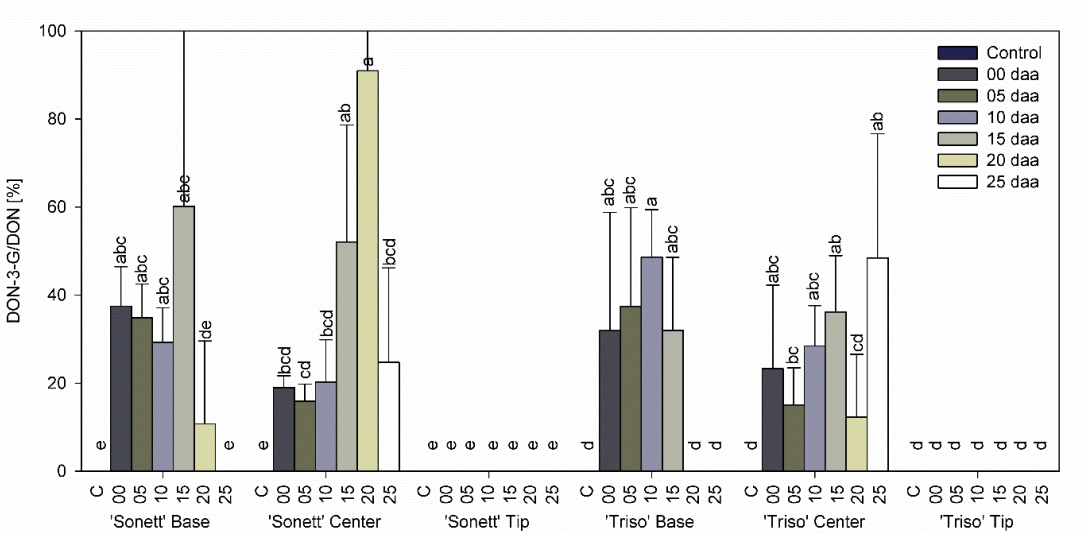

Figure 28. Deoxynivalenol-3-glucoside/Deoxynivalenol ratio in the tips, centers, and bases of the spikes of spring wheat varieties 'Sonett' and 'Triso' after inoculation of the central spikelets of the spike with *Fusarium graminearum* at different days after anthesis (daa), Kruskal-Wallis test, ($p < 0.0001$), $n = 6$; treatments with the same letters at the level of the variety are not significantly different.

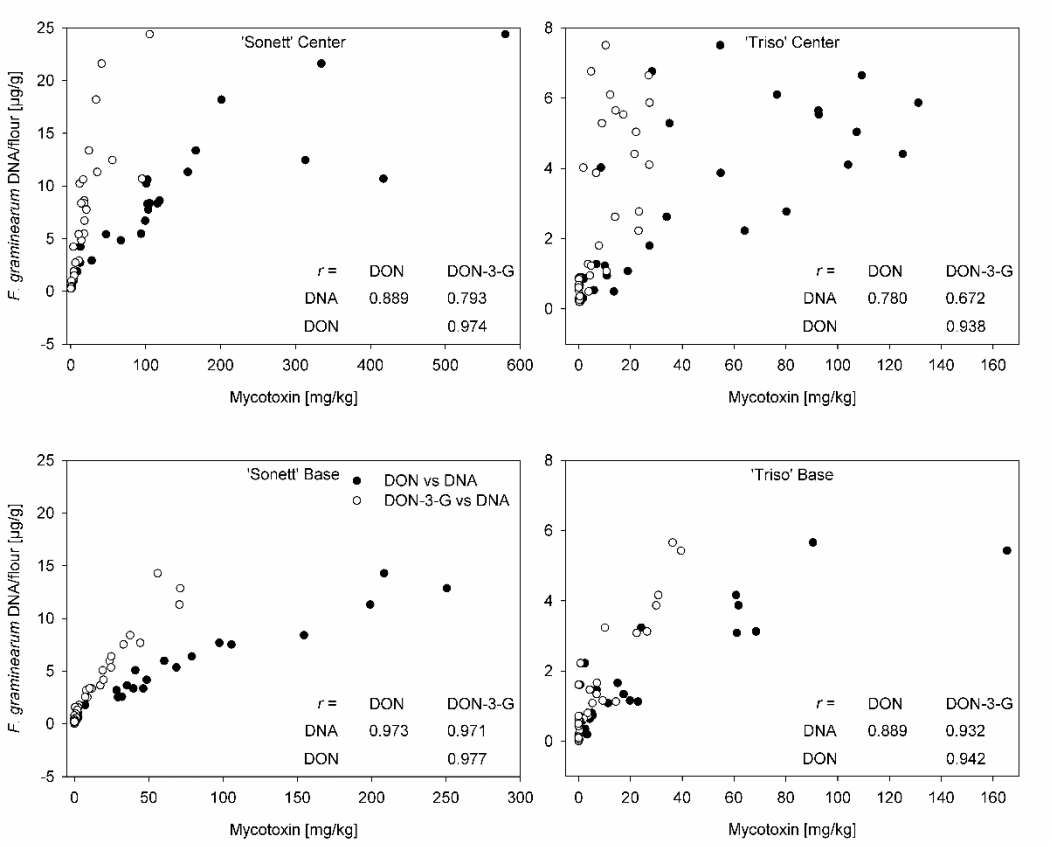

Figure 29. Pearson's correlation coefficient between fungal DNA and deoxynivalenol, fungal DNA and deoxynivalenol-3-glucoside, deoxynivalenol and deoxynivalenol-3-glucoside in the bases and centers of the spikes of spring wheat varieties 'Sonett' and 'Triso' after inoculation of the central spikelets of the spike with *Fusarium graminearum* at different days after anthesis (daa), ($p \leq 0.0001$, $n = 36$).

4.4.4. Discussion

The current study showed that the pathogen spreads from the inoculated spikelet downward at all inoculation times. This conclusion is based on the observation that the fungus was not isolated from the tips of the spikes but it was present in the centers containing the inoculated spikelets and the bases of both varieties. In addition, fungal DNA was not detectable in the tips of the spikes, while the largest amount of fungal DNA was found in the centers followed by the bases.

Predominantly downward-oriented growth of *F. graminearum* in wheat spikes was reported for the first time in 1905 by the U.S. plant pathologist Edward Freeman (Freeman 1905). Anatomical and micromorphological details of the infection of spikes were elucidated in microscopic studies for over a century. These studies confirmed that downward-oriented growth of *F. graminearum* from the point of inoculation was faster than upward-oriented growth (Atanasoff 1920; Miller et al. 2004). The qualitative character of histology however prevented quantitative comparisons. Several studies focusing on single spikelets and the neighboring tissues noticed the presence of hyphae below and above the inoculation point without attempting to compare the extent of colonization (Ilgen et al. 2009; Ribichich et al. 2000). The most revealing histological study so far regarding the direction of vertical growth of *F. graminearum* in wheat spikes examined ordered sections of the entire point-inoculated spike by optical and electron microscopy (Brown et al. 2010). The authors hypothesized that the lack of connection between the vascular vessels of the inoculated spikelet and the rachis above the point of inoculation accounted for the reduced colonization of the upper part of the spike. Another important finding of the study (Brown et al. 2010). was that two third of the colonized tissue appeared asymptomatic, indicating that visual symptoms do not provide a reliable assessment of infection.

Quantitative studies of the colonization of spikelets above and below the point of inoculation relied on visual symptoms, re-isolation of the fungus from individual spikelets, determination of fungal DNA content by qPCR, and indirectly on DON content. Visual symptoms are least reliable because seed infection poorly correlates with visual measurements (Argyris et al. 2005). Even authors who used visual assessment of spikelet infection in their work reported conjunction of symptoms caused by progressing infection with the stunting of kernels above the inoculation point due to plugged vascular tissue (Hallen-Adams et al. 2011). The

observation that colonized kernels might be asymptomatic (Brown et al. 2010) further diminishes the utility of visual symptoms for the assessment of infection.

Using re-isolation, Argyris et al. (2005) established downward-oriented growth of *F. graminearum* from point-inoculated spikelets for three out of four wheat varieties. Their results were confirmed for two other *F. graminearum* isolates in a greenhouse study (Siou et al. 2015b) and for a large number of *F. graminearum* isolates point-inoculated into the middle of wheat spikes in the field (Malbrán et al. 2012). Visual assessment of point-inoculated spikes of FHB-resistant variety 'Alsen', too, confirmed downward-oriented spread of *F. graminearum* within the spike. Infected kernels (less than 20 % of all kernels) were found up to three levels below the point of inoculation but only one level above (Hallen-Adams et al. 2011).

DON levels were reported for kernels below the point of inoculation in the same study, but not above the point of inoculation, apparently due to low sensitivity of the method (LOD of 20 µg/g) (Hallen-Adams et al. 2011). Similarly, much large amounts of DON were found in spikelets below than above the inoculation point in another study (Savard et al. 2000). These results are in line with the finding of the current study (Figure 26). Apparently, transport of DON to upper parts of the spike with the transpiration stream does not significantly affect DON content in kernels (see below).

Can *F. graminearum* colonize wheat spike in an upward direction? Some published results suggested that it might be possible. Argyris et al. (2005) reported 100% colonization of spikelets below and above the point of inoculation in their most susceptible accession. When comparing the results from Argyris et al. (2005), several aspects have to be considered critically. The breeding line 'GA 89482-E7' perhaps possessed lower Type II resistance than the susceptible commercial variety 'Sonett' used in the current study. Furthermore, the inoculation conditions differed: Argyris et al. (2005) kept inoculated plants at 25-35 °C and 100% humidity for 72 h, while inoculated plants in the current study were kept at 20 °C and 95% humidity only for 48 h. We assume that the combination of high susceptibility of the host plant and highly conducive infection conditions accounted for the heavy infection of spikelets of this particular variety above the point of inoculation. These conditions may occur in some growing areas.

Ha et al. (2016) investigated the effect of wheat variety on hyphal growth of *F. graminearum*. They showed abundant growth of fungal hyphae in the inoculated spikelet of the susceptible

variety ‘Milan’ compared with the resistant ‘Sumai 3’. Fungal DNA amount decreased with infection timing from 5 daa in the centers of both varieties. This tendency was more obvious in the bases of the susceptible variety ‘Sonett’ than in the resistant ‘Triso’. This corresponds to the results of former studies, which showed that the amount of DNA of *F. graminearum* in wheat kernels decreased with infection timing after spray inoculation. Siou et al., (2014) reported decreasing amounts of fungal DNA of two aggressive isolates of *F. graminearum* in wheat kernels between 8 daa and 28 daa. Similarly, Beccari et al. (2019) described decreasing accumulation of fungal DNA from 3 daa until 9 daa.

Previous reports documented DON translocation within the plant tissues above the inoculation site. Kang & Buchenauer (1999) showed that the hyphae of *F. culmorum* could not be detected in third spikelets above the inoculated spikelet, but DON was present especially in the xylem vessels and phloem sieve tubes, suggesting that DON can be translocated upward through these tissues. DON translocation was also reported after stem-base-inoculation of bread wheat with different *Fusarium* species i.e. *F. pseudograminearum*, *F. culmorum,* and *F. graminearum*. Even if the fungus was not present in the spike tissue (including chaff, rachis, and kernels), DON was detectable in the spike tissue of the stem-base-infected plants (Beccari et al., 2018b). In contrast, the results of the current study did not confirm DON translocation from inoculated spikelets into the kernels at the tip of the spike for both varieties and all inoculation times. This is attributed to differences in the investigated tissues since former studies proved an upward DON translocation into spike tissue including the chaff and rachis, whereas the current study investigated DON translocation in wheat kernels above the inoculation site. In addition, in the stem-base-inoculation, the plants were inoculated at the seedling stage, which means the entire plant tissue was contaminated with DON before spike formation. In the current study, the plants were inoculated at the anthesis stage after spike emergence.

The DON content in wheat kernels is affected by several factors including the wheat variety, infection timing, and weather conditions especially post-anthesis moisture (Cowger et al. 2009; Yoshida and Nakajima 2010). Several studies showed that a significant amount of DON can be produced 20 daa, even when the plants were inoculated at anthesis. In addition, late infection resulted in healthy-appearing kernels contaminated with high levels of DON. The high level of DON was attributed to the long duration of post-anthesis moisture that provided optimal conditions for the fungus to induce infection and produce mycotoxins (Cowger and Arrellano 2010; Cowger and Arellano 2013; Yoshida and Nakajima 2010). This can also be achieved by incubating the plants under plastic bags for 48 h after inoculation. Alisaac et al. (2019) showed

that incubating wheat plants under plastic bags for 48 h after inoculation resulted in high fungal DNA content and DON contamination even with a concentration of 1×10^4 conidia/mL of inoculum. The current study demonstrated the ability of *F. graminearum* to infect and contaminate wheat kernels with DON up to 25 daa. However, the amount of the inoculum that was delivered directly into the space between the palea and the lemma helped to induce the infection even 25 daa. This amount of inoculum will not be available within the wheat spikelets under natural conditions. Therefore, the time window for successful infection under natural conditions is likely to be narrower.

Variety resistance and infection timing had a significant effect on DON content in the kernels. The susceptible variety 'Sonett' showed decreasing DON content in the centers and the bases starting from 0 until 25 daa. These results correspond with the results of Siou et al. (2014) who reported decreasing DON contents in the highly susceptible wheat variety 'Royssac' from 0-28 daa. The moderately resistant variety 'Triso' exhibited increasing DON contents from 0-10 daa in the centers and from 0-5 daa in the bases. Beccari et al. (2019) reported the same trend of *F. graminearum* to cause higher DON contamination at 3 and 6 daa than 0 and 9 daa in the wheat variety 'Dyna-Gro Shirley'.

The content of fungal DNA correlated with DON content in both varieties for all inoculation times, which is similar to the results of Beccari et al. (2019) and Siou et al. (2014). The correlation appeared tighter in the bases than in the centers of the spikes (Figure 29). We assume that different age of hyphae in these tissues and a decline of DON production in aging hyphae (Boenisch and Schäfer 2011; Ilgen et al. 2009) might have accounted for this phenomenon. The centers of spikes contained young and old hyphae at varying ratios, while the bases were colonized by young hyphae sharing the same DON production rate. The correlation remained rather tight even in the centers of spikes, indicating that fungal hyphae produced DON at the same rate in all parts of the spike. Hallen-Adams et al. (2011) attempted to relate the expression of *Tri*5, which is the key gene of DON synthesis, to the DON content in individual spikelets. They found gene expression levels inconsistent with DON levels. For instance, the highest observed DON level was associated with a low *Tri*5 expression while relatively high *Tri*5 expression was associated with much lower DON levels. The discrepancy is not surprising because DON accumulated in the tissue is the result of DON productivity (corresponding to gene expression) multiplied by the fungal biomass and time, rather than to DON productivity alone. Furthermore, the authors used the ratio of threshold cycles (Ct) of *Tri*5 and a housekeeping gene (*GAPDH*) as a measure of relative *Tri5* expression. This is

incorrect because Ct is inversely proportional to the logarithm of mRNA level; the difference of Ct values rather than ratio should have been used, as exemplified by the customary ΔΔCt method.

The current study demonstrated that the glycosylation ratio increased as DON content of the wheat kernels decreased at later inoculation times. This was clearly shown in the bases, which contained lower amounts of DON than the centers in both varieties, and even stronger in the centers (Figure 28). We speculate that protein synthesis was suppressed by DON in spikelets with higher DON content, reducing the synthesis of the enzyme responsible for the glycosylation. In addition, it was shown that variety resistance plays a role in DON detoxification, with the detoxification ratio being higher for 'Triso' compared with 'Sonett'. This corresponds well with former studies, which showed that DON content and variety resistance are the main factors affecting DON detoxification in wheat (Berthiller et al., 2005; Lemmens et al., 2016). The high levels of DON-3-G relative to DON in both varieties show that DON-3-G should be legislated and measured in wheat kernels used in the food and feed supply chain because DON-3-G can be reconverted to DON in humans and animals.

4.4.5. Conclusions

This study showed that *Fusarium graminearum* is able to infect wheat spikes and cause DON contamination in wheat kernels under greenhouse conditions even when inoculated 25 days after anthesis. The infection timing played a significant role in fungal growth expressed by fungal DNA and DON content in infected kernels. The fungus grew from the inoculation site downward within infected wheat spikes and DON accumulation was confined to the colonized tissue. Variety resistance and DON content correlated with the glycosylation of DON in infected wheat kernels.

5. General Discussion and Conclusions

Agricultural production is affected by abiotic and biotic stresses that reduce the quantity and the quality of the final product. Among biotic stresses, plant pathogens (i.e. viruses, bacteria, and fungi) contribute significantly to these losses, however, it is still difficult to give an accurate estimation for these losses (Oerke 2006; Savary et al. 2019). In wheat, plant pathogens, mainly, leaf diseases and FHB cause up to 21.5% of yield and quality losses (Savary et al. 2019). Reducing this damage contributes to stabilizing food security and food safety in addition to its economic benefits for the farmer.

The avoidance of yield and quality losses caused by plant diseases can be achieved by involving the integrated pest management strategy in the agricultural system. This, in turn, contains different practices i.e. cultural practices, planting resistant varieties, biological control, chemical control, and predicting and detecting disease incidence. Among these practices, fungicides application is laborious, expensive; in addition, the pathogen can develop fungicide-resistant strains that will not respond to the fungicide treatment in the future. Moreover, fungicides have negative effects on non-targeted organisms and may hazard the health of agricultural workers. However, the lack of sufficient resistance in the available varieties to specific diseases e.g. FHB, makes fungicides application a necessity to control the disease. Therefore, decreasing fungicides applications will reduce labor and costs, contribute to protecting the environment and human health, and keep it as an effective tool to control the disease. This can be reached by reducing the number of treatments and using the local treatment to the infected plants in the field.

The damage caused by FHB includes yield losses and contamination of wheat kernels with mycotoxins. Therefore, applying fungicides at an early stage of pathogenicity should be considered in the management strategy of the disease (Torres et al. 2019). This, in turn, needs an accurate control of disease incidence under field conditions either for local treatment to the infected spots or for treating the entire crop. In addition, the selective harvest of healthy spikes could be an option to avoid infected spikes and reduces mycotoxin contamination (Bauriegel and Herppich 2014). This shows the need for effective tools for real-time detection and identification of plant diseases in the field. Optical sensors proved feasibility to detect and identify plant disease under controlled and field conditions (Mahlein 2016). Former studies successfully implemented HSI and CFI to detect to discriminate healthy and FHB-infected spikes (Bauriegel et al. 2011a,b).

The results of the current studies showed the applicability of optical sensors i.e. IRT, CFI, and HSI to detect FHB on the spikelet scale as early as three days after inoculation using machine learning approach. Fusing data of different sensors promoted the overall classification accuracy during the pathogenicity with the best combination between IRT-HSI (Mahlein et al. 2019). This will support the decision-making strategy with the required information about FHB incidence to apply fungicides against FHB at an early stage of pathogenicity.

Based on the SVIs of wheat spikes, it was also possible to discriminate between healthy and FHB-infected spikes as well as spikes infected with different *Fusarium* species (Alisaac et al. 2018). Using SVIs in FHB detection reduces the required data and time for FHB detection because these indices are calculated based on a few numbers of wavebands within the electromagnetic spectrum. This shows the feasibility of using multispectral instead of hyperspectral sensors for real-time detection and identification of FHB under field conditions. This, in turn, gives the possibility of local treatment of infected spots in the field and reduces the quantities of plant protection chemicals required for disease management. In addition, selective harvest aided by spectral sensors helps to avoid the infected spikes during harvest and reduces mycotoxin contamination of the harvested wheat kernels.

The high yielding varieties with sufficient resistance to plant diseases and pests are required to fulfill the global demand for food and feed. In addition, the involvement of resistant varieties in the agricultural systems will reduce the use of plant protection chemicals substantially. This requires finding new sources of genetic variations with sufficient resistance to pathogens and pests, increasing the size of the breeding programs with faster breeding cycles, improving the selection accuracy, and developing decision-making tools (Araus et al. 2018). Accelerating the breeding programs requires also interdisciplinary research involving plant pathology plant genetics, statistical models of plant genomic and phenomic data, as well as the development of plant phenotyping techniques in the field (Bolger et al. 2017).

Besides the yield, different plant traits (e.g. plant height, lodging, tolerance of drought and salinity, and diseases and pests resistance), have to be assessed simultaneously during the phenotyping process. The genotype-environment interaction is another important factor that has to be assessed during the phenotyping and this, in turn, means repeating the phenotyping at multiple locations with different environmental conditions. This makes the phenotyping under field conditions challenging process because it is laborious, time-consuming, and subjected to human error. In this term, using optical sensors especially multi- and hyperspectral

imaging sensors in phenotyping can provide an objective assessment for plant traits in addition to reduce the time and the labor in the field. These sensors showed feasibility to assess plant-pathogen interaction as a plant-resistance trait under controlled and field conditions (Mahlein et al. 2018).

Wheat resistance to FHB can be assessed as the number of infected spikes (disease incidence) that represents Type I resistance, and the number of infected spikelets per spike (disease severity) that represents Type II resistance (Bai and Shaner 1994). Assessment of either Type I or Type II resistance requires multiple observation of disease symptoms during the pathogenicity and combining these observations into one value represented by the AUDPC (Simko and Piepho 2012). Thereafter, wheat varieties are ranked according to their resistance to FHB based on the values of AUDPC.

The results of the current research showed the feasibility of HSI to quantify FHB symptoms on wheat spikes based on the SVIs derived from the mean spectral signature of wheat spikes during the disease development. A main output of the current research is designing an automated model to rank wheat varieties according to their resistance to FHB based on multiple hyperspectral assessments of disease development during the pathogenicity (Alisaac et al. 2018). This approach provides an objective tool to phenotype wheat resistance to FHB automatically. This in turn reduces the time and the labor required during the phenotyping process.

Another factor to be considered during the phenotyping process is after-harvest-phenotyping that targets the kernels. This includes phenotyping of Type III, Type IV, and Type V resistance that denote to resistance to kernel infection, tolerance against FHB, and resistance to trichothecenes respectively (Foroud et al. 2019; Mesterházy et al. 1999). The assessment of Type III and Type IV resistance needs pathogen re-isolation on selective media, which takes a long time to calculate the infection ratio. In addition, pathogen re-isolation gives only qualitative results (i.e. healthy vs infected) without any quantitative information about the fungal biomass in the infected kernels. Detection and quantification of *Fusarium* DNA content in wheat kernels using qPCR is an alternative tool to assess Type III and Type IV resistance. This tool provides quantitative information about the fungal biomass in the infected kernels. Moreover, trichothecenes detection and quantification using the immunological method (ELISA) or the chemical method (HPLC) is essential for phenotyping of Type V resistance (Góral et al. 2019). All the methods mentioned above are destructive, time-consuming,

laborious, and in the case of mycotoxin quantification, they are expensive (Bock 2020). For the aforementioned reasons, phenotyping of these types of resistance is only performed for the advanced lines at the latest stages of the breeding program. Recently, HSI showed feasibility for detecting FDK and DON contamination in wheat kernels (Femenias et al. 2020).

The results of the current work proved the applicability of HSI to detect wheat kernels and flour contaminated with multiple levels of DON and fungal DNA of different *Fusarium* species (Alisaac et al. 2019). This allows the screening of a large number of wheat entries within a short time according to their DON and *Fusarium* DNA contents. Moreover, this technology will reduce the costs, labor, and time required for wheat kernel phenotyping against FHB.

Recent studies proved a change in *Fusarium* profile causing FHB on wheat in southern central and northern Europe with a dominancy of *F. graminearum*. They attributed the conversion in the *Fusarium* profile to the climate change in the world and emphasized the need for tolerant varieties and modern fungicides to control FHB on wheat (Moretti et al. 2019). In Europe, these climate changes are expected to be an increase in temperature between 2.5-5°C with longer drought periods which might decrease crop yields in southern and western Europe. While in central and northern Europe the increase in temperature is expected to be between 3-4.5°C with significantly increased rainfall and a potential increase in crop yields (Magan et al. 2011). Recent modeling studies investigated the potential effect of climate changes on wheat phenology mainly anthesis and maturity dates in correlation with FHB epidemics and DON contamination. Madgwick et al. (2011) expected an earlier anthesis date with more severe FHB epidemics and increased DON contamination in wheat by the 2050s in the UK. In the Netherlands, van der Fels-Klerx et al. (2013) showed that wheat anthesis and maturity dates will advance 5-11 and 10-17 days respectively with a significant increase in DON contamination by the 2040s. Comparable results were obtained using data from Norway, Sweden, and Finland (van der Fels-Klerx et al. 2012). All the models reviewed above expect a significant increase in DON contamination in small cereal grains in the future (van der Fels-Klerx et al. 2016). This raises the question about the effect of *Fusarium* infection timing with reference to wheat anthesis and the role of variety resistance on DON accumulation in wheat kernels.

The results of the current study showed that *F. graminearum* grows for the infection site downward and DON contamination is confined only with the infected tissue. In addition, it showed the ability of *F. graminearum* to infect wheat kernels and cause DON and DON-3-G

contamination even when the infection was done close to maturity. It proved also that the major DON contamination occurred when the infection took place from 0-10 days after anthesis. Variety resistance played a role in DON contamination and DON detoxification in infected wheat kernels while lower DON content was observed in moderately resistant variety compared with susceptible variety. The DON content played a role in detoxification ratio with a tendency to higher detoxification ratio with a lower DON content in infected wheat kernels. The high levels of DON-3-G in infected wheat kernels are of concern during the food and feed processing for two reasons. Firstly, it can not be detected during the traditional DON analysis. Secondly, it is hydrolyzed into its parental mycotoxins through digestion (Rychlik et al. 2014). This shows the necessity for controlling this mycotoxin in the food chain.

In summary, this work showed that optical sensors, mainly IRT and HSI are promising tools to monitor FHB infection on wheat. These tools can be used to prevent quality and quantity losses caused by FHB in wheat yield. Besides, the results showed the feasibility of HSI to phenotype wheat resistance to FHB on the spike scale as well as to phenotype FHB infection and mycotoxin contamination on the kernel scale. This would be an effective advantage to accelerate the phenotyping process in the breeding programs. The results emphasized that the masked mycotoxin deoxynivalenol-3-glucoside should be legislated and monitored during the food and feed processing due to the high levels of this mycotoxin even with the late infection with FHB.

6. References

Aboukhaddour, R., Fetch, T., McCallum, B. D., Harding, M. W., Beres, B. L., and Graf, R. J. 2020. Wheat diseases on the prairies: a Canadian story. Plant Pathol. 69:418–432.

Alisaac, E., Behmann, J., Kuska, M. T., Dehne, H. W., and Mahlein, A. K. 2018. Hyperspectral quantification of wheat resistance to *Fusarium* head blight: comparison of two *Fusarium* species. Eur. J. Plant Pathol. 152:869–884.

Alisaac, E., Behmann, J., Rathgeb, A., Karlovsky, P., Dehne, H.-W., and Mahlein, A.-K. 2019. Assessment of *Fusarium* infection and mycotoxin contamination of wheat kernels and flour using hyperspectral imaging. Toxins. 11:556.

Alkadri, D., Nipoti, P., Döll, K., Karlovsky, P., Prodi, A., and Pisi, A. 2013. Study of fungal colonization of wheat kernels in Syria with a focus on *Fusarium* species. Int. J. Mol. Sci. 14:5938–5951.

Alkadri, D., Rubert, J., Prodi, A., Pisi, A., Mañes, J., and Soler, C. 2014. Natural co-occurrence of mycotoxins in wheat grains from Italy and Syria. Food Chem. 157:111–118.

Al Masri, A., Hau, B., Dehne, H. W., Mahlein, A. K., and Oerke, E. C. 2017. Impact of primary infection site of *Fusarium* species on head blight development in wheat ears evaluated by IR-thermography. Eur. J. Plant Pathol. 147:855–868.

Alshannaq, A., and Yu, J. H. 2017. Occurrence, toxicity, and analysis of major mycotoxins in food. Int. J. Environ. Res. Public Health. 14:632.

Alvarez, C. L., Azcarate, M. P., and Pinto, V. F. 2009. Toxigenic potential of *Fusarium graminearum* sensu stricto isolates from wheat in Argentina. Int. J. Food Microbiol. 135:131–135.

Amarasinghe, C. C., Tamburic-Ilincic, L., Gilbert, J., Brûlé-Babel, A. L., and Dilantha Fernando, W. G. 2013. Evaluation of different fungicides for control of *Fusarium* head blight in wheat inoculated with 3ADON and 15ADON chemotypes of *Fusarium graminearum* in Canada. Can. J. Plant Pathol. 35:200–208.

Anonymous. 2013. Descriptive list of varieties, the Federal Plant Variety Office, Hannover, Germany. Getreide, Mais, Öl- und Faserpflanzen, Legum. Rüben, Zwischenfrüchte. Available at: https://www.bundessortenamt.de/bsa/media/Files/BSL/bsl_getreide_2013.pdf.

Anonymous. 2017. Descriptive list of varieties, the Federal Plant Variety Office, Hannover, Germany. Getreide, Mais, Öl- und Faserpflanzen, Legum. Rüben, Zwischenfrüchte. Available at: https://www.bundessortenamt.de/bsa/media/Files/BSL/bsl_getreide_2017.pdf.

Anonymous. 2014. *Keys to soil taxonomy*. Twelfth Ed. ed. D. W. Smith. United States Department of Agriculture, Natural Resources Conservation Service.

Aoki, T., O'Donnell, K., and Geiser, D. M. 2014. Systematics of key phytopathogenic *Fusarium* species: current status and future challenges. J. Gen. Plant Pathol. 80:189–201.

Araus, J. L., Kefauver, S. C., Zaman-Allah, M., Olsen, M. S., and Cairns, J. E. 2018. Translating high-throughput phenotyping into genetic gain. Trends Plant Sci. 23:451–466.

Argyris, J., TeKrony, D., Hershman, D., VanSanford, D., Hall, M., Kennedy, B., et al. 2005. *Fusarium* head blight infection following point inoculation in the greenhouse compared with movement of *Fusarium graminearum* in seed and floral components. Crop Sci. 45:626–634.

Atanasoff, D. 1920. *Fusarium* blight (scab) of wheat and other cereals. J. Agric. Res. 20:1–32.

Ayeneh, A., Van Ginkel, M., Reynolds, M. P., and Ammar, K. 2002. Comparison of leaf, spike, peduncle and canopy temperature depression in wheat under heat stress. F. Crop. Res. 79:173–184.

Bai, G., and Shaner, G. 1994. Scab of wheat: prospects for control. Plant Dis. 78:760–766.

Bai, G., Su, Z., and Cai, J. 2018. Wheat resistance to *Fusarium* head blight. Can. J. Plant Pathol. 40:336–346.

Baker, N. R. 2008. Chlorophyll fuorescence: a probe of photosynthesis *in vivo*. Annu. Rev. Plant Biol. 59:89–113.

REFERENCES

Barbedo, J. G. A., Tibola, C. S., and Fernandes, J. M. C. 2015. Detecting *Fusarium* head blight in wheat kernels using hyperspectral imaging. Biosyst. Eng. 131:65–76.

Barros, G., Zanon, M. S. A., Palazzini, J. M., Haidukowski, M., Pascale, M., and Chulze, S. 2012. Trichothecenes and zearalenone production by *Fusarium equiseti* and *Fusarium semitectum* species isolated from Argentinean soybean. Food Addit. Contam. - Part A. 29:1436–1442.

Basler, R. 2016. Diversity of *Fusarium* species isolated from UK forage maize and the population structure of *F. graminearum* from maize and wheat. PeerJ. 4:e2143.

Bauriegel, E., Giebel, A., and Herppich, W. B. 2010. Rapid *Fusarium* head blight detection on winter wheat ears using chlorophyll fluorescence imaging. J. Appl. Bot. Food Qual. 83:196–203.

Bauriegel, E., Giebel, A., Geyer, M., Schmidt, U., and Herppich, W. B. 2011a. Early detection of *Fusarium* infection in wheat using hyper-spectral imaging. Comput. Electron. Agric. 75:304–312.

Bauriegel, E., Giebel, A., and Herppich, W. B. 2011b. Hyperspectral and chlorophyll fluorescence imaging to analyse the impact of *Fusarium culmorum* on the photosynthetic integrity of infected wheat ears. Sensors. 11:3765–3779.

Bauriegel, E., and Herppich, W. B. 2014. Hyperspectral and chlorophyll fluorescence imaging for early detection of plant diseases, with special reference to *Fusarium* spec. infections on wheat. Agriculture. 4:32–57.

Beccari, G., Colasante, V., Tini, F., Senatore, M. T., Prodi, A., Sulyok, M., et al. 2018a. Causal agents of *Fusarium* head blight of durum wheat (*Triticum durum* Desf.) in central Italy and their *in vitro* biosynthesis of secondary metabolites. Food Microbiol. 70:17–27.

Beccari, G., Prodi, A., Pisi, A., Nipoti, P., Onofri, A., Nicholson, P., et al. 2018b. Development of three *Fusarium* crown rot causal agents and systemic translocation of deoxynivalenol following stem base infection of soft wheat. Plant Pathol. 67:1055–1065.

Beccari, G., Arellano, C., Covarelli, L., Tini, F., Sulyok, M., and Cowger, C. 2019. Effect of wheat infection timing on *Fusarium* head blight causal agents and secondary metabolites in grain. Int. J. Food Microbiol. 290:214–225.

Behmann, J., Mahlein, A. K., Rumpf, T., Römer, C., and Plümer, L. 2015. A review of advanced machine learning methods for the detection of biotic stress in precision crop protection. Precis. Agric. 16:239–260.

Behmann, J., Acebron, K., Emin, D., Bennertz, S., Matsubara, S., Thomas, S., et al. 2018. Specim IQ: evaluation of a new, miniaturized handheld hyperspectral camera and its application for plant phenotyping and disease detection. Sensors. 18:441.

Berdugo, C. A., Zito, R., Paulus, S., and Mahlein, A. K. 2014. Fusion of sensor data for the detection and differentiation of plant diseases in cucumber. Plant Pathol. 63:1344–1356.

Bertero, A., Moretti, A., Spicer, L. J., and Caloni, F. 2018. *Fusarium* molds and mycotoxins: potential species-specific effects. Toxins. 10:1–27.

Berthiller, F., Dall'Asta, C., Schuhmacher, R., Lemmens, M., Adam, G., and Krska, A. R. 2005. Masked mycotoxins: determination of a deoxynivalenol glucoside in artificially and naturally contaminated wheat by liquid chromatography-tandem mass spectrometry. J. Agric. Food Chem. 53:3421–3425.

Berthiller, F., Crews, C., Dall'Asta, C., Saeger, S. De, Haesaert, G., Karlovsky, P., et al. 2013. Masked mycotoxins: a review. Mol. Nutr. Food Res. 57:165–186.

Beukes, I., Rose, L. J., van Coller, G. J., and Viljoen, A. 2018. Disease development and mycotoxin production by the *Fusarium graminearum* species complex associated with South African maize and wheat. Eur. J. Plant Pathol. 150:893–910.

Beule, L., Lehtsaar, E., Rathgeb, A., and Karlovsky, P. 2019. Crop diseases and mycotoxin accumulation in temperate agroforestry systems. Sustain. 11:2925.

Beyer, M., Pogoda, F., Ronellenfitsch, F. K., Hoffmann, L., and Udelhoven, T. 2010. Estimating deoxynivalenol contents of wheat samples containing different levels of *Fusarium*-damaged kernels by diffuse reflectance spectrometry and partial least square regression. Int. J. Food Microbiol. 142:370–374.

REFERENCES

Birzele, B., Meier, A., Hindorf, H., Krämer, J., and Dehne, H. W. 2002. Epidemiology of *Fusarium* infection and deoxynivalenol content in winter wheat in the Rhineland, Germany. Eur. J. Plant Pathol. 108:667–673.

Blackburn, G. A. 1998a. Quantifying chlorophylls and carotenoids at leaf and canopy scales: an evaluation of some hyperspectral approaches. Remote Sens. Environ. 66:273–285.

Blackburn, G. A. 1998b. Spectral indices for estimating photosynthetic pigment concentrations: a test using senescent tree leaves. Int. J. Remote Sens. 19:657–675.

Blandino, M., Haidukowski, M., Pascale, M., Plizzari, L., Scudellari, D., and Reyneri, A. 2012. Integrated strategies for the control of *Fusarium* head blight and deoxynivalenol contamination in winter wheat. F. Crop. Res. 133:139–149.

Bock, C. H., Poole, G. H., Parker, P. E., and Gottwald, T. R. 2010. Plant disease severity estimated visually, by digital photography and image analysis, and by hyperspectral imaging. CRC. Crit. Rev. Plant Sci. 29:59–107.

Bock, C. H. 2020. From visual estimates to fully automated sensor-based measurements of plant disease severity: status and challenges for improving accuracy. 2:9.

Boenisch, M. J., and Schäfer, W. 2011. *Fusarium graminearum* forms mycotoxin producing infection structures on wheat. BMC Plant Biol. 11:110.

Bolger, M., Schwacke, R., Gundlach, H., Schmutzer, T., Chen, J., Arend, D., et al. 2017. From plant genomes to phenotypes. J. Biotechnol. 261:46–52.

Borg, I., and Groenen, P. J. F. 2005. *Modern multidimensional scaling: Theory and applications*. 2nd Ed. New York: Springer.

Bottalico, A., and Perrone, G. 2002. Toxigenic *Fusarium* species and mycotoxins associated with head blight in small-grain cereals in Europe. Eur. J. Plant Pathol. 108:611–624.

Bragulat, M. R., Martínez, E., Castellá, G., and Cabañes, F. J. 2004. Selective efficacy of culture media recommended for isolation and enumeration of *Fusarium* spp. J. Food Prot. 67:207–211.

Brandfass, C., and Karlovsky, P. 2006. Simultaneous detection of *Fusarium culmorum* and *F. graminearum* in plant material by duplex PCR with melting curve analysis. BMC Microbiol. 6:4.

Braun, M. S., and Wink, M. 2018. Exposure, occurrence, and chemistry of fumonisins and their cryptic derivatives. Compr. Rev. Food Sci. Food Saf. 17:769–791.

Brown, N. A., Urban, M., van de Meene, A. M. L., and Hammond-Kosack, K. E. 2010. The infection biology of *Fusarium graminearum*: defining the pathways of spikelet to spikelet colonisation in wheat ears. Fungal Biol. 114:555–571.

Brugger, A., Kuska, M. T., and Mahlein, A. K. 2018. Impact of compatible and incompatible barley-*Blumeria graminis* f.sp. *hordei* interactions on chlorophyll fluorescence parameters. J. Plant Dis. Prot. 125:177–186.

Brunner, K., Farnleitner, A., and Mach, R. L. 2012. Novel methods for the quantification of pathogenic fungi in crop plants: quantitative PCR and ELISA accurately determine *Fusarium* biomass. In *Plant pathology*, ed. C. J. Cumagun. London: IntechOpen Limited, p. 203–218.

Buerstmayr, H., Ban, T., and Anderson, J. A. 2009. QTL mapping and marker-assisted selection for *Fusarium* head blight resistance in wheat: a review. Plant Breed. 128:1–26.

Bürling, K. 2011. Potential of fluorescence techniques with special reference to fluorescence lifetime determination for sensing and differentiating biotic and abiotic stresses in *Triticum aestivum* L. Available at: http://nbn-resolving.de/urn:nbn:de:hbz:5N-25907.

Bushnell, W. R., Hazen, B. E., and Pritsch, C. 2003. Histology and physiology of *Fusarium* head blight. In *Fusarium head blight of wheat and barley*, ed. W. R. Leonard, and K. J. Bushnell. St. Paul, MN, USA: American Phytopathological Society Press, p. 44–83.

Butler, W. L., and Kitajima, M. 1975. Fluorescence quenching in Photosystem II of chloroplasts. Biochim. Biophys. Acta - Bioenerg. 376:116–125.

REFERENCES

CABI, Centre for Agriculture and Bioscience International. 2020. Crop Protection Compendium. Available at: https://www.cabi.org/cpc/datasheet/55203 [Accessed March 3, 2020].

Cainong, J. C., Bockus, W. W., Feng, Y., Chen, P., Qi, L., Sehgal, S. K., et al. 2015. Chromosome engineering, mapping, and transferring of resistance to *Fusarium* head blight disease from *Elymus tsukushiensis* into wheat. Theor. Appl. Genet. 128:1019–1027.

Calderón, R., Navas-Cortés, J. A., and Zarco-Tejada, P. J. 2015. Early detection and quantification of *Verticillium* wilt in olive using hyperspectral and thermal imagery over large areas. Remote Sens. 7:5584–5610.

Castañares, E., Albuquerque, D. R., Dinolfo, M. I., Pinto, V. F., Patriarca, A., and Stenglein, S. A. 2014. Trichothecene genotypes and production profiles of *Fusarium graminearum* isolates obtained from barley cultivated in Argentina. Int. J. Food Microbiol. 179:57–63.

Chaerle, L., Van Caeneghem, W., Messens, E., Lambers, H., Van Montagu, M., and Van Der Straeten, D. 1999. Presymptomatic visualization of plant-virus interactions by thermography. Nat. Biotechnol. 17:813–816.

Chaerle, L., Valcke, R., and Van Der Straeten, D. 2003. Imaging techniques in plant physiology and agronomy: from simple to multispectral approaches. In *Plant physiology and plant molecular biology in the new millennium*, ed. A. Hemantaranjan. Jodhpur, India: Scientific Publisher, p. 135–155.

Chaerle, L., Leinonen, I., Jones, H. G., and Van Der Straeten, D. 2007. Monitoring and screening plant populations with combined thermal and chlorophyll fluorescence imaging. J. Exp. Bot. 58:773–784.

Chandler, E. A., Simpson, D. R., Thomsett, M. A., and Nicholson, P. 2003. Development of PCR assays to *Tri7* and *Tri13* trichothecene biosynthetic genes, and characterisation of chemotypes of *Fusarium graminearum*, *Fusarium culmorum* and *Fusarium cerealis*. Physiol. Mol. Plant Pathol. 62:355–367.

Chen, Y., Kistler, H. C., and Ma, Z. 2019. *Fusarium graminearum* trichothecene mycotoxins: biosynthesis, regulation, and management. Annu. Rev. Phytopathol. 57:15–39.

Chetouhi, C., Bonhomme, L., Lecomte, P., Cambon, F., Merlino, M., Biron, D. G., et al. 2015. A proteomics survey on wheat susceptibility to *Fusarium* head blight during grain development. Eur. J. Plant Pathol. 141:407–418.

Chu, X., Wang, W., Yoon, S. C., Ni, X., and Heitschmidt, G. W. 2017. Detection of aflatoxin B1 (AFB1) in individual maize kernels using short wave infrared (SWIR) hyperspectral imaging. Biosyst. Eng. 157:13–23.

Comby, M., Gacoin, M., Robineau, M., Rabenoelina, F., Ptas, S., Dupont, J., et al. 2017. Screening of wheat endophytes as biological control agents against *Fusarium* head blight using two different *in vitro* tests. Microbiol. Res. 202:11–20.

Cortes, C., and Vapnik, V. 1995. Support-vector networks. Mach. Learn. 20:273–297.

Covarelli, L., Beccari, G., Prodi, A., Generotti, S., Etruschi, F., Meca, G., et al. 2015a. Biosynthesis of beauvericin and enniatins *in vitro* by wheat *Fusarium* species and natural grain contamination in an area of central Italy. Food Microbiol. 46:618–626.

Covarelli, L., Beccari, G., Prodi, A., Generotti, S., Etruschi, F., Juan, C., et al. 2015b. *Fusarium* species, chemotype characterisation and trichothecene contamination of durum and soft wheat in an area of central Italy. J. Sci. Food Agric. 95:540–551.

Cowger, C., Patton-Özkurt, J., Brown-Guedira, G., and Perugini, L. 2009. Post-anthesis moisture increased *Fusarium* head blight and deoxynivalenol levels in North Carolina winter wheat. Phytopathology. 99:320–327.

Cowger, C., and Arrellano, C. 2010. Plump kernels with high deoxynivalenol linked to late *Gibberella zeae* infection and marginal disease conditions in winter wheat. Phytopathology. 100:719–728.

Cowger, C., and Arellano, C. 2013. *Fusarium graminearum* infection and deoxynivalenol concentrations during development of wheat spikes. Phytopathology. 103:460–471.

Cowger, C., Smith, J., Boos, D., Bradley, C. A., Ransom, J., and Bergstrom, G. C. 2020. Managing a destructive, episodic crop disease: a national survey of wheat and barley growers' experience with *Fusarium* head blight. Plant Dis. 104:634–648.

REFERENCES

Crippin, T., Renaud, J. B., Sumarah, M. W., and David Miller, J. 2019. Comparing genotype and chemotype of *Fusarium graminearum* from cereals in Ontario, Canada. PLoS One. 14:e0216735.

Cséfalvay, L., Gaspero, G. Di, Matouš, K., Bellin, D., Ruperti, B., and Olejníčková, J. 2009. Pre-symptomatic detection of *Plasmopara viticola* infection in grapevine leaves using chlorophyll fluorescence imaging. Eur. J. Plant Pathol. 125:291–302.

Cuthbert, P. A., Somers, D. J., Thomas, J., Cloutier, S., and Brule´-Babel, A. 2006. Fine mapping *Fhb1* , a major gene controlling *Fusarium* head blight resistance in bread wheat (*Triticum aestivum* L .). Theor. Appl. Genet. 112:1465–1472.

Cuthbert, P. A., Somers, D. J., and Brulé-babel, A. 2007. Mapping of *Fhb2* on chromosome 6BS: a gene controlling *Fusarium* head blight field resistance in bread wheat (*Triticum aestivum* L .). Theor. Appl. Genet. 114:429–437.

D'Angelo, D. L., Bradley, C. A., Ames, K. A., Willyerd, K. T., Madden, L. V., and Paul, P. A. 2014. Efficacy of fungicide applications during and after anthesis against *Fusarium* head blight and deoxynivalenol in soft red winter wheat. Plant Dis. 98:1387–1397.

Dall'Asta, C., Berthiller, F., Schuhmacher, R., Adam, G., Lemmens, M., and Krska, R. 2005. DON-glycosides: characterisation of synthesis products and screening for their occurrence in DON-treated wheat samples. Mycotoxin Res. 21:123–127.

Dall'Asta, C., and Battilani, P. 2016. Fumonisins and their modified forms, a matter of concern in future scenario? World Mycotoxin J. 9:727–739.

Daub, M. E., and Ehrenshaft, M. 2000. The photoactivated *Cercospora* toxin cercosporin: contributions to plant disease and fundamental biology. Annu. Rev. Phytopathol. 38:461–490.

Daughtry, C. S. T. 2001. Discriminating crop residues from soil by shortwave infrared reflectance. Agron. J. 93:125–131.

Delalieux, S., Somers, B., Verstraeten, W. W., van Aardt, J. A. N., Keulemans, W., and Coppin, P. 2009. Hyperspectral indices to diagnose leaf biotic stress of apple plants, considering leaf phenology. Int. J. Remote Sens. 30:1887–1912.

Delwiche, S. R. 2003. Classification of scab- and other mold-damaged wheat kernels by near-infrared reflectance spectroscopy. Trans. Am. Soc. Agric. Eng. 46:731–738.

Delwiche, S. R., and Hareland, G. A. 2004. Detection of scab-damaged hard red spring wheat kernels by near-infrared reflectance. Cereal Chem. 81:643–649.

Delwiche, S. R. 2009. Enhancement of *Fusarium* head blight detection in free-falling wheat kernels using a bichromatic pulsed LED design. Opt. Eng. 48:023602–1.

Delwiche, S. R., Kim, M. S., and Dong, Y. 2011. *Fusarium* damage assessment in wheat kernels by VIS/NIR hyperspectral imaging. Sens. Instrum. Food Qual. Saf. 5:63–71.

Desjardins, A. E. 2006. *Fusarium mycotoxins: Chemistry, genetics, and biology*. St. Paul, MN, USA: American Phytopathological Society Press.

Dill-Macky, R., and Jones, R. K. 2000. The effect of previous crop residues and tillage on *Fusarium* head blight of wheat. Plant Dis. 84:71–76.

Divon, H. H., Bøe, L., Tveit, M. M. N., and Klemsdal, S. S. 2019. Infection pathways and penetration modes of *Fusarium langsethiae*. Eur. J. Plant Pathol. 154:259–271.

Dong, F., Xu, J., Zhang, X., Wang, S., Xing, Y., Mokoena, M. P., et al. 2020. Gramineous weeds near paddy fields are alternative hosts for the *Fusarium graminearum* species complex that causes *Fusarium* head blight in rice. Plant Pathol. 69:433–441.

Dowell, F. E., Ram, M. S., and Seitz, L. M. 1999. Predicting scab, vomitoxin, and ergosterol in single wheat kernels using near-infrared spectroscopy. Cereal Chem. 76:573–576.

Drakopoulos, D., Luz, C., Torrijos, R., Meca, G., Weber, P., Bänziger, I., et al. 2019. Use of botanicals to suppress different stages of the life cycle of *Fusarium graminearum*. Phytopathology. 109:2116–2123.

REFERENCES

Dweba, C. C., Figlan, S., Shimelis, H. A., Motaung, T. E., Sydenham, S., Mwadzingeni, L., et al. 2017. *Fusarium* head blight of wheat: pathogenesis and control strategies. Crop Prot. 91:114–122.

Ezekiel, C. N., Odebode, A. C., and Fapohunda, S. O. 2008. Zearalenone production by naturally occurring *Fusarium* species on maize, wheat and soybeans from Nigeria. J. Biol. Environ. Sci. 2:77–82.

Fahlgren, N., Feldman, M., Gehan, M. A., Wilson, M. S., Shyu, C., Bryant, D. W., et al. 2015. A versatile phenotyping system and analytics platform reveals diverse temporal responses to water availability in Setaria. Mol. Plant. 8:1520–1535.

FAO, Food and Agriculture Organization of the United Nations. 2020. FAOSTAT. Available at: http://www.fao.org/faostat/en/#data/QC [Accessed March 3, 2020].

van der Fels-Klerx, H. J., Goedhart, P. W., Elen, O., Börjesson, T., Hietaniemi, V., and Booij, C. J. H. 2012. Modeling deoxynivalenol contamination of wheat in northwestern Europe for climate change assessments. J. Food Prot. 75:1099–1106.

van der Fels-Klerx, H. J., van Asselt, E. D., Madsen, M. S., and Olesen, J. E. 2013. Impact of climate change effects on contamination of cereal grains with deoxynivalenol. PLoS One. 8:e73602.

van der Fels-Klerx, H. J., Liu, C., and Battilani, P. 2016. Modelling climate change impacts on mycotoxin contamination. World Mycotoxin J. 9:717–726.

Femenias, A., Gatius, F., Ramos, A. J., Sanchis, V., and Marín, S. 2020. Use of hyperspectral imaging as a tool for *Fusarium* and deoxynivalenol risk management in cereals: a review. Food Control. 108:106819.

Ferrigo, D., Raiola, A., and Causin, R. 2016. *Fusarium* toxins in cereals: occurrence, legislation, factors promoting the appearance and their management. Molecules. 21:627.

Del Fiore, A., Reverberi, M., Ricelli, A., Pinzari, F., Serranti, S., Fabbri, A. A., et al. 2010. Early detection of toxigenic fungi on maize by hyperspectral imaging analysis. Int. J. Food Microbiol. 144:64–71.

Foroud, N. A., Baines, D., Gagkaeva, T. Y., Thakor, N., Badea, A., Steiner, B., et al. 2019. Trichothecenes in cereal grains – an update. Toxins. 11:634.

Fourty, T., and Baret, F. 1997. Vegetation water and dry matter contents estimated from top-of-the-atmosphere reflectance data: a simulation study. Remote Sens. Environ. 61:34–45.

Fraeyman, S., Croubels, S., Devreese, M., and Antonissen, G. 2017. Emerging *Fusarium* and *Alternaria* mycotoxins: occurrence, toxicity and toxicokinetics. Toxins. 9:228.

Francl, L., Shaner, G., Bergstrom, G., Gilbert, J., Pedersen, W., Dill-Macky, R., et al. 1999. Daily inoculum levels of *Gibberella zeae* on wheat spikes. Plant Dis. 83:662–666.

Freeman, E. M. 1905. *Minnesota plant diseases (geological and natural history survey of Minnesota).* Botanical series 5. St. Paul, MN, USA.

Furbank, R. T., and Tester, M. 2011. Phenomics - technologies to relieve the phenotyping bottleneck. Trends Plant Sci. 16:635–644.

Gamon, J. A., Peñuelas, J., and Field, C. B. 1992. A narrow-waveband spectral index that tracks diurnal changes in photosynthetic efficiency. Remote Sens. Environ. 41:35–44.

Gan, Z., R. Marquardt, R., Abramson, D., and Clear, R. M. 1997. The characterization of chicken antibodies raised against *Fusarium* spp. by enzyme-linked immunosorbent assay and immunoblotting. Int. J. Food Microbiol. 38:191–200.

Gärtner, B. H., Munich, M., Kleijer, G., and Mascher, F. 2008. Characterisation of kernel resistance against *Fusarium* infection in spring wheat by baking quality and mycotoxin assessments. Eur. J. Plant Pathol. 120:61–68.

Gebbers, R., and Adamchuk, V. I. 2010. Precision agriculture and food security. Science. 327:828–831.

Geiser, D. M., Aoki, T., Bacon, C. W., Baker, S. E., Bhattacharyya, M. K., Brandt, M. E., et al. 2013. One fungus, one name: defining the genus *Fusarium* in a scientifically robust way that preserves longstanding use. Phytopathology. 103:400–408.

REFERENCES

Genty, B., Briantais, J. M., and Baker, N. R. 1989. The relationship between the quantum yield of photosynthetic electron transport and quenching of chlorophyll fluorescence. Biochim. Biophys. Acta. 990:87–92.

Gilbert, J., and Haber, S. 2013. Overview of some recent research developments in *Fusarium* head blight of wheat. Can. J. Plant Pathol. 35:149–174.

Glenn, A. E. 2007. Mycotoxigenic *Fusarium* species in animal feed. Anim. Feed Sci. Technol. 137:213–240.

Gomez, S. 2014. Infection and spread of *Peronospora sparsa* on *Rosa* sp. (Berk.)—A microscopic and a thermographic approach. Available at: http://nbn-resolving.de/urn:nbn:de:hbz:5n-34738.

Góral, T., Wiśniewska, H., Ochodzki, P., Nielsen, L. K., Walentyn-Góral, D., and Stępień, Ł. 2019. Relationship between *Fusarium* head blight, kernel damage, concentration of *Fusarium* biomass, and *Fusarium* toxins in grain of winter wheat inoculated with *Fusarium culmorum*. Toxins. 11:2.

Goswami, R. S., and Kistler, H. C. 2004. Heading for disaster: *Fusarium graminearum* on cereal crops. Mol. Plant Pathol. 5:515–525.

Goswami, R. S., and Kistler, H. C. 2005. Pathogenicity and in planta mycotoxin accumulation among members of the *Fusarium graminearum* species complex on wheat and rice. Phytopathology. 95:1397–1404.

Guo, J., Zhang, X., Hou, Y., Cai, J., Shen, X., Zhou, T., et al. 2015. High-density mapping of the major FHB resistance gene *Fhb7* derived from *Thinopyrum ponticum* and its pyramiding with *Fhb1* by marker-assisted selection. Theor. Appl. Genet. 128:2301–2316.

Guo, Z., DoÏl, K., Dastjerdi, R., Karlovsky, P., Dehne, H. W., and Altincicek, B. 2014. Effect of fungal colonization of wheat grains with *Fusarium* spp. on food choice, weight gain and mortality of meal beetle larvae (*Tenebrio molitor*). PLoS One. 9:e100112.

Guo, Z., Pfohl, K., Karlovsky, P., Dehne, H. W., and Altincicek, B. 2018. Dissemination of *Fusarium proliferatum* by mealworm beetle *Tenebrio molitor*. PLoS One. 13:e0204602.

Ha, X., Koopmann, B., and von Tiedemann, A. 2016. Wheat blast and *Fusarium* head blight display contrasting interaction patterns on ears of wheat genotypes differing in resistance. Phytopathology. 106:270–281.

Haile, J. K., N'Diaye, A., Walkowiak, S., Nilsen, K. T., Clarke, J. M., Kutcher, H. R., et al. 2019. *Fusarium* head blight in durum wheat: recent status, breeding directions, and future research prospects. Phytopathology. 109:1664–1675.

Hallen-Adams, H. E., Wenner, N., Kuldau, G. A., and Trail, F. 2011. Deoxynivalenol biosynthesis-related gene expression during wheat kernel colonization by *Fusarium graminearum*. Phytopathology. 101:1091–1096.

Hellin, P., Duvivier, M., Dedeurwaerder, G., Bataille, C., De Proft, M., and Legrève, A. 2018. Evaluation of the temporal distribution of *Fusarium graminearum* airborne inoculum above the wheat canopy and its relationship with *Fusarium* head blight and DON concentration. Eur. J. Plant Pathol. 151:1049–1064.

Henson, J. M., and French, R. 1993. The polymerase chain reaction and plant disease diagnosis. Annu. Rev. Phytopathol. 31:81–109.

Hettiarachchy, N. S., and Boyacioğlu, D. 1995. Changes in some biochemical components of wheat grain that was infected with *Fusarium graminearum*. J. Cereal Sci. 21:57–62.

Hill, N. S., Schwarz, P., Dahleen, L. S., Neate, S. M., Horsley, R., Glenn, A. E., et al. 2006. ELISA analysis for *Fusarium* in barley: development of methodology and field assessment. Crop Sci. 46:2636–2642.

Hong, S. Y., Kang, M. R., Cho, E. J., Kim, H. K., and Yun, S. H. 2010. Specific PCR detection of four quarantine *Fusarium* species in Korea. Plant Pathol. J. 26:409–416.

Huang, W., Lamb, D. W., Niu, Z., Zhang, Y., Liu, L., and Wang, J. 2007. Identification of yellow rust in wheat using in-situ spectral reflectance measurements and airborne hyperspectral imaging. Precis. Agric. 8:187–197.

Hunt, E. R., and Rock, B. N. 1989. Detection of changes in leaf water content using Near- and Middle-Infrared reflectances. Remote Sens. Environ. 30:43–54.

REFERENCES

Igor, J., Dudaš, T., Krstovic, S., Krska, R., Sulyok, M., Bagi, F., et al. 2019. Emerging *Fusarium* mycotoxins fusaproliferin, beauvericin, enniatins, and moniliformin in Serbian maize. Toxins. 11:357.

Ilgen, P., Hadeler, B., Maier, F. J., and Schäfer, W. 2009. Developing kernel and rachis node induce the trichothecene pathway of *Fusarium graminearum* during wheat head infection. Mol. Plant-Microbe Interact. 22:899–908.

Iori, A., Scala, V., Cesare, D., Pinzari, F., D'Egidio, M. G., Fanelli, C., et al. 2015. Hyperspectral and molecular analysis of *Stagonospora nodorum* blotch disease in durum wheat. Eur. J. Plant Pathol. 141:689–702.

Ivanova, L., Fæste, C. K., Van Pamel, E., Daeseleire, E., Callebaut, A., and Uhlig, S. 2014. Presence of enniatin B and its hepatic metabolites in plasma and liver samples from broilers and eggs from laying hens. World Mycotoxin J. 7:167–175.

Jestoi, M. 2008. Emerging *Fusarium*-mycotoxins fusaproliferin, beauvericin, enniatins, and moniliformin-a review. Crit. Rev. Food Sci. Nutr. 48:21–49.

Jin, X., Jie, L., Wang, S., Qi, H. J., and Li, S. W. 2018. Classifying wheat hyperspectral pixels of healthy heads and *Fusarium* head blight disease using a deep neural network in the wild field. Remote Sens. 10:395.

Jirsa, O., and Polišenská, I. 2011. Identification of *Fusarium* damaged wheat kernels using image analysis. Acta Univ. Agric. Silvic. Mendelianae Brun. 59:125–130.

Joalland, S., Screpanti, C., Liebisch, F., Varella, H. V., Gaume, A., and Walter, A. 2017. Comparison of visible imaging, thermography and spectrometry methods to evaluate the effect of *Heterodera schachtii* inoculation on sugar beets. Plant Methods. 13:73.

Johnson, D. D., Flaskerud, G. K., Taylor, R. D., and Satyanarayana, V. 2003. Quantifying economic impacts of *Fusarium* head blight in wheat. In *Fusarium head blight of wheat and barley*, ed. W. R. Leonard, and K. J. Bushnell. St. Paul, MN, USA: American Phytopathological Society Press, p. 461–483.

Jung, B., Lee, S., Ha, J., Park, J. C., Han, S. S., Hwang, I., et al. 2013. Development of a selective medium for the fungal pathogen *Fusarium graminearum* using toxoflavin produced by the bacterial pathogen *Burkholderia glumae*. Plant Pathol. J. 29:446–450.

Jurado, M., Vázquez, C., Patiño, B., and González-Jaén, M. T. 2005. PCR detection assays for the trichothecene-producing species *Fusarium graminearum*, *Fusarium culmorum*, *Fusarium poae*, *Fusarium equiseti* and *Fusarium sporotrichioides*. Syst. Appl. Microbiol. 28:562–568.

Jurado, M., Vázquez, C., Marín, S., Sanchis, V., and Teresa González-Jaén, M. 2006. PCR-based strategy to detect contamination with mycotoxigenic *Fusarium* species in maize. Syst. Appl. Microbiol. 29:681–689.

Kang, Z., and Buchenauer, H. 1999. Immunocytochemical localization of *Fusarium* toxins in infected wheat spikes by *Fusarium culmorum*. Physiol. Mol. Plant Pathol. 55:275–288.

Kautzman, M. E., Wickstrom, M. L., and Scott, T. A. 2015. The use of near infrared transmittance kernel sorting technology to salvage high quality grain from grain downgraded due to *Fusarium* damage. Anim. Nutr. 1:41–46.

Kelly, A. C., Clear, R. M., O'Donnell, K., McCormick, S., Turkington, T. K., Tekauz, A., et al. 2015. Diversity of *Fusarium* head blight populations and trichothecene toxin types reveals regional differences in pathogen composition and temporal dynamics. Fungal Genet. Biol. 82:22–31.

Khan, M. R., and Doohan, F. M. 2009. Comparison of the efficacy of chitosan with that of a fluorescent pseudomonad for the control of *Fusarium* head blight disease of cereals and associated mycotoxin contamination of grain. Biol. Control. 48:48–54.

Khan, N. I., Schisler, D. A., Boehm, M. J., Slininger, P. J., and Bothast, R. J. 2001. Selection and evaluation of microorganisms for biocontrol of *Fusarium* head blight of wheat incited by *Gibberella zeae*. Plant Dis. 85:1253–1258.

Khan, N. I., Schisler, D. A., Boehm, M. J., Lipps, P. E., and Slininger, P. J. 2004. Field testing of antagonists of *Fusarium* head blight incited by *Gibberella zeae*. Biol. Control. 29:245–255.

REFERENCES

Kimuli, D., Lawrence, K. C., Yoon, S. C., Wang, W., Heitschmidt, G. W., and Zhao, X. 2017. A SWIR hyperspectral imaging method for classifying aflatoxin B 1 contaminated maize kernels. In *ASABE annual international meeting*, Spokane, Washington: American Society of Agricultural and Biological Engineers, p. 1700764.

Kluger, B., Bueschl, C., Lemmens, M., Michlmayr, H., Malachova, A., Koutnik, A., et al. 2015. Biotransformation of the mycotoxin deoxynivalenol in *Fusarium* resistant and susceptible near isogenic wheat lines. PLoS One. 10:e0119656.

Kovalsky, P., Kos, G., Nährer, K., Schwab, C., Jenkins, T., Schatzmayr, G., et al. 2016. Co-occurrence of regulated, masked and emerging mycotoxins and secondary metabolites in finished feed and maize–an extensive survey. Toxins. 8:863.

Kreuzberger, M., Limsuwan, S., Eggert, K., Karlovsky, P., and Pawelzik, E. 2015. Impact of *Fusarium* spp. infection of bread wheat (*Triticum aestivum* L.) on composition and quality of flour in association with EU maximum level for deoxynivalenol. J. Appl. Bot. Food Qual. 88:177–185.

Krska, R., Schubert-Ullrich, P., Molinelli, A., Sulyok, M., MacDonald, S., and Crews, C. 2008. Mycotoxin analysis: an update. Food Addit. Contam. - Part A. 25:152–163.

Kruskal, J. B. 1964. Multidimensional scaling by optimizing goodness of fit to a nonmetric hypothesis. Psychometrika. 29:1–27.

Kubo, K., Fujita, M., Kawada, N., Nakajima, T., Nakamura, K., Maejima, H., et al. 2013. Minor differences in anther extrusion affect resistance to *Fusarium* head blight in wheat. J. Phytopathol. 161:308–314.

Kuckenberg, J., Tartachnyk, I., and Noga, G. 2009. Temporal and spatial changes of chlorophyll fluorescence as a basis for early and precise detection of leaf rust and powdery mildew infections in wheat leaves. Precis. Agric. 10:34–44.

Kuhnem, P. R., Del Ponte, E. M., Dong, Y., and Bergstrom, G. C. 2015. *Fusarium graminearum* isolates from wheat and maize in New York show similar range of aggressiveness and toxigenicity in cross-species pathogenicity tests. Phytopathology. 105:441–448.

Kuska, M., Wahabzada, M., Leucker, M., Dehne, H. W., Kersting, K., Oerke, E. C., et al. 2015. Hyperspectral phenotyping on the microscopic scale: towards automated characterization of plant-pathogen interactions. Plant Methods. 11:28.

Kuska, M. T., Brugger, A., Thomas, S., Wahabzada, M., Kersting, K., Oerke, E. C., et al. 2017. Spectral patterns reveal early resistance reactions of barley against *Blumeria graminis* f.sp. *hordei*. Phytopathology. 107:1388–1398.

Kuska, M. T., and Mahlein, A. K. 2018. Aiming at decision making in plant disease protection and phenotyping by the use of optical sensors. Eur. J. Plant Pathol. 152:987–992.

Kuzdraliński, A., Solarska, E., and Muszyńska, M. 2013. Deoxynivalenol and zearalenone occurence in beers analysed by an enzyme-linked immunosorbent assay method. Food Control. 29:22–24.

Kuzdraliński, A., Kot, A., Szczerba, H., Nowak, M., and Muszyńska, M. 2017. A review of conventional PCR assays for the detection of selected phytopathogens of wheat. J. Mol. Microbiol. Biotechnol. 27:175–189.

Lancashire, P. D., Bleiholder, H., van den Boom, T., Langelüddeke, P., Stauss, R., Weber, E., et al. 1991. A uniform decimal code for growth stages of crops and weeds. Ann. Appl. Biol. 119:561–601.

van der Lee, T., Zhang, H., van Diepeningen, A., and Waalwijk, C. 2015. Biogeography of *Fusarium graminearum* species complex and chemotypes: a review. Food Addit. Contam. - Part A. 32:453–460.

Lehoczki-Krsjak, S., Varga, M., and Mesterházy, Á. 2015. Distribution of prothioconazole and tebuconazole between wheat ears and flag leaves following fungicide spraying with different nozzle types at flowering. Pest Manag. Sci. 71:105–113.

Lemmens, M., Haim, K., Lew, H., and Ruckenbauer, P. 2004. The effect of nitrogen fertilization on *Fusarium* head blight development and deoxynivalenol contamination in wheat. J. Phytopathol. 152:1–8.

REFERENCES

Lemmens, M., Scholz, U., Berthiller, F., Dall'Asta, C., Koutnik, A., Schuhmacher, R., et al. 2005. The ability to detoxify the mycotoxin deoxynivalenol colocalizes with a major quantitative trait locus for *Fusarium* head blight resistance in wheat. Mol. Plant-Microbe Interact. 18:1318–1324.

Lemmens, M., Steiner, B., Sulyok, M., Nicholson, P., Mesterhazy, A., and Buerstmayr, H. 2016. Masked mycotoxins: does breeding for enhanced *Fusarium* head blight resistance result in more deoxynivalenol-3-glucoside in new wheat varieties? World Mycotoxin J. 9:741–754.

Leucker, M., Mahlein, A. K., Steiner, U., and Oerke, E. C. 2016. Improvement of lesion phenotyping in *Cercospora beticola*-sugar beet interaction by hyperspectral imaging. Phytopathology. 106:177–184.

Leucker, M., Wahabzada, M., Kersting, K., Peter, M., Beyer, W., Steiner, U., et al. 2017. Hyperspectral imaging reveals the effect of sugar beet quantitative trait loci on *Cercospora* leaf spot resistance. Funct. Plant Biol. 44:1–9.

Li, M., Yang, C., Mao, Y., Hong, X., and Du. D. 2019. Zearalenone contamination in corn, corn products, and swine feed in China in 2016–2018 as assessed by magnetic bead immunoassay. Toxins. 11:451.

Lindenthal, M., Steiner, U., Dehne, H. W., and Oerke, E. C. 2005. Effect of downy mildew development on transpiration of cucumber leaves visualized by digital infrared thermography. Phytopathology. 95:233–240.

Lofgren, L., Riddle, J., Dong, Y., Kuhnem, P. R., Cummings, J. A., Del Ponte, E. M., et al. 2018. A high proportion of NX-2 genotype strains are found among *Fusarium graminearum* isolates from northeastern New York State. Eur. J. Plant Pathol. 150:791–796.

López-Díaz, C., Rahjoo, V., Sulyok, M., Ghionna, V., Martín-Vicente, A., Capilla, J., et al. 2018. Fusaric acid contributes to virulence of *Fusarium oxysporum* on plant and mammalian hosts. Mol. Plant Pathol. 19:440–453.

Lu, Q., Lillemo, M., Skinnes, H., He, X., Shi, J., Ji, F., et al. 2013. Anther extrusion and plant height are associated with Type I resistance to *Fusarium* head blight in bread wheat line 'Shanghai-3/Catbird.' Theor. Appl. Genet. 126:317–334.

Lucas, J. A. 2011. Advances in plant disease and pest management. J. Agric. Sci. 149:91–114.

Ma, H., Huang, W., Jing, Y., Pignatti, S., Laneve, G., Dong, Y., et al. 2020. Identification of *Fusarium* head blight in winter wheat ears using continuous wavelet analysis. Sensors. 20:20.

Madgwick, J. W., West, J. S., White, R. P., Semenov, M. A., Townsend, J. A., Turner, J. A., et al. 2011. Impacts of climate change on wheat anthesis and *Fusarium* ear blight in the UK. Eur. J. Plant Pathol. 130:117–131.

Magan, N., Medina, A., and Aldred, D. 2011. Possible climate-change effects on mycotoxin contamination of food crops pre- and postharvest. Plant Pathol. 60:150–163.

Mahlein, A. K., Steiner, U., Dehne, H. W., and Oerke, E. C. 2010. Spectral signatures of sugar beet leaves for the detection and differentiation of diseases. Precis. Agric. 11:413–431.

Mahlein, A. K., Oerke, E. C., Steiner, U., and Dehne, H. W. 2012a. Recent advances in sensing plant diseases for precision crop protection. Eur. J. Plant Pathol. 133:197–209.

Mahlein, A. K., Steiner, U., Hillnhütter, C., Dehne, H. W., and Oerke, E. C. 2012b. Hyperspectral imaging for small-scale analysis of symptoms caused by different sugar beet diseases. Plant Methods. 8:3.

Mahlein, A. K., Rumpf, T., Welke, P., Dehne, H. W., Plümer, L., Steiner, U., et al. 2013. Development of spectral indices for detecting and identifying plant diseases. Remote Sens. Environ. 128:21–30.

Mahlein, A. K. 2016. Plant disease detection by imaging sensors – parallels and specific demands for precision agriculture and plant phenotyping. Plant Dis. 100:241–251.

Mahlein, A. K., Kuska, M. T., Behmann, J., Polder, G., and Walter, A. 2018. Hyperspectral sensors and imaging technologies in phytopathology: state of the art. Annu. Rev. Phytopathol. 56:535–558.

REFERENCES

Mahlein, A. K., Alisaac, E., Al Masri, A., Behmann, J., Dehne, H. W., and Oerke, E. C. 2019. Comparison and combination of thermal, fluorescence, and hyperspectral imaging for monitoring *Fusarium* head blight of wheat on spikelet scale. Sensors. 19:2281.

Malbrán, I., Mourelos, C. A., Girotti, J. R., Aulicino, M. B., Balatti, P. A., and Lori, G. A. 2012. Aggressiveness variation of *Fusarium graminearum* isolates from Argentina following point inoculation of field grown wheat spikes. Crop Prot. 42:234–243.

Marín, P., Moretti, A., Ritieni, A., Jurado, M., Vázquez, C., and González-Jaén, M. T. 2012. Phylogenetic analyses and toxigenic profiles of *Fusarium equiseti* and *Fusarium acuminatum* isolated from cereals from Southern Europe. Food Microbiol. 31:229–237.

McCormick, S. 2003. The Role of DON in Pathogenicity. In *Fusarium head blight of wheat and barley*, ed. W. R. Leonard, and K. J. Bushnell. St. Paul, MN, USA: American Phytopathological Society Press, p. 165–183.

McCormick, S. P., Stanley, A. M., Stover, N. A., and Alexander, N. J. 2011. Trichothecenes: from simple to complex mycotoxins. Toxins. 3:802–814.

McKee, G., Cowger, C., Dill-Macky, R., Friskop, A., Gautam, P., Ransom, J., et al. 2019. Disease management and estimated effects on DON (deoxynivalenol) contamination in *Fusarium* infested barley. Agriculture. 9:155.

McLean, M. 1995. The phytotoxicity of selected mycotoxins on mature, germinating *Zea mays* embryos. Mycopathologia. 132:173–183.

McMullen, M., Jones, R., and Gallenberg, D. 1997. Scab of wheat and barley: a re-emerging disease of devastating impact. Plant Dis. 81:1340–1348.

McMullen, M., Bergstrom, G., De Wolf, E., Dill-Macky, R., Hershman, D., Shaner, G., et al. 2012. *Fusarium* head blight disease cycle, symptoms, and impact on grain yield and quality frequency and magnitude of epidemics since 1997. Plant Dis. 96:1712–1728.

Meneely, J. P., Ricci, F., van Egmond, H. P., and Elliott, C. T. 2011. Current methods of analysis for the determination of trichothecene mycotoxins in food. Trends Anal. Chem. 30:192–203.

Menesatti, P., Antonucci, F., Pallottino, F., Giorgi, S., Matere, A., Nocente, F., et al. 2013. Laboratory vs. in-field spectral proximal sensing for early detection of *Fusarium* head blight infection in durum wheat. Biosyst. Eng. 114:289–293.

Merzlyak, M. N., Gitelson, A. A., Chivkunova, O. B., and Rakitin, V. Y. 1999. Non-destructive optical detection of pigment changes during leaf senescence and fruit ripening. Physiol. Plant. 106:135–141.

Mesterházy. Á. 1995. Types and components of resistance to *Fusarium* head blight of wheat. Plant Breed. 114:377–386.

Mesterházy, Á., Bartók, T., Mirocha, C. G., and Komoróczy, R. 1999. Nature of wheat resistance to *Fusarium* head blight and the role of deoxynivalenol for breeding. Plant Breed. 118:97–110.

Mesterházy, Á., Buerstmayr, H., Tóth, B., Lehoczki-Krsjak, S., Szabó-Hevér, Á., and Lemmens, M. 2007. An improved strategy for breeding FHB resistant wheat must include Type I resistance. In *Proceedings of the 5th Canadian workshop on Fusarium head blight*, ed. R. Clear. Delta Winnipeg, p. 51–66.

Mesterházy, Á., Tóth, B., Varga, M., Bartók, T., Szabó-Hevér, Á., Farády, L., et al. 2011. Role of fungicides, application of nozzle types, and the resistance level of wheat varieties in the control of *Fusarium* head blight and deoxynivalenol. Toxins. 3:1453–1483.

Mesterházy, Á., Lehoczki-Krsjak, S., Varga, M., Szabó-Hevér, Á., Tóth, B., and Lemmens, M. 2015. Breeding for FHB resistance via *Fusarium* damaged kernels and deoxynivalenol accumulation as well as inoculation methods in winter wheat. Agric. Sci. 6:970–1002.

Miller, J. D., and Arnison, P. G. 1986. Degradation of deoxynivalenol by suspension cultures of the *Fusarium* head blight resistant wheat cultivar Frontana. Can. J. Plant Pathol. 8:147–150.

Miller, J., Culley, J., Fraser, K., Hubbard, S., Meloche, F., Ouellet, T., et al. 1998. Effect of tillage practice on *Fusarium* head blight of wheat. Can. J. Plant Pathol. 20:95–103.

REFERENCES

Miller, S. S., Chabot, D. M. P., Ouellet, T., Harris, L. J., and Fedak, G. 2004. Use of a *Fusarium graminearum* strain transformed with green fluorescent protein to study infection in wheat (*Triticum aestivum*). Can. J. Plant Pathol. 26:453–463.

Mishra, P. K., Fox, R. T. V., and Culham, A. 2003. Development of a PCR-based assay for rapid and reliable identification of pathogenic *Fusaria*. FEMS Microbiol. Lett. 218:329–332.

Möller, E. M., Chełkowski, J., and Geiger, H. H. 1999. Species-specific PCR assays for the fungal pathogens *Fusarium moniliforme* and *Fusarium subglutinans* and their application to diagnose maize ear rot disease. J. Phytopathol. 147:497–508.

Moradi, M. 2008. Microbiological and molecular assessment of interactions among the major *Fusarium* head blight pathogens on wheat ears. Available at: http://nbn-resolving.de/urn:nbn:de:hbz:5N-13956.

Moretti, A., Pascale, M., and Logrieco, A. F. 2019. Mycotoxin risks under a climate change scenario in Europe. Trends Food Sci. Technol. 84:38–40.

Moroni, M., Lupo, E., and Cenedese, A. 2013. Hyperspectral proximal sensing of *Salix alba* trees in the sacco river valley (Latium, Italy). Sensors. 13:14633–14649.

Moshou, D., Bravo, C., Oberti, R., West, J., Bodria, L., McCartney, A., et al. 2005. Plant disease detection based on data fusion of hyper-spectral and multi-spectral fluorescence imaging using Kohonen maps. Real-Time Imaging. 11:75–83.

Mourelos, C. A., Malbrán, I., Balatti, P. A., Ghiringhelli, P. D., and Lori, G. A. 2014. Gramineous and non-gramineous weed species as alternative hosts of *Fusarium graminearum*, causal agent of *Fusarium* head blight of wheat, in Argentina. Crop Prot. 65:100–104.

Murchie, E. H., and Lawson, T. 2013. Chlorophyll fluorescence analysis: a guide to good practice and understanding some new applications. J. Exp. Bot. 64:3983–3998.

MycoBank, An initiative of the International Mycological Association (IMA) and the Westerdijk Fungal Biodiversity Institute. 2019. MYCOBANK DATABASE. Available at: http://www.mycobank.org/defaultinfo.aspx?Page=Home [Accessed October 21, 2019].

Mylona, K., Garcia-Cela, E., Sulyok, M., Medina, A., and Magan, N. 2019. Influence of two garlic-derived compounds, propyl propane thiosulfonate (PTS) and propyl propane thiosulfinate (PTSO), on growth and mycotoxin production by *Fusarium* species *in vitro* and in stored cereals. Toxins. 11:495.

Nagler, P. L., Inoue, Y., Glenn, E. P., Russ, A. L., and Daughtry, C. S. T. 2003. Cellulose absorption index (CAI) to quantify mixed soil-plant litter scenes. Remote Sens. Environ. 87:310–325.

Nazari, L., Pattori, E., Terzi, V., Morcia, C., and Rossi, V. 2014. Influence of temperature on infection, growth, and mycotoxin production by *Fusarium langsethiae* and *F. sporotrichioides* in durum wheat. Food Microbiol. 39:19–26.

Nelson, R. 2020. International plant pathology: past and future contributions to global food security. Phytopathology. 110:245–253.

Nicholson, P., Lees, A. K., Maurin, N., Parry, D. W., and Rezanoor, H. N. 1996. Development of a PCR assay to identify and quantify *Microdochium nivale* var. *nivale* and *Microdochium nivale* var. *majus* in wheat. Physiol. Mol. Plant Pathol. 48:257–271.

Nicholson, P., Simpson, D. R., Weston, G., Rezanoor, H. N., Lees, A. K., Parry, D. W., et al. 1998. Detection and quantification of *Fusarium culmorum* and *Fusarium graminearum* in cereals using PCR assays. Physiol. Mol. Plant Pathol. 53:17–37.

Nicolaisen, M., Suproniene, S., Nielsen, L. K., Lazzaro, I., Spliid, N. H., and Justesen, A. F. 2009. Real-time PCR for quantification of eleven individual *Fusarium* species in cereals. J. Microbiol. Methods. 76:234–240.

Nielsen, L. K., Cook, D. J., Edwards, S. G., and Ray, R. V. 2014. The prevalence and impact of *Fusarium* head blight pathogens and mycotoxins on malting barley quality in UK. Int. J. Food Microbiol. 179:38–49.

Nightingale, M. J., Marchylo, B. A., Clear, R. M., Dexter, J. E., and Preston, K. R. 1999. *Fusarium* head blight: effect of fungal proteases on wheat storage proteins. Cereal Chem. 76:150–158.

REFERENCES

O'Donnell, K., Ward, T. J., Geiser, D. M., Kistler, H. C., and Aoki, T. 2004. Genealogical concordance between the mating type locus and seven other nuclear genes supports formal recognition of nine phylogenetically distinct species within the *Fusarium graminearum* clade. Fungal Genet. Biol. 41:600–623.

Obanor, F., Neate, S., Simpfendorfer, S., Sabburg, R., Wilson, P., and Chakraborty, S. 2013. *Fusarium graminearum* and *Fusarium pseudograminearum* caused the 2010 head blight epidemics in Australia. Plant Pathol. 62:79–91.

Oerke, E. C. 2006. Crop losses to pests. J. Agric. Sci. 144:31–43.

Oerke, E. C., Steiner, U., Dehne, H. W., and Lindenthal, M. 2006. Thermal imaging of cucumber leaves affected by downy mildew and environmental conditions. J. Exp. Bot. 57:2121–2132.

Oerke, E. C., Meier, A., Dehne, H. W., Sulyok, M., Krska, R., and Steiner, U. 2010. Spatial variability of *Fusarium* head blight pathogens and associated mycotoxins in wheat crops. Plant Pathol. 59:671–682.

Oerke, E. C., and Steiner, U. 2010. Potential of digital thermography thermography for disease control. In *Precision crop protection - The challenge and use of heterogeneity*, eds. E. C. Oerke, R. Gerhards, G. Menz, and R. A. Sikora. Dordrecht: Springer Netherlands, p. 167–182.

Oerke, E. C., Fröhling, P., and Steiner, U. 2011. Thermographic assessment of scab disease on apple leaves. Precis. Agric. 12:699–715.

Oerke, E. C., Mahlein, A. K., and Steiner, U. 2014. Proximal sensing of plant diseases. In *Detection and diagnostics of plant pathogens*, ed. P. J. M. Gullino, and M. L. Bonants. Dordrecht: Springer Netherlands, p. 55–68.

Osborne, L. E., and Stein, J. M. 2007. Epidemiology of *Fusarium* head blight on small-grain cereals. Int. J. Food Microbiol. 119:103–108.

Palazzini, J. M., Groenenboom-de Haas, B. H., Torres, A. M., Köhl, J., and Chulze, S. N. 2013. Biocontrol and population dynamics of *Fusarium* spp. On wheat stubble in Argentina. Plant Pathol. 62:859–866.

Palazzini, J. M., Fumero, V., Yerkovich, N., Barros, G., Cuniberti, M., and Chulze, S. 2015. Correlation between *Fusarium graminearum* and deoxynivalenol during the 2012/13 wheat *Fusarium* head blight outbreak in Argentina. Cereal Res. Commun. 43:627–637.

Parry, D. W., Jenkinson, P., and McLeod, L. 1995. *Fusarium* ear blight (scab) in small grain cereals—a review. Plant Pathol. 44:207–238.

Parry, D. W., and Nicholson, P. 1996. Development of a PCR assay to detect *Fusarium poae* in wheat. Plant Pathol. 45:383–391.

Pasquali, M., Beyer, M., Logrieco, A., Audenaert, K., Balmas, V., Basler, R., et al. 2016. A European database of *Fusarium graminearum* and *F. culmorum* trichothecene genotypes. Front. Microbiol. 7:406.

Patiño, B., Mirete, S., González-Jaén, M. T., Mulé, G., Rodríguez, M. T., and Vázquez, C. 2004. PCR detection assay of fumonisin-producing *Fusarium verticillioides* strains. J. Food Prot. 67:1278–1283.

Paul, P. A., Bradley, C. A., Madden, L. V., Lana, F. D., Bergstrom, G. C., Dill-Macky, R., et al. 2018. Meta-analysis of the effects of QoI and DMI fungicide combinations on *Fusarium* head blight and deoxynivalenol in wheat. Plant Dis. 102:2602–2615.

Peiris, K. H. S., Pumphrey, M. O., and Dowell, F. E. 2009. NIR absorbance characteristics of deoxynivalenol and of sound and *Fusarium*-damaged wheat kernels. J. Near Infrared Spectrosc. 17:213–221.

Peiris, K. H. S., Pumphrey, M. O., Dong, Y., Maghirang, E. B., Berzonsky, W., and Dowell, F. E. 2010. Near-infrared spectroscopic method for identification of *Fusarium* head blight damage and prediction of deoxynivalenol in single wheat kernels. Cereal Chem. 87:511–517.

Penuelas, J., Baret, F., and Filella, I. 1995. Semi-empirical indices to assess carotenoids/chlorophyll a ratio from leaf spectral reflectance. Photosynthetica. 31:221–230.

Penuelas, J., Pinol, J., Ogaya, R., and Filella, I. 1997. Estimation of plant water concentration by the reflectance Water Index WI (R900/R970). Int. J. Remote Sens. 18:2869–2875.

REFERENCES

Pestka, J. J. 2010. Deoxynivalenol: mechanisms of action, human exposure, and toxicological relevance. Arch. Toxicol. 84:663–679.

Del Ponte, E. M., Fernandes, J. M. C., Pavan, W., and Baethgen, W. E. 2009. A model-based assessment of the impacts of climate variability on *Fusarium* head blight seasonal risk in southern Brazil. J. Phytopathol. 157:675–681.

Prosperini, A., Berrada, H., Ruiz, M. J., Caloni, F., Coccini, T., Spicer, L. J., et al. 2017. A review of the mycotoxin enniatin B. Front. Public Heal. 5:304.

Qi, L. L., Pumphrey, M. ., Friebe, B., P.D., C., and Gill, B. S. 2008. Molecular cytogenetic characterization of alien introgressions with gene *Fhb3* for resistance to *Fusarium* head blight disease of wheat. Theor. Appl. Genet. 117:1155–1166.

Ribichich, K. F., Lopez, S. E., and Vegetti, A. C. 2000. Histopathological spikelet changes produced by *Fusarium graminearum* in susceptible and resistant wheat cultivars. Plant Dis. 84:794–802.

Rotter, B. A., Prelusky, D. B., and Pestka, J. J. 1996. Toxicology of deoxynivalenol (vomitoxin). J Toxicol Env. Heal. 48:1–34.

Rouse, W., Haas, R. H., and Deering, D. W. 1974. Monitoring vegetation systems in the Great Plains with ERTS. In *Proceedings of the third earth resources technology satellite-1 symposium*, eds. S. C. Freden, E. P. Mercanti, and M. A. Becker. Greenbelt: NASA, p. 309–317.

Rumpf, T., Mahlein, A. K., Steiner, U., Oerke, E. C., Dehne, H. W., and Plümer, L. 2010. Early detection and classification of plant diseases with support vector machines based on hyperspectral reflectance. Comput. Electron. Agric. 74:91–99.

Rychlik, M., Humpf, H. U., Marko, D., Dänicke, S., Mally, A., Berthiller, F., et al. 2014. Proposal of a comprehensive definition of modified and other forms of mycotoxins including “masked” mycotoxins. Mycotoxin Res. 30:197–205.

Salgado, J. D., Madden, L. V., and Paul, P. A. 2014. Efficacy and economics of integrating in-field and harvesting strategies to manage *Fusarium* head blight of wheat. Plant Dis. 98:1407–1421.

Salgado, J. D., Madden, L. V., and Paul, P. A. 2015. Quantifying the effects of *Fusarium* head blight on grain yield and test weight in soft red winter wheat. Phytopathology. 105:295–306.

Savard, M. E., Sinha, R. C., Lloyd Seaman, W., and Fedak, G. 2000. Sequential distribution of the mycotoxin deoxynivalenol in wheat spikes after inoculation with *Fusarium graminearum*. Can. J. Plant Pathol. 22:280–285.

Savary, S., Willocquet, L., Pethybridge, S. J., Esker, P., McRoberts, N., and Nelson, A. 2019. The global burden of pathogens and pests on major food crops. Nat. Ecol. Evol. 3:430–439.

Schaad, N. W., and Frederick, R. D. 2002. Real-time PCR and its application for rapid plant disease diagnostics. Can. J. Plant Pathol. 24:250–258.

Scherm, B., Balmas, V., Spanu, F., Pani, G., Delogu, G., Pasquali, M., et al. 2013. *Fusarium culmorum*: causal agent of foot and root rot and head blight on wheat. Mol. Plant Pathol. 14:323–341.

Schilling, A. G., Möller, E. M., and Geiger, H. H. 1996. Polymerase chain reaction-based assays for species-specific detection of *Fusarium culmorum*, *F. graminearum*, and *F. avenaceum*. Phytopathology. 86:515–522.

Schisler, D. A., Khan, N. I., Boehm, M. J., and Slininger, P. J. 2002. Greenhouse and field evaluation of biological control of *Fusarium* head blight on durum wheat. Plant Dis. 86:1350–1356.

Scholes, J. D., and Rolfe, S. A. 2009. Chlorophyll fluorescence imaging as tool for understanding the impact of fungal diseases on plant performance: a phenomics perspective. Funct. Plant Biol. 36:880–892.

Schroeder, H. W., and Christensen, J. J. 1963. Factors affecting resistance of wheat to scab caused by *Gibberella zeae*. Phytopathology. 53:831–838.

Scott, P. M. 2012. Recent research on fumonisins: a review. Food Addit. Contam. - Part A. 29:242–248.

Serrano, L., Peñuelas, J., and Ustin, S. L. 2002. Remote sensing of nitrogen and lignin in Mediterranean vegetation from AVIRIS data: decomposing biochemical from structural signals. Remote Sens. Environ. 81:355–364.

Shah, D. A., De Wolf, E. D., Paul, P. A., and Madden, L. V. 2019. Functional data analysis of weather variables linked to *Fusarium* head blight epidemics in the United States. Phytopathology. 109:96–110.

Shahin, M. A., and Symons, S. J. 2012. Detection of *Fusarium* damage in Canadian wheat using visible/near-infrared hyperspectral imaging. J. Food Meas. Charact. 6:3–11.

Shi, W., Tan, Y., Wang, S., Gardiner, D. M., De Saeger, S., Liao, Y., et al. 2017. Mycotoxigenic potentials of *Fusarium* species in various culture matrices revealed by mycotoxin profiling. Toxins. 9:6.

Simko, I., and Piepho, H. P. 2012. The area under the disease progress stairs: calculation, advantage, and application. Phytopathology. 102:381–389.

Simpson, D. R., Weston, G. E., Turner, J. A., Jennings, P., and Nicholson, P. 2001. Differential control of head blight pathogens of wheat by fungicides and consequences for mycotoxin contamination of grain. Eur. J. Plant Pathol. 107:421–431.

Sims, D. A., and Gamon, J. A. 2002. Relationships between leaf pigment content and spectral reflectance across a wide range of species, leaf structures and developmental stages. Remote Sens. Environ. 81:337–354.

Singh, A., Ganapathysubramanian, B., Singh, A. K., and Sarkar, S. 2016. Machine learning for high-throughput stress phenotyping in plants. Trends Plant Sci. 21:110–124.

Singh, C. B., Jayas, D. S., Paliwal, J., and White, N. D. G. 2008. Detection of sprouted and midge-damaged wheat kernels using near-infrared hyperspectral imaging. In *Proceedings of the CSBE/SCGAB 2008 annual conference*, North Vancouver, BC, Canada, p. CSBE08-198.

Singh, C. B., Jayas, D. S., Paliwal, J., and White, N. D. G. 2009. Detection of insect-damaged wheat kernels using near-infrared hyperspectral imaging. J. Stored Prod. Res. 45:151–158.

Siou, D., Gélisse, S., Laval, V., Repinçay, C., Canalès, R., Suffert, F., et al. 2014. Effect of wheat spike infection timing on *Fusarium* head blight development and mycotoxin accumulation. Plant Pathol. 63:390–399.

Siou, D., Gélisse, S., Laval, V., Elbelt, S., Repinçay, C., Bourdat-Deschamps, M., et al. 2015a. Interactions between head blight pathogens: consequences for disease development and toxin production in wheat spikes. Appl. Environ. Microbiol. 81:957–965.

Siou, D., Gélisse, S., Laval, V., Suffert, F., and Lannou, C. 2015b. Mutual exclusion between fungal species of the *Fusarium* head blight complex in a wheat spike. Appl. Environ. Microbiol. 81:4682–4689.

Siuda, R., Grabowski, A., Lenc, L., Ralcewicz, M., and Spychaj-Fabisiak, E. 2010. Influence of the degree of fusariosis on technological traits of wheat grain. Int. J. Food Sci. Technol. 45:2596–2604.

Skinnes, H., Semagn, K., Tarkegne, Y., Marøy, A. G., and Bjørnstad, Å. 2010. The inheritance of anther extrusion in hexaploid wheat and its relationship to *Fusarium* head blight resistance and deoxynivalenol content. Plant Breed. 129:149–155.

Smith, W. 1884. New diseases of wheat, barley, and rye-grass. In *Diseases of field and garden crops*, London: MacMillan and Co., p. 208–213.

Spanic, V., Lemmens, M., and Drezner, G. 2010. Morphological and molecular identification of *Fusarium* species associated with head blight on wheat in east Croatia. Eur. J. Plant Pathol. 128:511–516.

Spanic, V., Zdunic, Z., Drezner, G., and Sarkanj, B. 2019. The pressure of *Fusarium* disease and its relation with mycotoxins in the wheat grain and malt. Toxins. 11:198.

Stack, R. W., and McMullen, M. P. 1998. A visual scale to estimate severity of *Fusarium* head blight in wheat. North Dakota State Univ. Ext. Serv. :PP-1095.

Stack, R. W. 2003. History of *Fusarium* head blight with emphasis on north America. In *Fusarium head blight of wheat and barley*, ed. W. R. Leonard, and K. J. Bushnell. St. Paul, MN, USA: American Phytopathological Society Press, p. 1–34.

REFERENCES

Stanciu, O., Juan, C., Miere, D., Loghin, F., and Mañes, J. 2017a. Presence of enniatins and beauvericin in Romanian wheat samples: from raw material to products for direct human consumption. Toxins. 9:189.

Stanciu, O., Juan, C., Miere, D., Loghin, F., and Mañes, J. 2017b. Occurrence and co-occurrence of *Fusarium* mycotoxins in wheat grains and wheat flour from Romania. Food Control. 73:147–155.

Stanciu, O., Juan, C., Berrada, H., Miere, D., Loghin, F., and Mañes, J. 2019. Study on trichothecene and zearalenone presence in Romanian wheat relative to weather conditions. Toxins. 11:163.

Steiner, B., Buerstmayr, M., Michel, S., Schweiger, W., Lemmens, M., and Buerstmayr, H. 2017. Breeding strategies and advances in line selection for *Fusarium* head blight resistance in wheat. Trop. Plant Pathol. 42:165–174.

Stenglein, S. A. 2009. *Fusarium poae*: a pathogen that needs more attention. J. Plant Pathol. 91:25–36.

Stenglein, S. A., Dinolfo, M. I., Barros, G., Bongiorno, F., Chulze, S. N., and Moreno, M. V. 2014. *Fusarium poae* pathogenicity and mycotoxin accumulation on selected wheat and barley genotypes at a single location in Argentina. Plant Dis. 98:1733–1738.

Stoll, M., Schultz, H. R., Baecker, G., and Berkelmann-Loehnertz, B. 2008. Early pathogen detection under different water status and the assessment of spray application in vineyards through the use of thermal imagery. Precis. Agric. 9:407–417.

Strange, R. N., Majer, J. R., and Smith, H. 1974. The isolation and identification of choline and betaine as the two major components in anthers and wheat germ that stimulate *Fusarium graminearum in vitro*. Physiol. Plant Pathol. 4:277–290.

Summerell, B. A. 2019. Resolving *Fusarium*: current status of the genus. Annu. Rev. Phytopathol. 57:323–339.

Suproniene, S., Kadziene, G., Irzykowski, W., Sneideris, D., Ivanauskas, A., Sakalauskas, S., et al. 2019. Weed species within cereal crop rotations can serve as alternative hosts for *Fusarium graminearum* causing *Fusarium* head blight of wheat. Fungal Ecol. 37:30–37.

Talas, F., Parzies, H. K., and Miedaner, T. 2011. Diversity in genetic structure and chemotype composition of *Fusarium graminearum* sensu stricto populations causing wheat head blight in individual fields in Germany. Eur. J. Plant Pathol. 131:39–48.

Tedjiotsop Feudjio, F., Dornetshuber, R., Lemmens, M., Hoffmann, O., Lemmens-Gruber, R., and Berger, W. 2010. Beauvericin and enniatin: emerging toxins and/or remedies? World Mycotoxin J. 3:415–430.

Thomas, S., Wahabzada, M., Kuska, M. T., Rascher, U., and Mahlein, A. K. 2017. Observation of plant-pathogen interaction by simultaneous hyperspectral imaging reflection and transmission measurements. Funct. Plant Biol. 44:23–34.

Thomas, S., Kuska, M. T., Bohnenkamp, D., Brugger, A., Alisaac, E., Wahabzada, M., et al. 2018. Benefits of hyperspectral imaging for plant disease detection and plant protection: a technical perspective. J. Plant Dis. Prot. 125:5–20.

Thrane, U. 1996. Comparison of three selective media for detecting *Fusarium* species in foods: a collaborative study. Int. J. Food Microbiol. 29:149–156.

Torres, A. M., Palacios, S. A., Yerkovich, N., Palazzini, J. M., Battilani, P., Leslie, J. F., et al. 2019. *Fusarium* head blight and mycotoxins in wheat: prevention and control strategies across the food chain. World Mycotoxin J. 12:333–355.

Trail, F. 2009. For blighted waves of grain: *Fusarium graminearum* in the postgenomics era. Plant Physiol. 149:103–110.

Tralamazza, S. M., Bemvenuti, R. H., Zorzete, P., De Souza Garcia, F., and Corrêa, B. 2016. Fungal diversity and natural occurrence of deoxynivalenol and zearalenone in freshly harvested wheat grains from Brazil. Food Chem. 196:445–450.

Umpiérrez-Failache, M., Garmendia, G., Pereyra, S., Rodríguez-Haralambides, A., Ward, T. J., and Vero, S. 2013. Regional differences in species composition and toxigenic potential among *Fusarium* head blight isolates from Uruguay indicate a risk of nivalenol contamination in new wheat production areas. Int. J. Food Microbiol. 16:135–140.

REFERENCES

Varga, E., Wiesenberger, G., Hametner, C., Ward, T. J., Dong, Y., Schöfbeck, D., et al. 2015. New tricks of an old enemy: isolates of *Fusarium graminearum* produce a type A trichothecene mycotoxin. Environ. Microbiol. 17:2588–2600.

Vesonder, R. F., Goliński, P., Plattner, R., and Zietkiewicz, D. L. 1991. Mycotoxin formation by different geographic isolates of *Fusarium crookwellense*. Mycopathologia. 113:11–14.

Vogelgsang, S., Beyer, M., Pasquali, M., Jenny, E., Musa, T., Bucheli, T. D., et al. 2019. An eight-year survey of wheat shows distinctive effects of cropping factors on different *Fusarium* species and associated mycotoxins. Eur. J. Agron. 105:62–77.

Wang, J., Wieser, H., Pawelzik, E., Weinert, J., Keutgen, A. J., and Wolf, G. A. 2005. Impact of the fungal protease produced by *Fusarium culmorum* on the protein quality and breadmaking properties of winter wheat. Eur. Food Res. Technol. 220:552–559.

Wang, W., Heitschmidt, G. W., Windham, W. R., Feldner, P., Ni, X., and Chu, X. 2015. Feasibility of detecting aflatoxin B1 on inoculated maize kernels surface using VIS/NIR hyperspectral imaging. J. Food Sci. 80:M116–M122.

Wang, X., Zhang, M., Zhu, J., and Geng, S. 2008. Spectral prediction of *Phytophthora infestans* infection on tomatoes using artificial neural network (ANN). Int. J. Remote Sens. 29:1693–1706.

Ward, T. J., Clear, R. M., Rooney, A. P., O'Donnell, K., Gaba, D., Patrick, S., et al. 2008. An adaptive evolutionary shift in *Fusarium* head blight pathogen populations is driving the rapid spread of more toxigenic *Fusarium graminearum* in North America. Fungal Genet. Biol. 45:473–484.

Wegulo, S. N., Bockus, W. W., Nopsa, J. H., de Wolf, E. D., Eskridge, K. M., Peiris, K. H. S., et al. 2011. Effects of integrating cultivar resistance and fungicide application on *Fusarium* head blight and deoxynivalenol in winter wheat. Plant Dis. 95:554–560.

Wegulo, S. N., Baenziger, P. S., Hernandez Nopsa, J., Bockus, W. W., and Hallen-Adams, H. 2015. Management of *Fusarium* head blight of wheat and barley. Crop Prot. 73:100–107.

Wieser, H. 2000. Simple determination of gluten protein types in wheat flour by turbidimetry. Cereal Chem. 77:48–52.

Williams, K. J., Dennis, J. I., Smyl, C., and Wallwork, H. 2002. The application of species-specific assays based on the polymerase chain reaction to analyse *Fusarium* crown rot of durum wheat. Australas. Plant Pathol. 31:119–127.

Wilson, A., Simpson, D., Chandler, E., Jennings, P., and Nicholson, P. 2004. Development of PCR assays for the detection and differentiation of *Fusarium sporotrichioides* and *Fusarium langsethiae*. FEMS Microbiol. Lett. 233:69–76.

Winter, M., Koopmann, B., Döll, K., Karlovsky, P., Kropf, U., Schlüter, K., et al. 2013. Mechanisms regulating grain contamination with trichothecenes translocated from the stem base of wheat (*Triticum aestivum*) infected with *Fusarium culmorum*. Phytopathology. 103:682–689.

Xu, K., He, X., Dreisigacker, S., He, Z., and Singh, P. K. 2020. Anther extrusion and its association with *Fusarium* head blight in CIMMYT wheat germplasm. Agronomy. 10:47.

Xu, X. M., Nicholson, P., Thomsett, M. A., Simpson, D., Cooke, B. M., Doohan, F. M., et al. 2008. Relationship between the fungal complex causing *Fusarium* head blight of wheat and environmental conditions. Phytopathology. 98:69–78.

Xue, A. G., Chen, Y., Seifert, K., Guo, W., Blackwell, B. A., Harris, L. J., et al. 2019. Prevalence of *Fusarium* species causing head blight of spring wheat, barley and oat in Ontario during 2001–2017. Can. J. Plant Pathol. 41:392–402.

Xue, J., and Su, B. 2017. Significant remote sensing vegetation indices: a review of developments and applications. J. Sensors. 2017:1353691.

Xue, S., Li, G., Jia, H., Xu, F., Lin, F., Tang, M., et al. 2010. Fine mapping *Fhb4* , a major QTL conditioning resistance to *Fusarium* infection in bread wheat (*Triticum aestivum* L.). Theor. Appl. Genet. 121:147–156.

REFERENCES

Xue, S., Xu, F., Tang, M., Zhou, Y., Li, G., An, X., et al. 2011. Precise mapping *Fhb5* , a major QTL conditioning resistance to *Fusarium* infection in bread wheat (*Triticum aestivum* L.). Theor. Appl. Genet. 123:1055–1063.

Yoder, W. T., and Christianson, L. M. 1998. Species-specific primers resolve members of *Fusarium* section *Fusarium*. Fungal Genet. Biol. 23:68–80.

Yoshida, M., and Nakajima, T. 2010. Deoxynivalenol and nivalenol accumulation in wheat infected with *Fusarium graminearum* during grain development. Phytopathology. 100:763–773.

Zachetti, V. G. L., Cendoya, E., Nichea, M. J., Chulze, S. N., and Ramirez, M. L. 2019. Preliminary study on the use of chitosan as an eco-friendly alternative to control *Fusarium* growth and mycotoxin production on maize and wheat. Pathogens. 8:29.

Zhang, P., Zhu, Y., Ma, D., Xu, W., Zhou, J., Yan, H., et al. 2019. Screening, identification, and optimization of fermentation conditions of an antagonistic endophyte to wheat head blight. Agronomy. 9:476.

Zhao, Y., Selvaraj, J. N., Xing, F., Zhou, L., Wang, Y., Song, H., et al. 2014. Antagonistic action of *Bacillus subtilis* strain SG6 on *Fusarium graminearum*. PLoS One. 9:e92486.

Zhu, Z., Hao, Y., Mergoum, M., Bai, G., Humphreys, G., Cloutier, S., et al. 2019. Breeding wheat for resistance to *Fusarium* head blight in the Global North: China, USA, and Canada. Crop J. 7:730–738.